An Examination of Metamorphic Uranium Occurrences in Coosa County, Alabama

by

Jessica Horwitz

A thesis submitted to the Graduate Faculty of
Auburn University
in partial fulfillment of the
requirements for the Degree of
Master of Science

Auburn, Alabama
August 9, 2010

Keywords: Uranium, Coosa County, Alabama

Approved by

Robert Cook, Chair, Professor Emeritus of Geology
Willis Hames, Professor of Geology
Mark Steltenpohl, Professor of Geology

Abstract

Coosa County, Alabama, is host to one or more presumably metamorphosed uranium occurrences of unknown size or grade. The exact location, size and mode of emplacement of each uranium occurrence is currently unknown. This thesis expands on existing knowledge of these occurrences through fieldwork, and geochemical and petrographic studies. Geochemical maps document that most of the anomalous uranium occurrences are within Section 30 T. 23 N, R. 18 E, overlapping with radiometric contour highs reported in surveys conducted during the 1970's. Geochemical analyses document concentrations of barium and vanadium within anomalously green micas (mean values of 5,894.50 and 3,470.10 ppm respectively). Microprobe analyses indicate a decrease in uranium and vanadium in the micas with alteration (mean values of 1.50 to 1.07 and 0.92 to 0.27 weight percent, respectively). Uranium is present in small quantities within the anomalously green mica, but higher abundances are indicated by individual whole-rock samples (mean values of 7.51 and 4.89 ppm respectively). The likely prototype for the uranium occurrences is similar to the occurrences in the Colorado Plateau or the Mauch Chunk Formation in the eastern United States. Recrystallized micas and quartz indicate temperatures of ~400°C, and brittle fractures within quartz indicate temperatures >300°C suggesting two stages of metamorphism, the first of which was sillimanite grade and occurred during the Acadian Orogeny. The rocks underwent retrograde metamorphism occurring during the Alleghanian Orogeny at which time the uranium and vanadium

moved from the muscovites and into other unidentified sites (such as minor shear zones) within the host rock.

Acknowledgments

The author would like to thank Mark Wassweiler (deceased) for funding the research and Brad McLauchlin at Resource Land Management for allowing access to the field area. Fieldwork could not have been completed without the help of fellow students Kevin Bogdan, Andy Drake, Thomas Key and Amanda Reynolds. Special thanks to Amanda Savrda for helping with the bulk of the fieldwork. Thanks also to family members Joan, Michael and Mara for their support. The author would especially like to thank Wes Buchanan for his understanding, support and patience throughout the duration of the thesis project.

Table of Contents

List of Tables

List of Figures

INTRODUCTION

Nuclear energy became a popular and thought-provoking reality after the detonation of the first atom bomb in 1945. Since that time, exploration for uranium has increased dramatically. Between the late 1940's and mid 1950's, there was a uranium boom. Internationally, nuclear reactors were seen as new energy sources, and, in 1954, the USSR's Obninsk Nuclear Power Plant became the first operational nuclear power plant. After the Three Mile Island and Chernobyl accidents in 1979 and 1986, respectively, the construction of new nuclear reactors was slowed.

Due to the increased demands of fossil fuels and increasing concerns for the amounts of CO_2 and other greenhouse gasses released into the environment, energy companies have had renewed interest in nuclear energy and how it can be used safely. The economy at the time of this report reflects this increased attention; the value of uranium, as U_3O_8 in the form of yellowcake, increased from $20.00 per pound in 2004 to $42.00 per pound in February of 2010. Currently, the United States imports about 80% of the uranium it consumes annually. If nuclear power is seen as the future of energy within the United States, new domestic deposits must be found.

Coosa County, Alabama, is host to one or more presumably metamorphosed uranium occurrences of unknown size and grade. The exact location and mode of occurrence of the uranium within the rocks of Coosa County is currently unknown. This thesis expands existing knowledge of these occurrences through fieldwork, and geochemical and

petrographic studies. Although preliminary geochemical work has been performed on the occurrences, no database contains all the geologic and geochemical information pertaining to the uranium occurrences within Coosa County. Previously existing and new geochemical and structural data have been compiled into a database. The data were compared to known deposit types with similar characteristics, which allows for a depositional model to be developed. The uranium occurrences are in close proximity to a northeast trend of abandoned graphite mines and prospects. Scintillometer readings are generally higher in areas underlain by siliceous units of the Higgins Ferry Group containing green vanadium-rich mica, previously referred to loosely as roscoelite, which is believed to be the host for the uranium. The siliceous units of the Higgins Ferry Group form a prominent northeast/southwest striking ridge within in the field area.

Geographic Setting and Access

The study area is within Coosa County, Alabama, and can be located on the Flag Mountain 7 1/2' U.S.G.S. Topographic Quadrangle. The site is centered within Sections 19, 20, 29, 30, and 31, T. 23 N, R. 18 E (Figs. 1 and 2). Two data points are outside of the central area; one in Section 36, T. 22 N, R. 17 E and one in Section 9, T. 23 N, R. 18 E. Access to the field area is limited. One entrance is a poorly maintained dirt road located off County Road 29. The second entrance, also from County Road 29, is gated and locked. Within the field area, roads degrade into logging and ATV trails, which become impassable during rainy weather. Within the field area, many roads are gated by hunting clubs that lease the land, and by the logging companies that own the land.

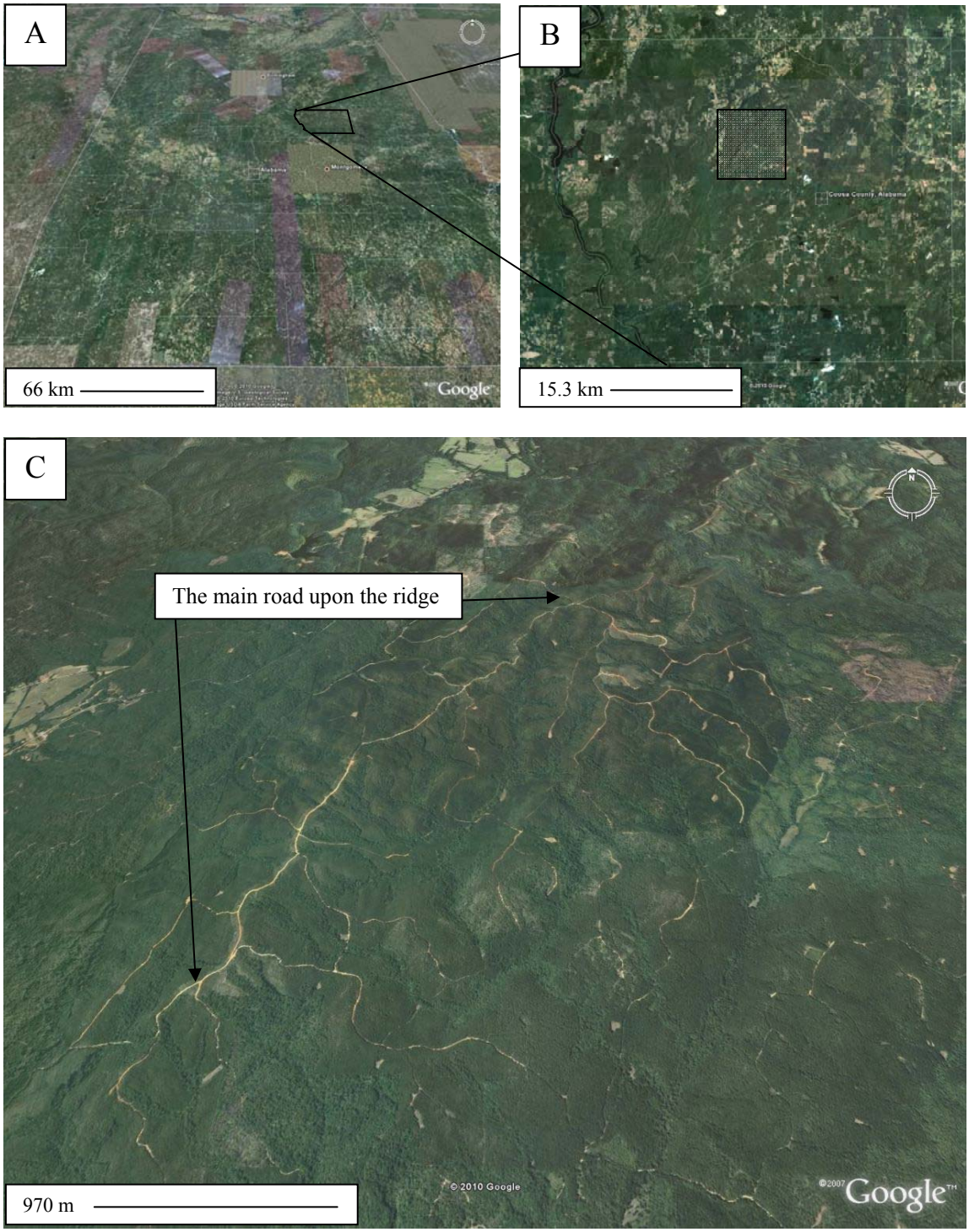

Fig. 1. Photos A and B show Coosa County, Alabama and the location of the field area. Photo C is the approximate field area, and the main road on top of the ridge is seen and is centered within the anomalous uranium zones (Google Earth photo).

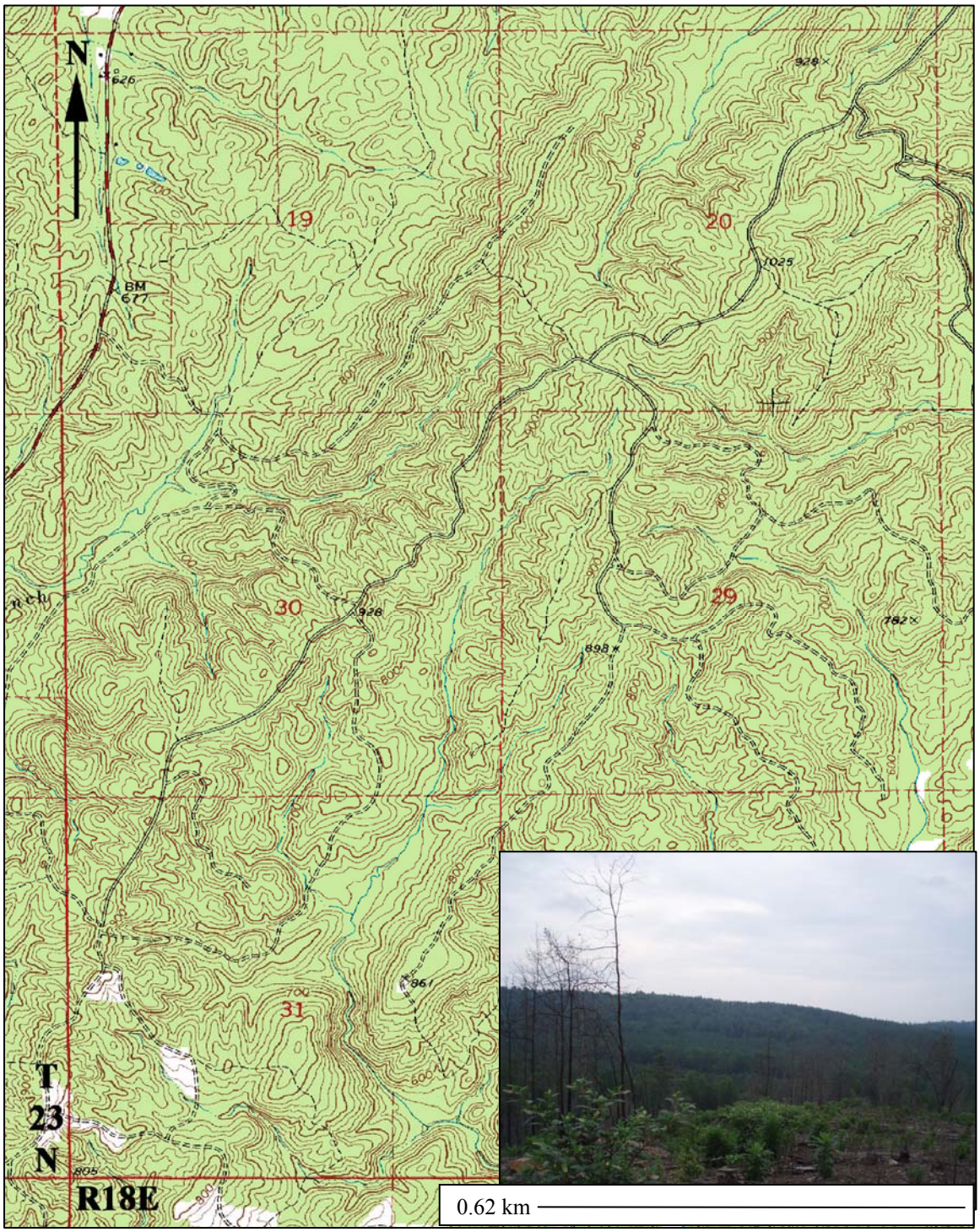

Fig. 2. Part of the United States Geological Survey Flag Mountain 7 1/2' Topographic Quadrangle showing the prominent ridge in the anomalous uranium area (sections 19, 20, 29, 30 and 31 T. 23 N., R. 18 E.) (modified from United States Geological Survey, 1971). The inset photograph is a view to the east of the same ridge.

General Geology of the Study Area

Terminology within the Southern Appalachians has been complicated by authors in Alabama and other states giving similar rocks different names. Specific to Alabama is the differentiation of Piedmont terrains as Northern, Inner and Southern (Raymond et al., 1988). Coosa County is located within the Northern Alabama Piedmont, which is bounded to the north by the Talladega-Cartersville fault and to the south by the Brevard Zone. Within the Northern Piedmont are three structural blocks - the Talladega, Coosa and Tallapoosa. These blocks change progressively from lower greenschist-facies in the northwestern Talladega Block to mid- and upper-amphibolite-facies in the Coosa and Tallapoosa Blocks (Tull, 1978; Drummond, 1986; Drummond et al. 1986; Raymond, et al., 1988).

The Coosa block is structurally controlled by the sinuous Hollins Line fault to the north and the relatively straight Enitachopco-Goodwater fault to the south (Fig. 3). The Hollins Line fault is truncated in several places by the Enitachopco-Goodwater fault, resulting in two sub-regional salients, which are separated by the Millerville reentrant (Raymond et al., 1988; Steltenpohl and Moore, 1988; Steltenpohl, 2005). Clay County contains the northeastern salient, and Coosa County contains the southwestern salient. Lithologically the rocks found within the two salients are the same; however, they have been named differently. The northeastern salient contains the Kahatchee Mountain, Sylacauga, Talladega, Unity and Poe Bridge Mountain Groups. The southwestern salient (Fig. 4) contains the Higgins Ferry, Hatchet Creek and Wedowee Groups (Raymond et al., 1988). The Higgins Ferry, Hatchet Creek, Poe Bridge Mountain and Mad Indian Groups within the two salients were originally named the Ashland Mica Schist by Adams (1926). Tull (1978) suggested the groups as a whole be termed the Ashland Supergroup.

The Poe Bridge Mountain Group, contained in the Clay County Salient, is lithologically the same as the Higgins Ferry group within Coosa County (Tull, 1978; Beg, 1980; Cook et al., 1982). As with the Higgins Ferry Group, anomalous uranium is found within the Poe Bridge Mountain Group. The uranium is generally associated with anomalously green mica along the general trend of graphite mines (Beg, 1980; Cook et al., 1982).

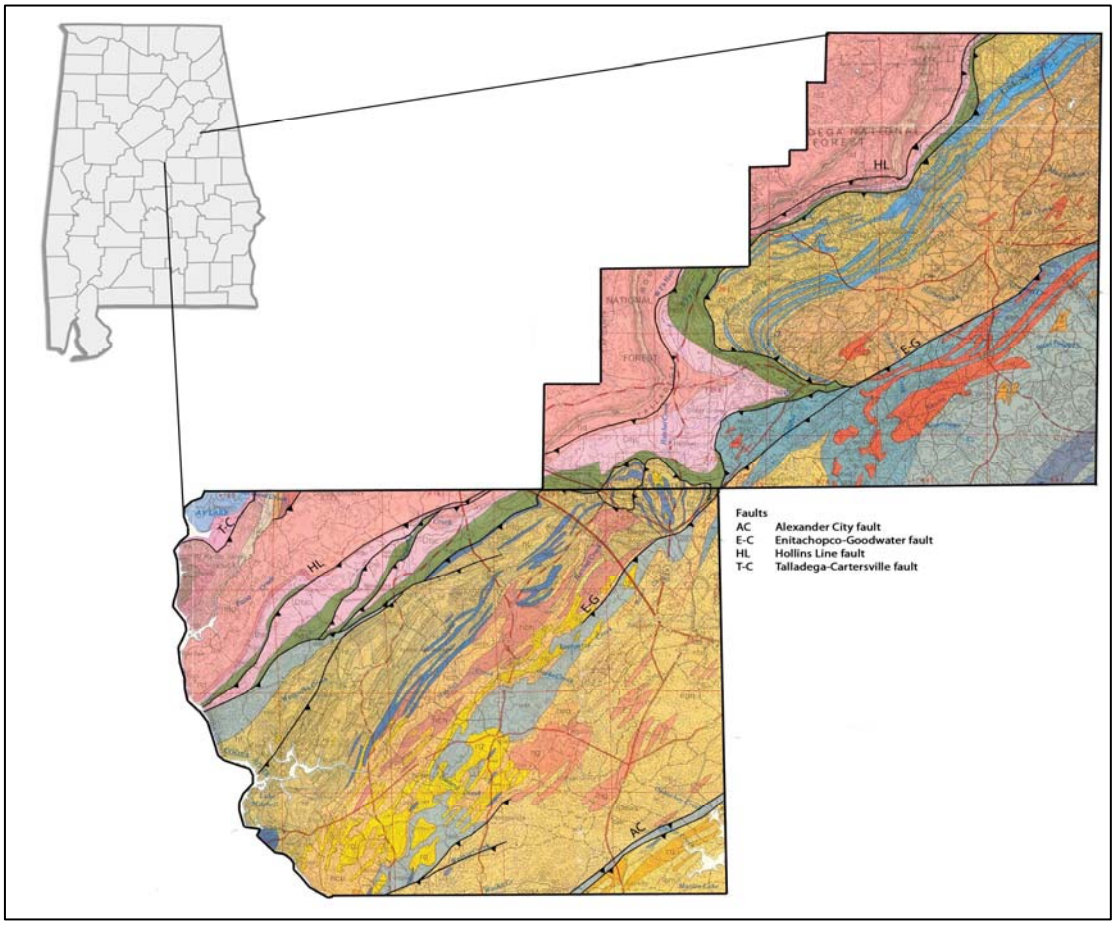

Fig. 3. Geologic map of the two structural salients in Clay and Coosa Counties (*after* Osborne et al., 1988). This map is located on the accompanying CD and can be viewed at an enlarged size.

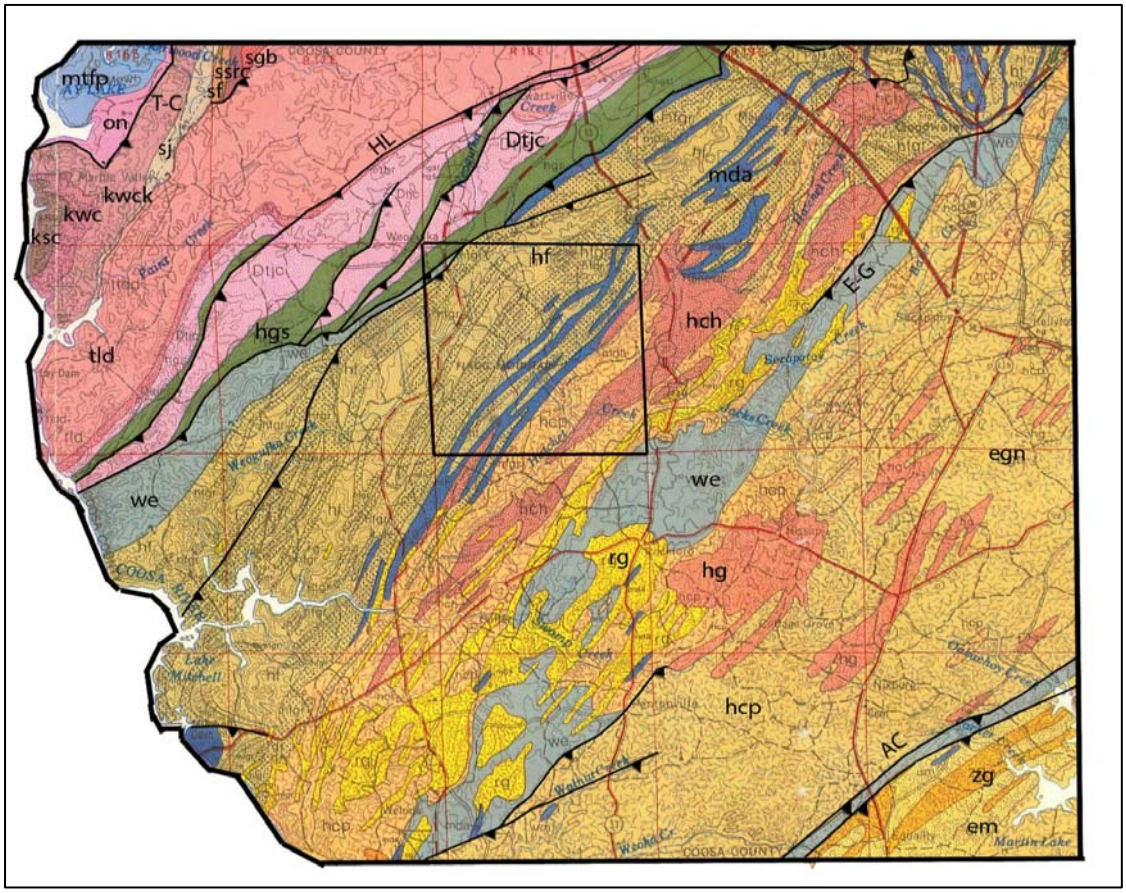

Fig. 4. Geologic map illustrating the faults and lithodemic units of Coosa County (*after* Osborne et al., 1988). The field area is outlined in black. The map is located on the accompanying CD and can be viewed at an enlarged size. Abbreviations are as follows: Dtjc-Jemison Chert and Chulfinnee Schist, egn-Elkahatchee Quartz Diorite Gneiss, em-Emuckfaw Group, hch-Hanover Schist, hcp-Pinchoulee Gneiss, hf-Higgins Ferry Group, hg-Hissop Granite, hgs-Hillabee Greenstone, ksc-Slumps Creek Formation, kwc-Wash Creek Shale, kwck-kalona Quartzite Member of the Wash Creek Shale, mda-Mitchell Dam Amphibolite, mtfp-Tuscumbia Limestone and Ft. Payne Chert, on-Newala Limestone, rg-Rockford Granite, sj-Jumbo Dolomite, tld-Lay Dam Formation, We-Wedowee Group, zg-Zana Granite. Abbreviations for faults are as follows: AF-Alexander City fault, E-G-Enitachopco-Goodwater fault, HL-Hollins Line Fault, T-C-Talladega-Cartersville fault.

In an effort to correlate Alabama terminology with that used in the rest of the Appalachians, researchers have begun calling the physiographic provinces within Alabama by the same names as those to the northeast. Using this 'new' terminology, the Northern Alabama Piedmont corresponds to the western Blue Ridge and the eastern Blue

Ridge (Fig. 5). The eastern Blue Ridge in Alabama is framed by the Hollins Line fault to the north and by the Brevard Zone to the south (Steltenpohl and Moore, 1988; Steltenpohl, 2005). The Hollins Line fault separates rocks of the Talladega belt from the rocks of the eastern Blue Ridge, and there is a stark contrast between the lower-grade greenschist facies rock of the Talladega belt and the rocks of the eastern Blue Ridge, which have been metamorphosed to mid- to upper-amphibolite-facies (Fig. 6) (kyanite and/or sillimanite grade) (Neathery and Tull, 1975; Steltenpohl, 2005). When using this terminology, areas are no longer defined as structural blocks; this does not negate the recognition of the two separate salients separated by the Millerville reentrant (Steltenpohl and Moore, 1988; Steltenpohl, 2005).

Rocks Within and Near the Field Area

Specific lithodemic units within the Higgins Ferry Group contain the anomalous uranium occurrences. The Higgins Ferry Group is comprised of coarse- to fine-grained biotite-feldspar-quartz gneiss, sericite-feldspar-muscovite schist, quartzite and garnet-bearing altered mafic rocks. Throughout the Higgins Ferry Group, kyanite and sillimanite porphyroblasts are common. Both graphitic schists and quartzites within the Higgins Ferry contain the anomalously green mica.

The Mitchell Dam Amphibolite is contained as lenticular bodies within the Higgins Ferry Group. Hornblendes from the unit have been dated at ~ 348 +/- 10 Ma based on potassium-argon isotopic analysis (Russell, 1978; Frinak, 1984; Drummond, 1986;

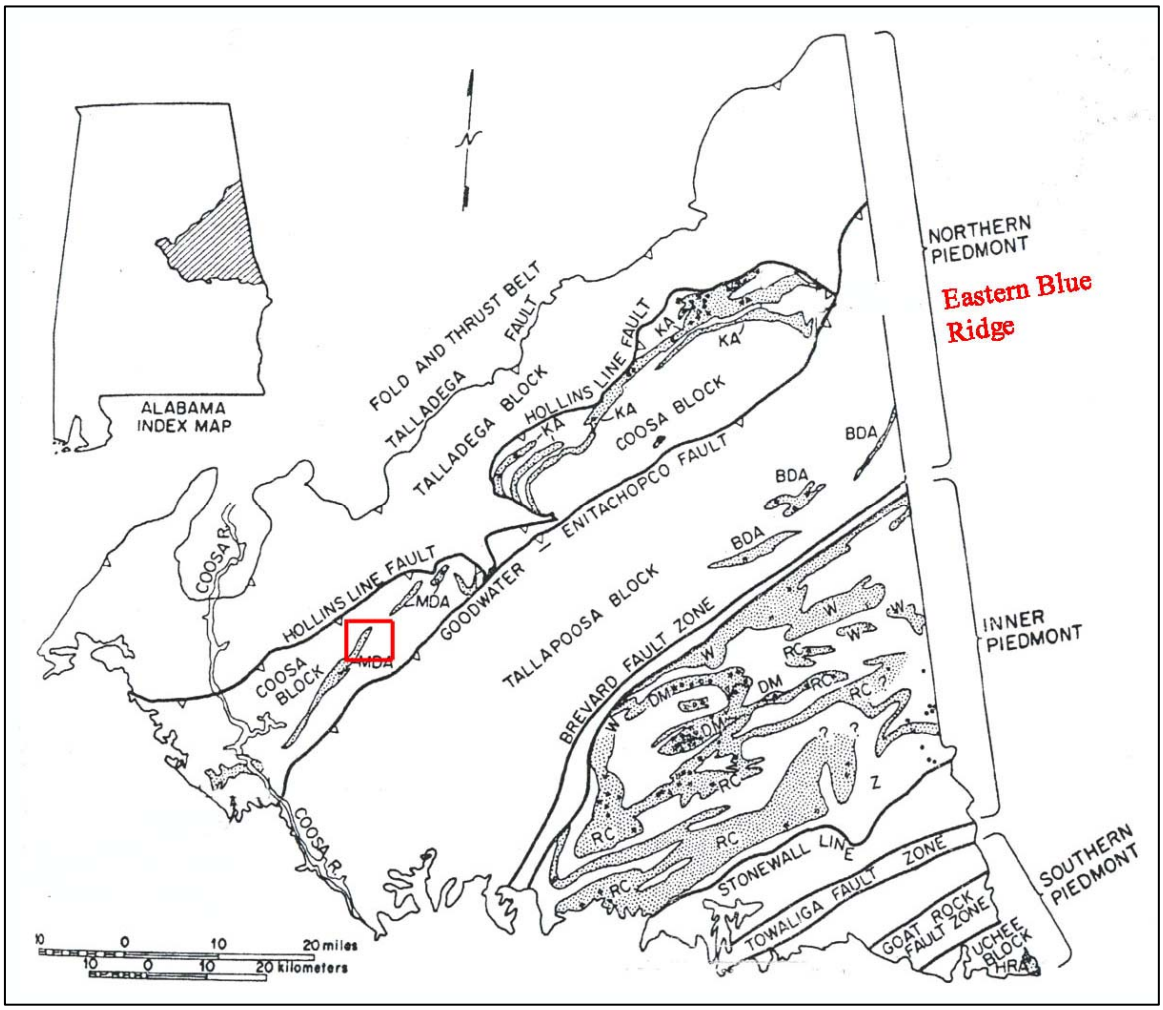

Fig. 5. Different nomenclatures of the rocks within Alabama. In black is the local terminology, and in red is the regionally accepted terminology (*after* Stow et al., 1984). The study area is outlined in the red box. Abbreviations are as follows: BDA-Beaver Dam Amphibolite, HRA-Hudson Rapids Amphibolite, KA-Ketchepedrakee Amphibolite, MDA-Mitchell Dam Amphibolite, RC-Ropes Creek Formation, W-Waresville Formation, Z-Zebulon Formation.

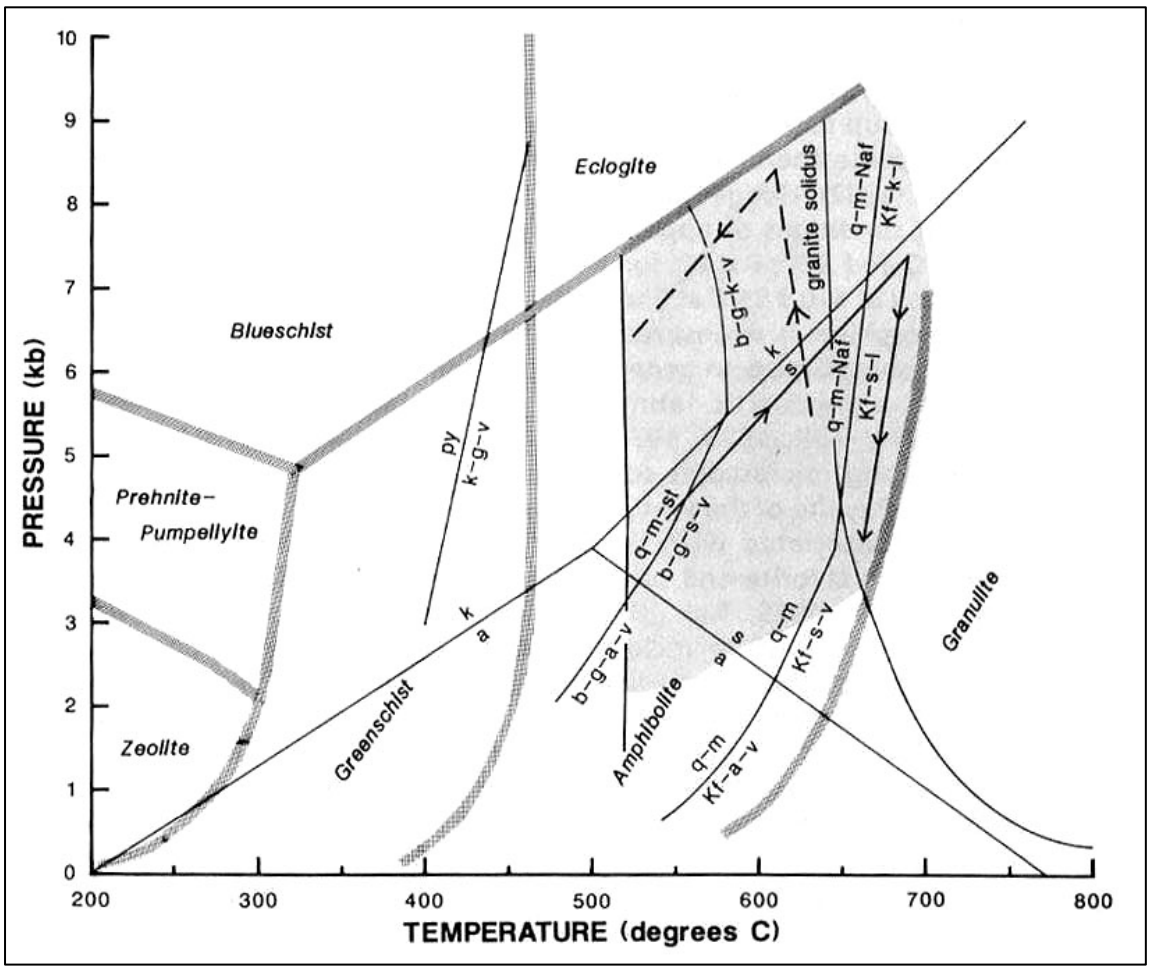

Fig. 6. Pressure-temperature diagram displaying the conditions for metamorphism of the eastern Blue Ridge belt of Alabama (shaded area), which includes rocks of the study area. Abbreviations are as follows: a–andalusite, ab-albite, b-biotite, cc-calcite, di-diopside, do-dolomite, chl-chlorite, chd-chloritoid, fo-fosterite, g-garnet, gl-glaucophane, k-kyanite, Kf-k-feldspar, l-liquid, m-muscovite, Naf-plagioclase, py-pyrophyllite, q-quartz, s-sillimanite, st-staurolite, tc-talc, tr-tremolite, v-vapor (Steltenpohl and Moore, 1988).

Raymond et al., 1988; Steltenpohl and Moore, 1988). The amphibolite is interpreted as orthoamphibolite, whose protolith was a tholeiitic basalt formed in an ocean-rifting environment (Stow et al., 1984; Tull et al., 2007).

Southeast of the Higgins Ferry Group is the Hatchet Creek Group. These units are fine- to coarse-grained feldspathic schists and gneisses that have been termed the Hannover Schist-Gneiss Complex. The gneisses vary in composition from granitic to

dioritic. Similar to the Higgins Ferry Group are the graphitic-quartz schists within the complex. Locally the Hatchet Creek Group hosts pegmatite swarms (Frinak, 1984; Raymond et al., 1988).

Southeast of the Hatchet Creek Group is the Wedowee Group. This group comprises a sequence of quartz-graphite-sericite phyllites and chlorite-sericite phyllites that grade into schists (Raymond et al., 1988).

Within the three groups contained in the Coosa Block, granite and pegmatite intrusions are common. The block contains the Rockford Granite, an S-type granite that is associated with tin deposits in Coosa County near the town of Rockford. It is hosted by the Wedowee and Hatchet Creek Groups and is thought to have intruded during kyanite-sillimanite grade regional metamorphism (Hunter, 1944; Drummond, 1987a + b; Drummond and Allison, 1987).

Economic Resources

Coosa and surrounding counties contain abundant historical mineral resources. Deposits of graphite, mica and gold have been mined from the Higgins Ferry Group, as well as from other nearby rock units. Graphite, mica, tin, tantalum and pyrite have all been mined or prospected near the field area. Figure 7 show points of reference which are important to the economic resources in and surrounding Coosa County.

A 60-mile long northeast-trending belt of graphitic schist is found in Chilton, Coosa and Clay Counties (Jones, 1929) and extends from Verbena to southwest of Delta. An absence of graphite deposits is found between the towns of Goodwater and Millerville (Cameron and Weis, 1960). According to Drummond (1986), the graphite-rich units are the metamorphosed remnants of marine black shales formed from lithified anoxic mud.

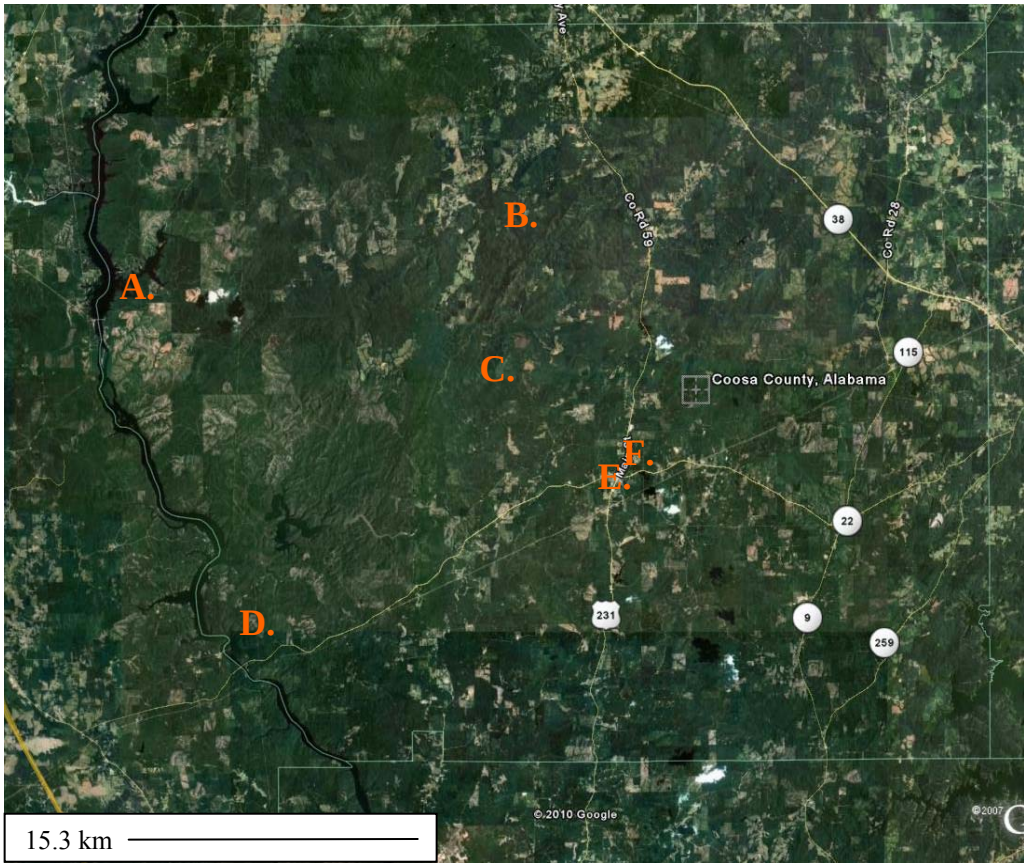

Fig. 7. Aerial photograph of Coosa County with points of reference labeled as follows: A-Lay Dam; B-Weogufka; C-Field Area; D-Mitchell Dam; E-McCallister Deposit; F-Rockford (Google Earth photo).

In many areas, the graphite is present in large enough quantities to have been mined and has been used to make crucibles for the manufacturing of steel. Graphite mines in Coosa County were important during World Wars I and II. Over 40 mills were built for the production of flake graphite during World War I. Only one was still in operation when World War II began and all had been shut down after 1953 (Pallister and Thoenen, 1948; Cameron and Weis, 1960; Dean, 2007). The most economic of the graphite occurrences were found in association with the Poe Bridge Mountain and Higgins Ferry Groups and can occur with vanadium-bearing mica. The graphite can occur as elongated lenses that range from a few inches to more than 100 feet in thickness (Dean, 2007).

Mica is abundant within the area, and is found in concentrations high enough for mining in multiple southwest-northeast trending belts of mineralization typically associated with pegmatite dikes. Abandoned muscovite mines are found within Randolph, Clay, Tallapoosa, Coosa, Cleburne, Chambers, Elmore, Talladega and Lee counties (Clark, 1921; Epperson and Rheams, 1984). During World Wars I and II, muscovite was mined extensively in Coosa County for the war efforts. Later it was mined for electrical purposes. In 1980, due to rising costs, the last Alabama scrap mica operation in Randolph County was closed (Epperson and Rheams, 1984). Current production is limited to an operation near Micaville in Cleburne County (Dean, 2007).

In 1880, residual masses of the tin oxide, cassiterite, were found near Rockford, Alabama, where it occurs within the Rockford granite and associated pegmatites. Most occurrences were located in the 1930's by a prospector named W. M. Hoyt. The United States Bureau of Mines prospected the area between 1939 and 1942 in an effort to discover new occurrences (Hunter, 1944; Neathery, 1977; Reed, 1950). Between 1970 and 1985, the area was again explored for tin deposits, and 39 tin and/or tin-tantalum occurrences were found using stream-sediment and soil geochemistry. These new discoveries included the McAllister deposit, located three kilometers west of Rockford, which contains both tin and tantalum. The deposit is within a large pegmatite hosted by the Rockford Granite, which contains extensive zones of replacement albite and greisen-like pipes (Cook et al., 1987; Dean and Cook, 1987; Foord and Cook, 1989). In the early 1990's the occurrence was mined (Dean, 2007).

Beginning in 1832, small placer and lode gold mines were active in Alabama for several decades. Alabama has two belts of mineralization where gold has been found. The Upper or Northern belt occurs in Talladega, Clay, Randolph and Cleburne Counties,

while the Lower or Southern belt is located in Chilton, Coosa, Tallapoosa, Elmore and Chambers Counties (Simpson and Neathery, 1980). Operations in Coosa County, near Rockford and Weogufka, mined lode gold from pyrite-rich quartz veins in the Higgins Ferry Group. Gold was also mined between Mitchell and Lay Dams on the Coosa River (Adams, 1930; Guthrie and Lesher, 1989; Dean 1989).

Although no copper has been mined in Coosa County, there is a record of prospecting gossan-like iron oxides that contained 'iridescent films' that were misidentified as copper. Copper was mined from nearby Cleburne County (Adams, 1930).

Little has been published on the uranium found in the area. Reed (1950) briefly mentioned that the pegmatites hosting the tin deposits near Rockford were radioactive due to "minor concentrations of autunite, a calcium-uranium-phosphate occurring in the pegmatites." The most recent work (Cook et al., 1982) provides information on the radiometric anomalies obtained by fieldwork and geochemical analysis. Uranium is concentrated within the rocks of the Higgins Ferry Group and is commonly associated with 'roscoelite'-bearing quartzite (Cook et al., 1982). Uranium occurs within the general trend of abandoned graphite mines in Coosa County.

Previous Work

Uranium Research: Beginning in the 1970's and continuing as this report was written, Coosa County has been explored for economic uranium occurrences. Through the United States Geological Survey (USGS), the United State's Government sponsored the National Uranium Resource Evaluation (NURE) program between 1975 and 1980, in the hope of discovering new economic sources of uranium. Stream-sediment and stream-water samples were collected throughout the nation and analyzed for a variety of

elements, including uranium and vanadium. In 1995, all of the NURE files were reformatted and added to either the national stream-sediment database or water-sample database, both of which are available online (Schweitzer, 2006). Within Coosa County there are 114 NURE data points for sediments, and 110 NURE data points for water samples; however, none of these data points are within the field area.

Neathery et al. (1976) discussed interpretations of aero-radioactivity maps that were generated by the Alabama Geological Survey and the USGS. They noted that the metavolcanics have a relatively low aero-radioactivity signature compared with the high-grade metamorphic rocks adjacent to the Hollins Line fault. Rocks producing the higher signature are graphitic schist and phyllite and garnet-bearing schist.

An unpublished report (Beg, 1980) on zones of anomalous radioactivity within the Piedmont mentions that shear zones containing oxidized dark-reddish brown to blackish-red clay may be associated with the anomalies. Average uranium content within the country rock was 25 ppm. Most uranium mineralization occurs within shear zones that are sub-parallel to the foliation of the country rock, allowing for mobilization of the uranium. Beg (1980) also commented that uranium occurrences within Clay County are in rocks of the Poe Bridge Mountain Group.

As previously mentioned, Cook et al. (1982) published maps and a report on uranium in Coosa and Clay Counties. Radiometric anomalies were initially identified by airborne surveys and followed up with ground radiometric surveys. Samples of stream sediment, saprolite and rock were collected and used to better define the uranium anomalies. In their study, surface anomaly threshold levels of 700 counts per second were found by using a scintillometer with a one cubic inch crystal. A threshold value of 2.1 ppm uranium in stream sediments was identified. Within rock samples, total uranium values

ranged from 2 to 613 ppm, with a threshold value of 267.3 ppm. Areas with anomalous radioactivity were recognized mainly within the rocks of the Higgins Ferry Group (Cook et al., 1982).

Private uranium mining corporations also have funded reconnaissance work in the area. In the 1970's, Amax Uranium Corporation and URANERZ U.S.A., Inc. studied the uranium anomalies in Coosa County with the hope of discovering one or more economic occurrences. Neither program was successful.

In 1979, the Drummond Company again prospected the area for possible economic deposits. The report resulting from this project indicates that the uranium is contained in one major lithologic unit, the Higgins Ferry Group, and is associated with anomalous molybdenum, copper, vanadium and barium. It was suggested that prior to regional metamorphism, the occurrences were similar to the sandstone-hosted deposits of the Colorado Plateau. Regional metamorphism and coincident deformation resulted in formation of the present uranium occurrences, none of which were found to be of economic-grade occurrences (Cook and Mallette, 1979).

Non-Uranium Research: Coosa County also has been the subject area for several Master's thesis investigations. Hicks (1981) mapped a portion of the Rockford Quadrangle, and Frinak (1984) mapped an adjacent part of the county; however, neither investigated the uranium contained in the Higgins Ferry Group. A Florida State University thesis by Mark Drummond (1986) described the igneous, metamorphic and structural history of the Alabama tin belt in Coosa County. Drummond's (1986) thesis did not focus on the uranium within the Higgins Ferry Group, but mentions the relationship between metasomatism and low amounts of uranium and thorium within the

trondhjemite of the Rockford Granite.

The field area of the current study is included within the general "Columbiana Area," which includes Chilton, Coosa and Clay Counties (Guthrie, 1994). Guthrie (1994) examined metamorphism and structure of rocks that transition from the foreland fold-thrust belt to those of the Talladega belt. He also discussed contacts between Mississippian to Pennsylvanian rocks and the underlying strata of the foreland fold-thrust belt.

Pallister and Thoenen (1948) presents information about the vanadium content of the green mica in graphite deposits of Coosa County. Samples of the mica were analyzed with each sample of graphite collected in his study, with the hope of generating a vanadium by-product when mining graphite. However, relatively low amounts of vanadium were recovered when the micas were processed (Pallister and Thoenen, 1948).

Uranium Deposits - A Brief Review

Uranium Deposits in Metamorphic Host Rocks: In general, uranium deposits found in metamorphic environments are either structurally controlled or linked to a local intrusion. Structurally controlled deposits are subdivided into vein or unconformity types. Intrusion-controlled deposits are subdivided into contact metasomatic or pegmatite/porphyry types (Elevatorski, 1979). Neither type conforms closely to regionally metamorphosed sedimentary-hosted deposits such as traditional 'roll front' types.

Structurally controlled uranium-vein deposits are classified either as granite related or non-granite related. Uranium minerals found associated with vein-type deposits are uraninite, coffinite and their alteration products. Common gangue minerals in vein-type

deposits are quartz, chalcedony, carbonates, fluorite and barite (Dahlkamp, 1993).

Granite-related deposits are either intragranitic, with veins in the granite, or perigranitic, with veins occurring near the igneous intrusion (Fig. 8). Intragranitic deposits are generally monometallic, with ore occurring as linear veins within fractured granite or as disseminated minerals throughout pipes within desilicifed granite. Perigranitic deposits can be mono- or polymetallic, with the latter commonly associated with cobalt, nickel, bismuth and silver minerals. Typically, the host rock is severely altered, up to widths of about two kilometers. Depth of ore emplacement can be up to 2,000 meters (Dahlkamp, 1993).

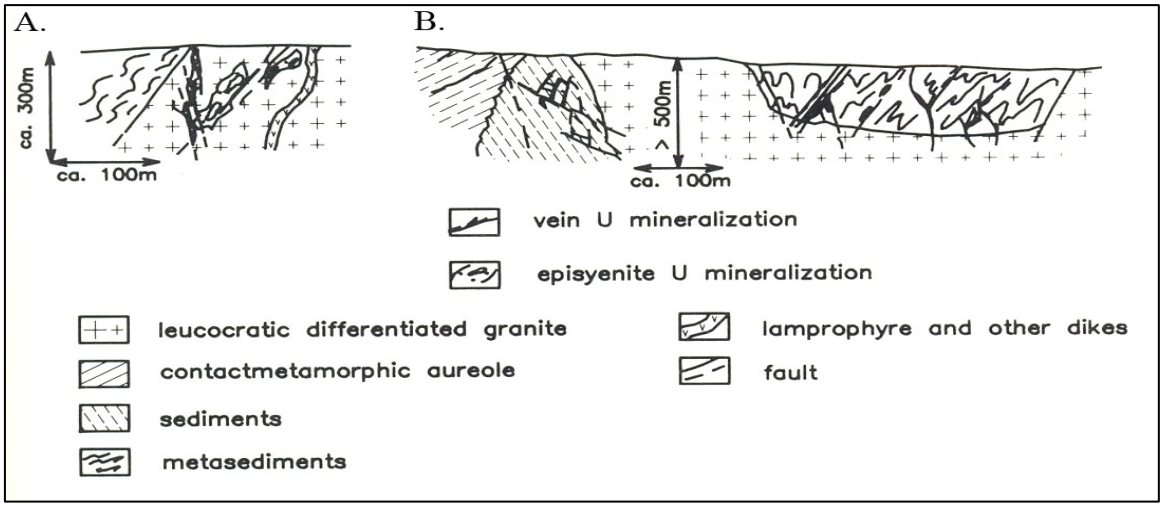

Fig. 8. A. Conceptualized model of intragranitic vein-type uranium deposit. B. Conceptualized model of perigranitic vein-type uranium deposit (*after* Dahlkamp, 1993).

Non-granitic vein-type deposits are commonly hosted by quartzite, schist or gneiss (Fig. 9). Deposits of this type may be folded and/or sheared, and may contain lenses and veinlets of mineralization (Elevatorski, 1979; Nash 1981; Dahlkamp, 1993). Ore grades in these deposits are moderate, on average between 0.2 and 0.45 percent, with ore forming at depths from 300-1,500 meters (Nash, 1981; Burns and Finch, 1999). The

mineralogy of the deposits can be simple, with uranium occurring as uraninite, or complex, with silver, cobalt, nickel, copper, gold, selenium and arsenic minerals (Nash, 1981).

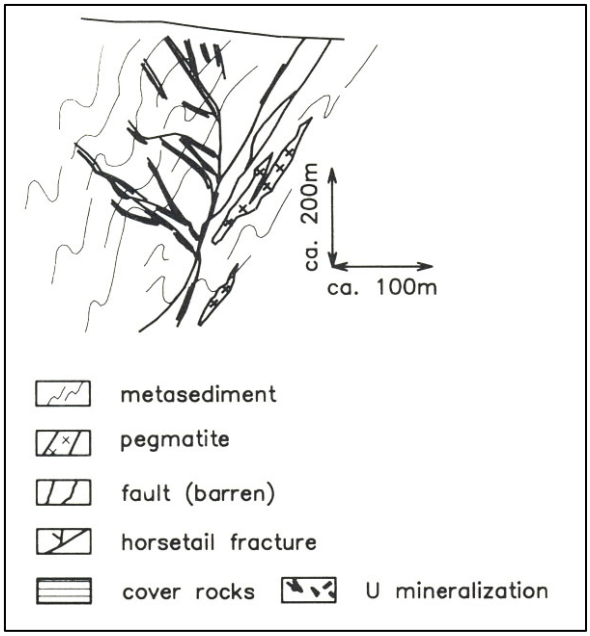

Fig. 9. Conceptualized model of non-granitic vein-type uranium deposit (*after* Dahlkamp, 1993).

During the 1970's, unconformity-type deposits were recognized within the intracratonic Athabasca Basin in Canada and the Pine Creek Geosyncline of Australia (Fig. 10). These deposits are hosted within Middle Proterozoic sandstones that are in contact with Lower Proterozoic rocks overlaying Achaean gneiss-granite complexes (Nash, 1981; Nash et al., 1981; Marmont, 1987; Ruzicka, 1993; McMillin, 1998). The basement rock of these deposits show lateritic weathering. Alternation around the mineralization is often seen within the basement rocks and post-unconformity rocks (International Atomic Energy Agency, 2009). Ore grades of these deposits are unusually high and can range from 1-10 percent (Gabelman, 1988). If the deposit is monometallic,

mineralization can occur below the unconformity in the basement rocks or above the basement rocks within sandstones. Polymetallic deposits occur at the unconformity between the sedimentary and basement rocks and contain varying amounts of nickel, cobalt, arsenic, lead, gold, platinum and copper (Ruzicka, 1993; International Atomic Energy Agency, 2009). Ore is commonly found within chloritized fault and fracture zones (Nash, 1981; Nash et al., 1981; Marmount, 1987; Gabelman, 1988; Ruzicka, 1993, McMillan, 1998). According to Nash (1981), most of the unconformity-type deposits occur in or near graphitic-mica schists, biotite-garnet schists and dolomitic-marble metamorphic sequences formed from marginal marine sedimentary rocks.

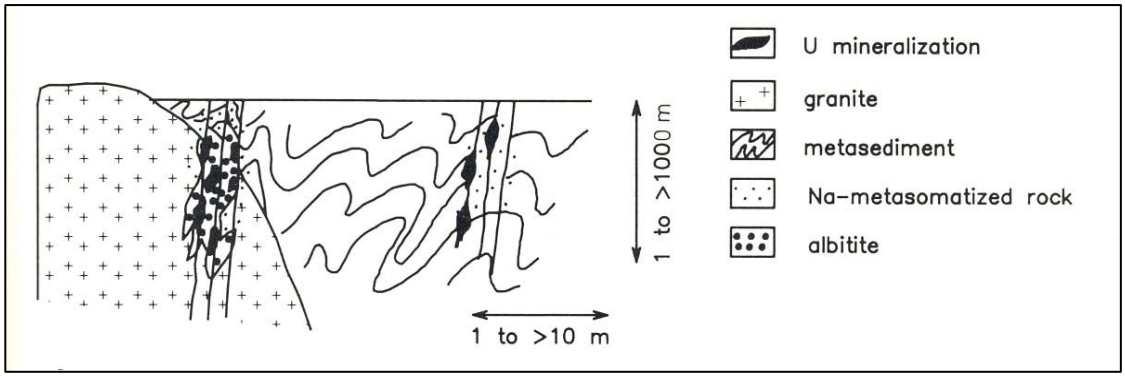

Fig. 10. Model of an unconformity-type uranium deposit (*after* Dahlkamp, 1993)

Uranium also can be deposited by metasomatic fluids during high-grade regional metamorphism that mobilizes the uranium into surrounding rocks (Fig. 11). Contact metasomatic and porphyry/pegmatites are associated with skarns, schists and hornsfels. These are commonly sheared and complexly folded (Elevatorski, 1979; Lentz, 1996). Uranium minerals within metasomatic deposits are uraninite, coffinite, uranothorianite, uranothorite and thorite. Associated minerals are allanite, monazite, zircon, apatite,

galena and magnetite. The uranium minerals generally are disseminated throughout the host rock and as fine veinlets (Dahlkamp, 1993).

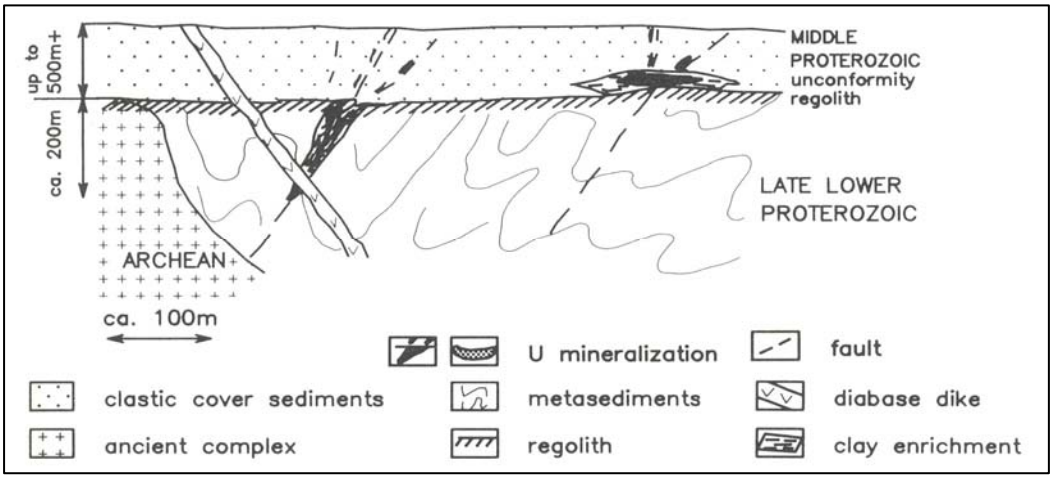

Fig. 11. Conceptualized model of a metasomatic uranium deposit (*after* Dahlkamp, 1993).

Igneous Uranium Deposits: Uranium is concentrated in some S-or I- type granites, usually as disseminated occurrences throughout the intrusion (Fig. 12). Occurrences containing muscovite and biotite are termed 'two mica granites' and are generally albitized (Simpson et al., 1979; Dahlkamp, 1993). Epigenetic uranium deposits are younger than the pluton in which they were formed (Nash, 1981). Uraninite is the typical ore mineral found within granitic uranium deposits (Dahlkamp, 1993).

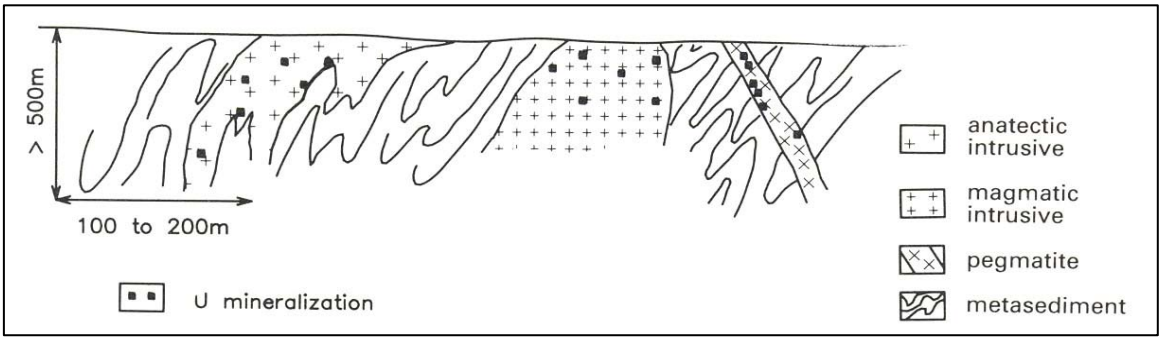

Fig. 12. Conceptualized model of an intrusion-related uranium deposit (*after* Dahlkamp, 1993).

Sedimentary Uranium Deposits: Sedimentary uranium deposits are commonly hosted in continental fluvial and mixed fluvial marine sandstones that are interbedded with less permeable horizons (Fig. 13). They are usually in porous, medium- to coarse-grained arkosic and quartzose sandstones that contain uranium and often vanadium. The sandstones may contain carbonaceous material, hydrocarbons, sulfides and volcanic ash. Ages range from the Paleozoic to Tertiary (Finch, 1967; DeVoto, 1978; Adams, 1981; Dahlkamp, 1993; International Atomic Energy Agency, 2009). Ground water geochemistry is a predominant factor in depositional history. As uranium is soluble in the hexavalent state, the groundwater must be oxygenated just enough to keep the uranium in solution, and then be reduced to a tetravalent state so that the uranium can be precipitated. To reduce the uranium to a tetravalent state, there must be a substance to reduce the ion. These substances include, but are not limited to carbonaceous material, sulfides, hydrocarbons, ferro-magnesium minerals and, in some cases, bacteria (Nash et al., 1981; Tilsley, 1981).

Sandstone hosted deposits are classified by the shape of the deposit. Roll-front deposits are crescent shaped and are convex in the down-gradient direction. This 'C' shape can be seen in cross-section. Tabular sandstone hosted deposits are irregularly shaped lenticular masses. The mineralized portions are often parallel to the depositional trend (Finch, 1967; DeVoto, 1978; Adams, 1981; Nash et al., 1981; Dahlkamp, 1993; 2009).

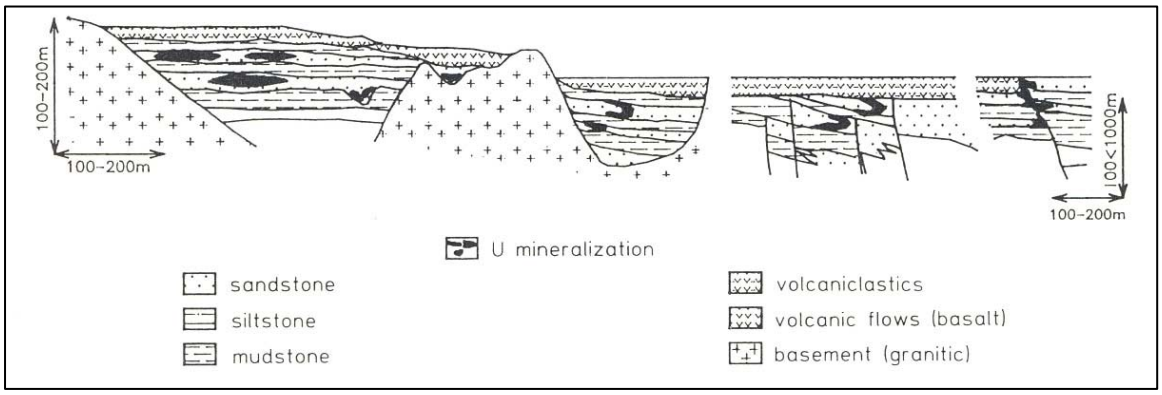

Fig. 13. Conceptualized model of a tabular sandstone-type uranium deposit (left), and conceptualized model of a roll-front-type uranium deposit (right) (*after* Dahlkamp, 1993).

OBJECTIVES

The overall goal of this thesis is to use data derived from this and prior investigations to achieve a comprehensive understanding of the uranium occurrences within Coosa County. A database of new and old information was created within Microsoft® Excel®, and a compiled dataset was entered into ArcMap™. Using ArcMap™, maps were produced to show relationships between elemental abundances.

An important aspect of the present investigation that has not been examined in detail before is how the uranium within the rocks relates to the other elements, specifically vanadium and barium. Geochemical data were evaluated to explore elemental relationships. Pearson correlation matrices and graphs were used to evaluate various geochemical and mineralogical relationships. These data were also used to evaluate what minerals within the rocks host the uranium, barium and vanadium.

No depositional models have been proposed for the occurrences in this study. In order to develop a depositional model for these occurrences, they were compared to known deposit types. Using the known deposit types, there can be a better understanding of the Coosa County occurrences, and one or more depositional models can be put forward. After the depositional models are proposed, information from regional geology is used to predict how the deposits may have attained their current form and distribution.

METHODS

Fieldwork

Fieldwork was conducted between June and September of 2007. Roads within the area were first driven to become acquainted with the geology of the area. Rock samples were collected near and off the roads and along streams; sample sizes were about seven by four by ten centimeters. Larger samples were collected if the rock contained the green mica. Two sediment samples in an area of anomalous radiation were also collected. Sample sites were logged using a Garmin Rino 120 GPS receiver. Effort was made to collect rocks within iron-stained fracture zones. A scintillometer was used to record background radiation within the study area. Strikes and dips of foliation at selected outcrops were measured using a Brunton Compass.

Geochemistry

Whole-rock and trace-element analyses were performed on rock samples from the study area. Samples were initially selected from throughout the study area to get a broad geochemical overview of the area. Sample sites with high concentrations of uranium, vanadium and barium were noted, and a second round of samples from near those areas were analyzed.

Analyses were performed by ALS Chemex in Vancouver, British Columbia, Canada. Samples were first prepared by taking a split from the samples and pulverizing the split to

> 85 percent passing a 75-micron screen. Samples for whole-rock analyses were then fused into glass disks by using lithium metaborate and were analyzed using x-ray fluorescence. Trace-element analyses also were done using fused lithium metaborate disks but using Inductively Coupled Plasma Mass Spectrometry (ICP-MS). Elements analyzed and detection ranges for the whole-rock and trace-element analyses are listed in Tables 1 and 2. Complete analytical results can be found on the accompanying CD and in the appendix.

Rocks containing anomalously green mica were crushed and the micas were handpicked. These mica grains were then crushed to < 200 mesh, weighed, and sent to ALS Chemex in Vancouver for trace-element analysis. The samples were again fused into glass disks by lithium metaborate fusion and were analyzed using Inductively Coupled Plasma Mass Spectrometry (ICP-MS). Elements analyzed and detection ranges were the same as that used on the trace-element analyses of the rock samples (Table 2).

Petrographic Analysis

Idaho Petrographics, in Grangeville, Idaho, prepared polished and unpolished thin sections of rock samples. Petrographic observations were made on standard one- by two-inch covered thin sections. Descriptions were written with emphasis on metamorphic mineral assemblages and paragenesis.

Table 1. Detection Range for Whole-Rock Analyses

	Detection Range		**Detection Range**
SiO_2	.01-100%	Cr_2O_3	.01-100%
Al_2O_3	.01-100%	TiO_2	.01-100%
Fe_2O_3	.01-100%	MnO	.01-100%
CaO	.01-100%	P_2O_5	.01-100%
MgO	.01-100%	SrO	.01-100%
Na_2O	.01-100%	BaO	.01-100%
K_2O	.01-100%	LOI	.01-100%

Table 2. Detection Range for Trace-Element Analyses

	Detection Range		**Detection Range**
Ag	1-1,000 ppm	Ni	5-10,000 ppm
Ba	0.5-10,000 ppm	Pb	5-10,000 ppm
Ce	0.5-10,000 ppm	Pr	0.03-1,000 ppm
Co	0.5-10,000 ppm	Rb	0.2-10,000 ppm
Cr	10-10,000 ppm	Sm	0.03-1,000 ppm
Cs	0.01-10,000 ppm	Sn	1-10,000 ppm
Cu	5-10,000 ppm	Sr	0.1-10,000 ppm
Dy	0.05-1,000 ppm	Ta	0.1-10,000 ppm
Er	0.03-1,000 ppm	Tb	0.01-1,000 ppm
Eu	0.03-1,000 ppm	Th	0.05-1,000 ppm
Ga	0.1-1,000 ppm	Tl	0.5-1,000 ppm
Gd	0.05-1,000 ppm	Tm	0.01-1,000 ppm
Hf	0.2-10,000 ppm	U	0.5-1,000 ppm
Ho	0.01-1,000 ppm	V	0.5-10,000 ppm
La	0.5-10,000 ppm	W	1-10,000 ppm
Lu	0.01-10,000 ppm	Y	0.5-10,000 ppm
Mo	2-10,000 ppm	Yb	0.03-1,000 ppm
Nb	0.2-10,000 ppm	Zn	5-10,000 ppm
Nd	0.1-10,000 ppm	Zr	0.5-10,000 ppm

Microprobe Analysis

Polished thin sections containing the anomalously green mica were carbon coated and analyzed using a JOEL 8600 electron microprobe at the University of Georgia's Geology Department, in Athens, Georgia. Grains within four thin sections were chosen for analysis. Photomicrographs were taken of the grains to locate analytical target areas. Target areas were within micas exhibiting various stages of apparent alteration. The micas were analyzed for silica, titanium, aluminum, magnesium, iron, calcium, manganese, potassium, sodium, chromium, barium, copper, uranium and vanadium.

The microprobe was operated at an accelerating voltage of 15KV and a beam current of 15nA. Quantitative analyses were performed using Wavelength Dispersive System (WDS) analysis. Natural and synthetic mineral standards were used. Results were calculated using Armstrong's phi (rho Z) matrix correlation (Armstrong, 1988). Quantitative analyses of silicate and oxide materials were performed by comparing Monte Carlo, ZAF, and phi (rho Z) correction procedures (Goldstein et al., 1975). The stage and spectrometers were automated with Geller Microanalytical Laboratory's dQUANT software.

Data Synthesis

Possible anomalous threshold values were calculated as the mean plus one and the mean plus two standard deviations of particular data populations. Graphs showing correlations between selected elements and Pearson Correlation Matrices were produced for complete data sets using Microsoft Excel®. To produce the correlations, data below detection limits were input as one-half the detection limit and data above detection limits

were input as the upper detection limit, as is standard practice. Correlations with values above 0.5 were considered statistically meaningful.

Data collected from this investigation, including sample-location coordinates, were first entered into Excel®, saved as a DBF-IV file, and added to ArcMap as a dataset. Data from previous investigations were added to ArcMap by digitizing layers on a topographic base map of the Flag Mountain Quadrangle. Strike and dip of foliation planes collected during this investigation were added to the map using an Excel DBF-IV file, which was converted into a shapefile through ArcCatalogue. Once geochemical data were added, maps were created and used to characterize the Coosa County occurrences.

The data have been collected into a comprehensive, computerized set, which is contained on the accompanying CD. Included on the CD are Pearson Correlation Matrices and the geochemical datasets. All maps produced from these data are also on the accompanying CD.

RESULTS

Geology of the Area

In order of increasing abundance, rocks observed during this investigation were poorly indurated amphibolites, quartzites and quartz-muscovite-graphite schists that locally contain anomalous green mica. Contacts between the schist and quartzite are gradational. Quartzite and schist underlie the main ridge within the field area. This ridge strikes to the northeast, parallel with the regional foliation. Foliation due to compositional mineral banding was observed. In general, outcrops of bedrock are smaller than 3.5 meters across. Due to sub-tropical weathering, most exposures are saprolitic.

Red soils are derived from schist and quartzite helping to distinguish their presence; amphibolites produce a brown soil where weathered (Fig. 14). Generally, the amphibolite outcrops are no more than 1.5 meters across. While most of the red soils are to the southeast of the main ridge, there is an inferred northwest trend of that soil unit. Movement of the red soils to their current location southeast of the ridge could be due to weathering and slumping down the southeastern slope.

Schists and quartzites contain megascopic quartz, graphite, muscovite, pyrite, iron oxides (Fig. 15), and locally, green secondary copper minerals. Graphite occurs in most of the rocks and was especially prevalent in those containing the anomalously green mica found on the prominent ridge within the field area. Pyrite, although a common accessory mineral, was found in relative abundance in two locations (32° 56.579, 86° 18.673 and

32° 57.071, 86° 18.857). Secondary copper minerals were observed in one location, about 100 meters east of the main ridge (32° 56.981, 86° 18.459) (Fig. 16).

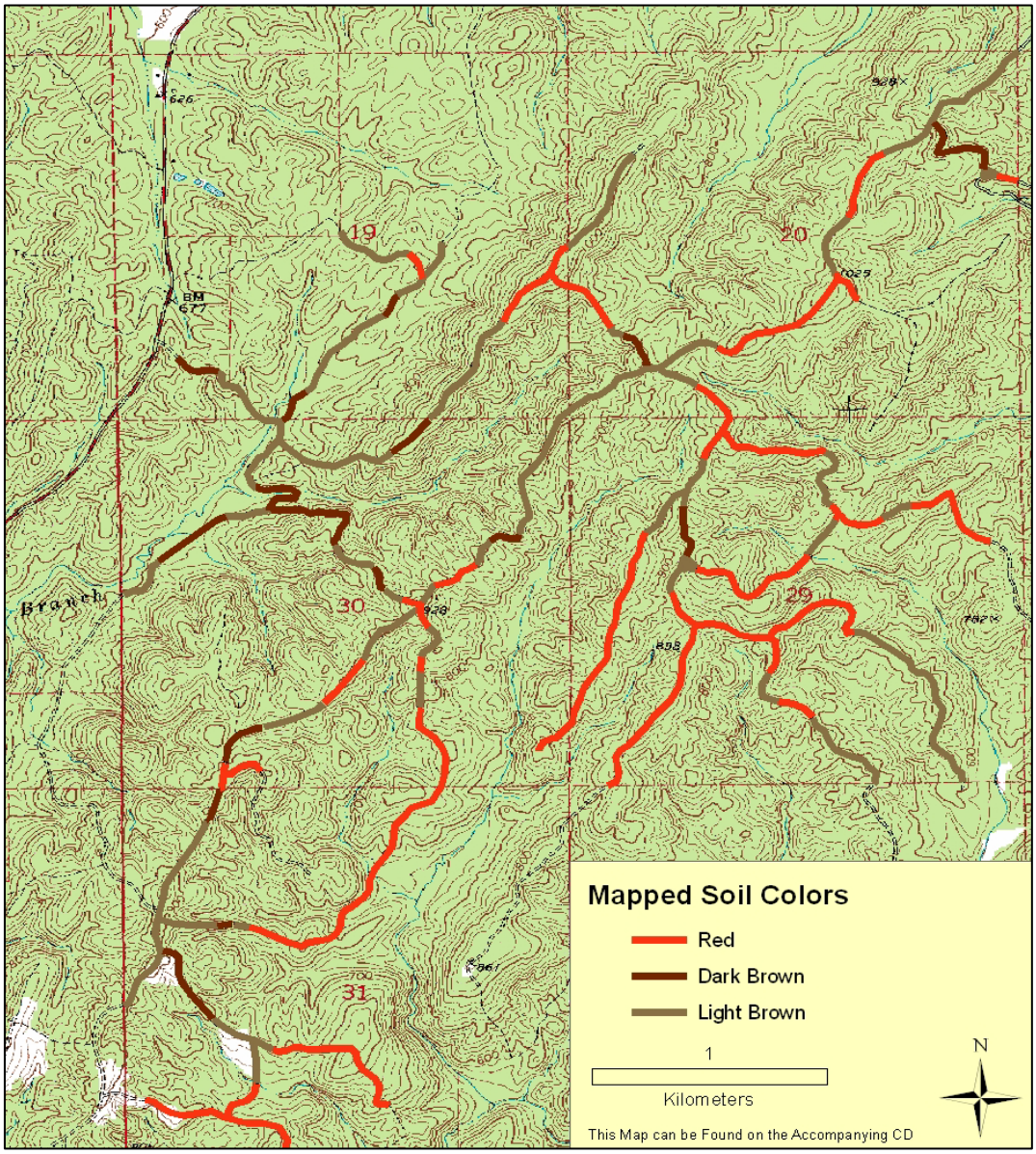

Fig. 14. Distribution of dominant soil units observed along field transects within sections 19, 20, 29, 30, 31 T. 23 N., R. 18 E. on the Flag Mountain 7 ½' Topographic Quadrangle (*modified from* United States Geological Survey, 1971).

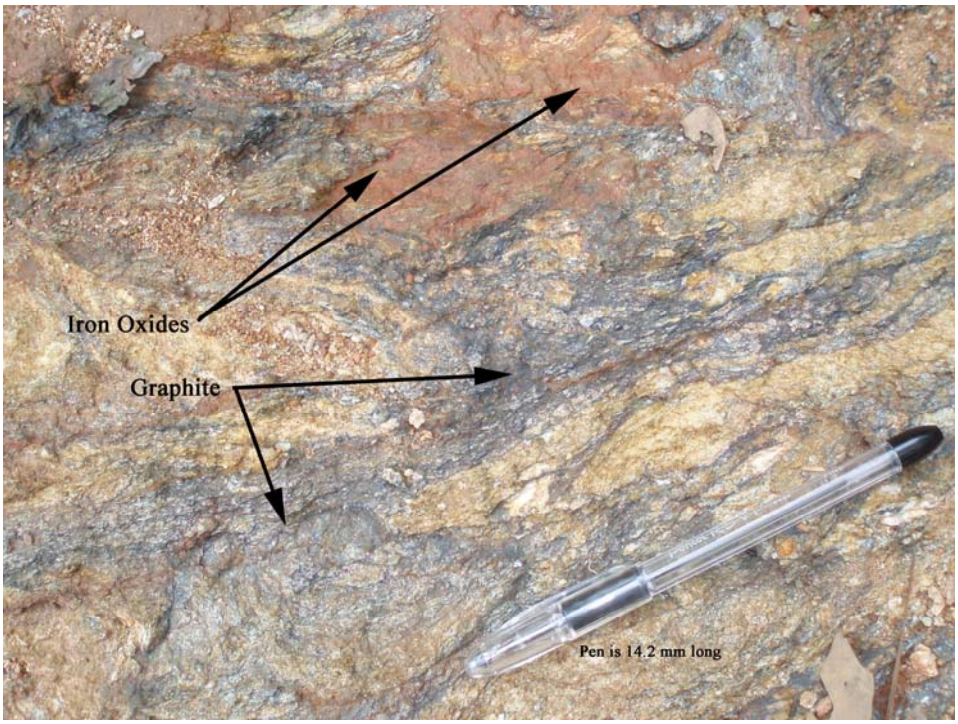

Fig. 15. Outcrop of a graphitic schist containing iron oxides.

Fig. 16. Aerial photograph showing the location of secondary copper minerals within the field area.

General structural observations and a total of 38 strike and dip measurements were entered into ArcMap to produce a foliation map (Fig. 17). In general, strike is to the northeast with southeasterly dips varying from 18 to 83 degrees (Fig. 18). Relatively small shear zones, usually no more than 0.67 m wide, occur in the northwest section of the field area within section 19. Fault gouge was found within some brittle shear zones.

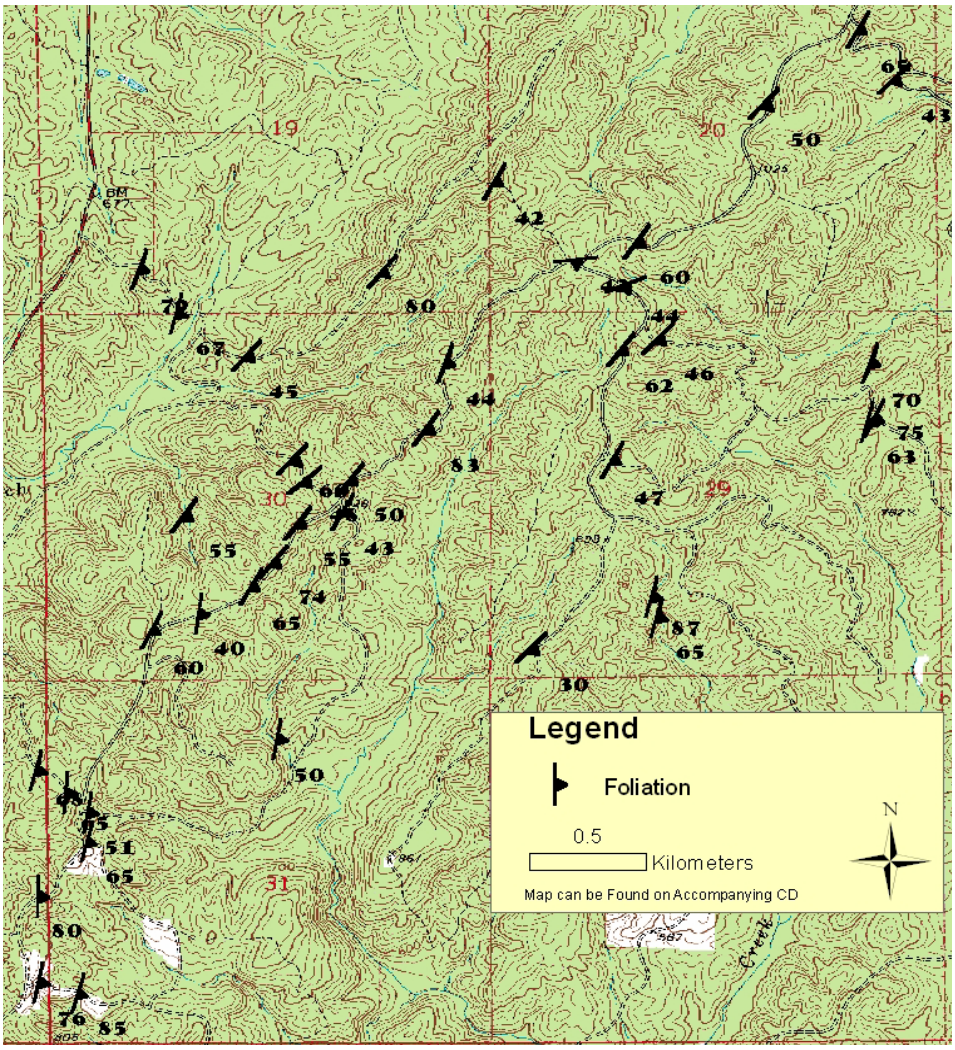

Fig. 17. Strike and dip of foliation within sections 19, 20, 29, 30, and 31, T. 23 N., R. 18 E. of the Flag Mountain 7 ½' Topographic Quadrangle (m*odified from* United States Geological Survey, 1971).

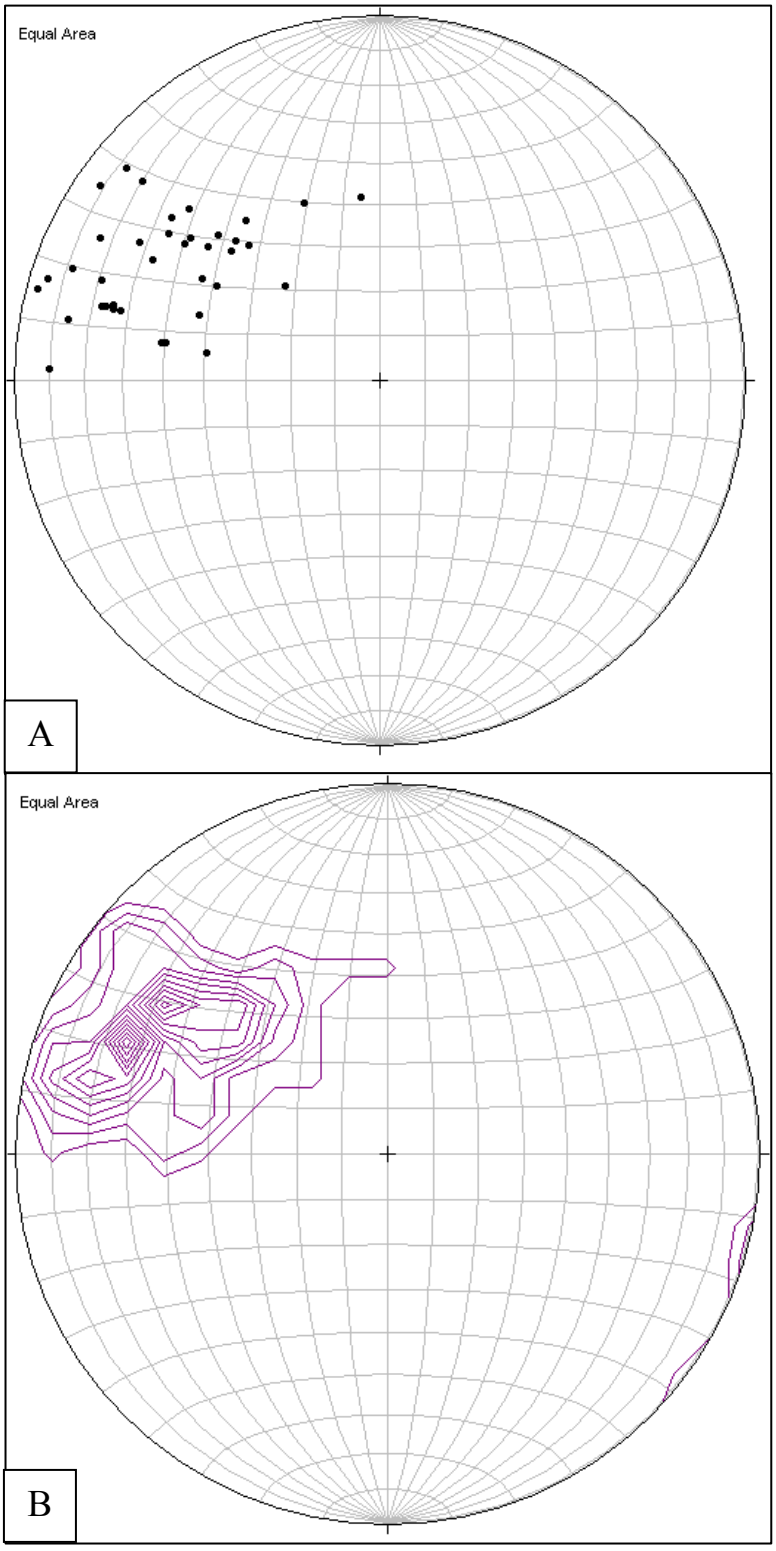

Fig. 18. Lower hemisphere stereographic projections of poles to foliation planes (n=38) (A). B shows the same data but is contoured, with a contour density of 2% per 1% area.

Petrography

Quartz-muscovite-graphite schist of the Higgins Ferry Group is the dominant rock type in the area. Most thin sections have a well-developed foliation produced by mineral segregation and parallel alignment. Textures include intragranular- interlobate, seriate-polygonal, inequigranular-polygonal and seriate - interlobate. Average grain sizes of quartz, graphite and muscovite are between 0.25-2.00 mm, 0.25-0.75 mm, and 0.5-4.0 mm, respectively. Photomicrographs of representative rocks are in Figure 19. Figures 20 and 21 compare examples of the most and least schistose rocks, mostly separated into dark bands of mica and graphite and light quartz ribbons.

Compositional foliation is developed within the schistose rocks. Graphite and muscovite grains are aligned parallel to one another, creating foliation by mineral alignment. Tabular graphite grains generally lie between quartz grains. Some graphite grains are included within muscovite. Quartz forms ribbons within the rock containing prominent subgrains occurring within segregated mineral bands parallel with those dominated by micas. Generally quartz within these bands has subparallel extinction.

Prograde metamorphic assemblages contain variable amounts of quartz, muscovite, graphite, garnet, plagioclase and sillimanite. Retrograde assemblages are characterized by sericitic mica and calcite. Sillimanite occurs either as ‘fibrolite’ masses or as larger, individual, acicular grains. Neither individual grains nor masses of fibrolite were larger than 0.50 mm. Opaque minerals within the thin sections were determined by oblique illumination to be graphite (Fig. 22) and pyrite (Fig. 23). Albite twinning is characteristic in plagioclase (Fig. 24).

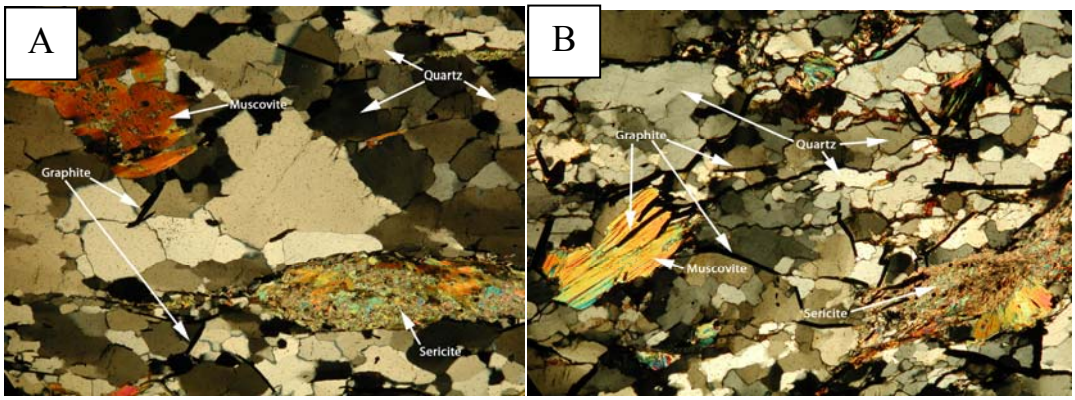

Fig. 19. Typical views of quartz-muscovite-graphite schist. Samples CC20E (A) and CC219 (B). Crossed polars; fields of view are 3 mm wide.

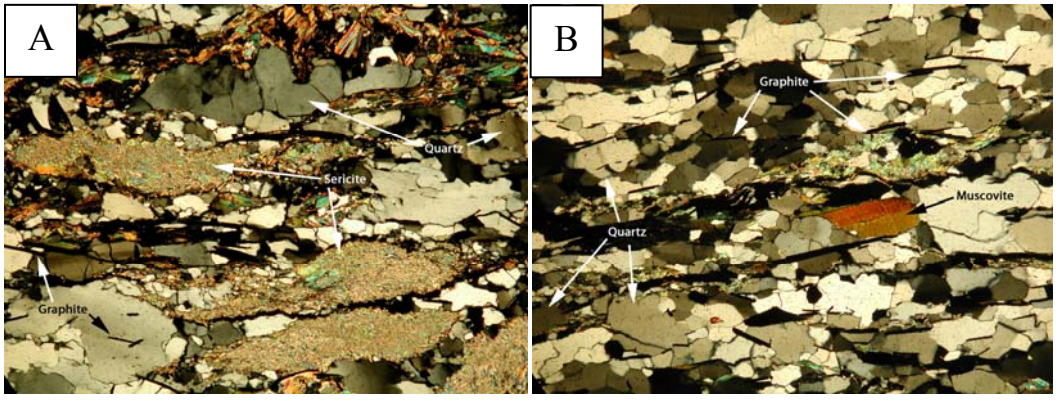

Fig. 20. Well-developed foliation within quartz-muscovite-graphite schist. Samples CC20E (A) and CC169 (B) ; crossed polars; fields of view are 3 mm wide.

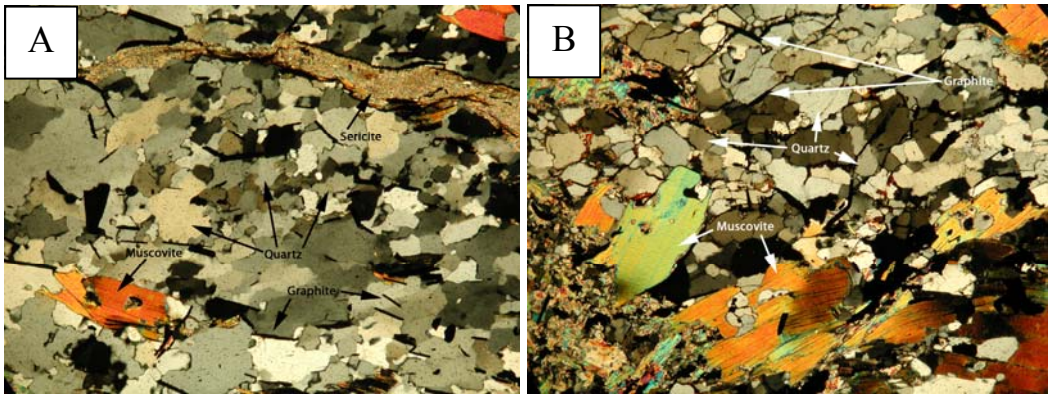

Fig. 21. Weakly developed foliation within graphite-rich quartzite. Samples CC180 (A) CC219 (B). Crossed polars; fields of view are 3 mm.

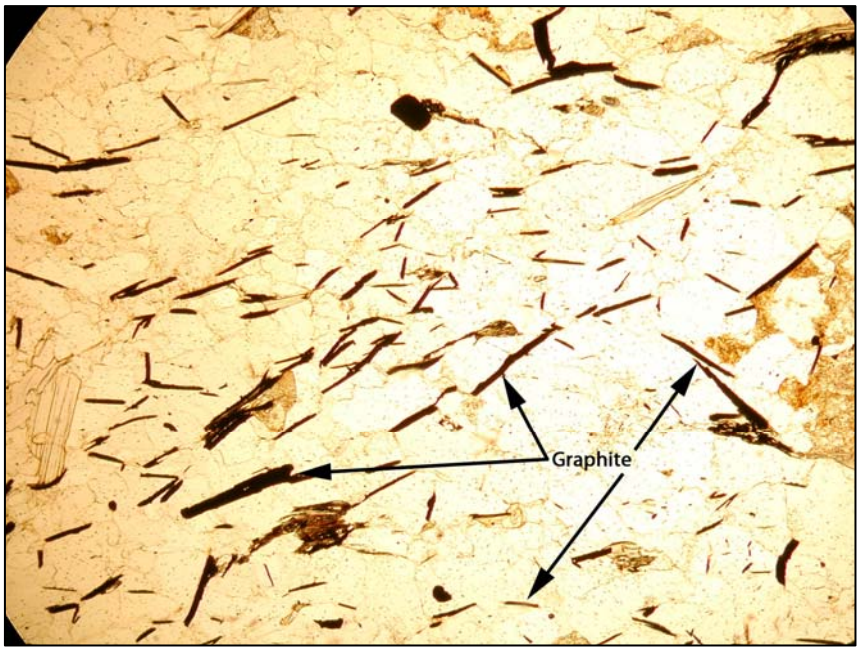

Fig. 22. Tabular graphite grains within a quartz-muscovite-graphite schist. Sample CC21, plane polarized light, field of view is 3 mm wide.

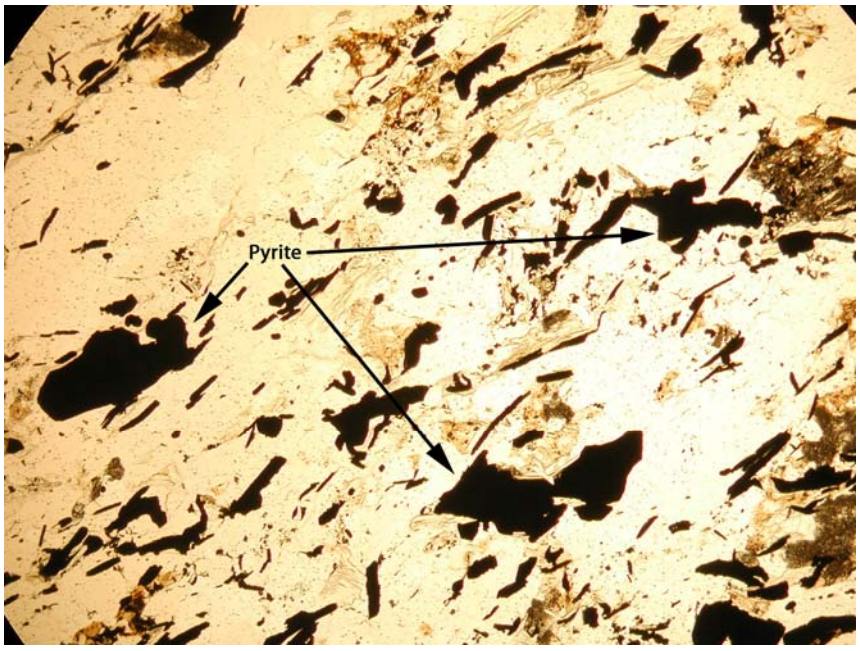

Fig. 23. Globular pyrite grains within a quartz-muscovite-graphite schist. Sample CC177, plane polarized light, field of view is 3 mm wide.

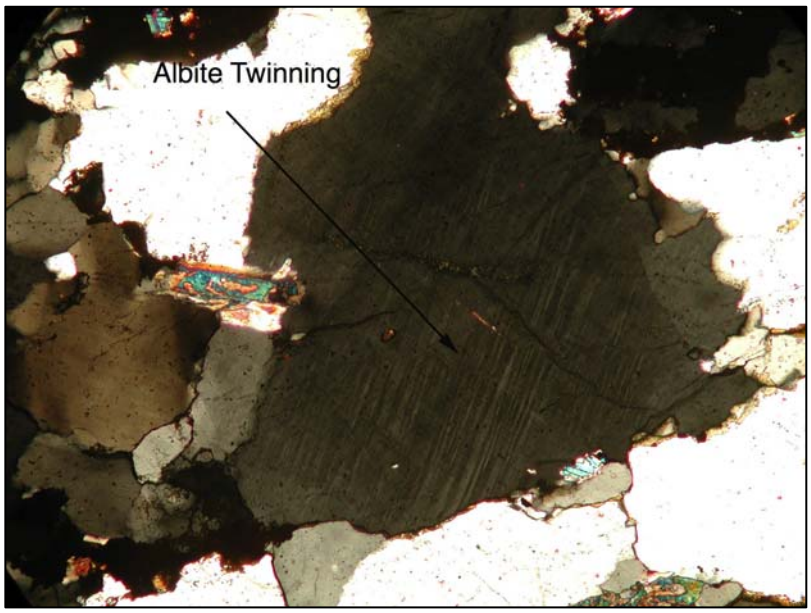

Fig. 24. Albite twins within plagioclase contained in a quartz-muscovite-graphite schist. Sample CC50C, crossed polars, field of view is 1.5 mm wide.

Alteration of minerals observed in thin sections is likely due to retrograde metamorphism. Sericitic alteration of muscovite, plagioclase and sillimanite can be seen in thin section (Figs. 25 and 26). In general, most of the sericite occurs within or around larger grains of prograde muscovite. Sericitic masses commonly preserve the original shape of the muscovite grains. Garnets in two thin sections are altered or weathered to iron oxides along fractures (Fig. 27).

Fractures interpreted to be the result of radiation damage were seen within the prograde and retrograde micas. Pleochroic halos indicating radiation damage were seen in muscovite and biotite (Fig. 28) that contain monazite and/or zircon. Sample CC219 contains two types of fracturing; internal fracturing is interpreted as radiation damage, and fractures surrounding the mass are due to volume change during alteration (Fig. 29).

Fig. 25. Sericitic alteration of muscovite fish in a quartz-muscovite-graphite schist. Sample CC66; crossed polars; field of view is 3 mm wide.

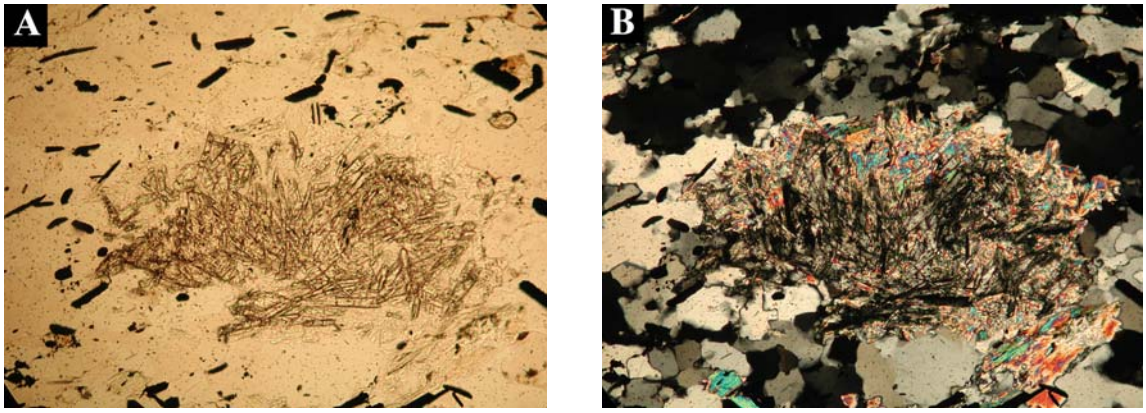

Fig. 26. Sericitic alteration of sillimanite within quartz-muscovite-graphite schist. Sample CC177; plane polarized light (A) and crossed polars (B); fields of view are 1.5 mm wide.

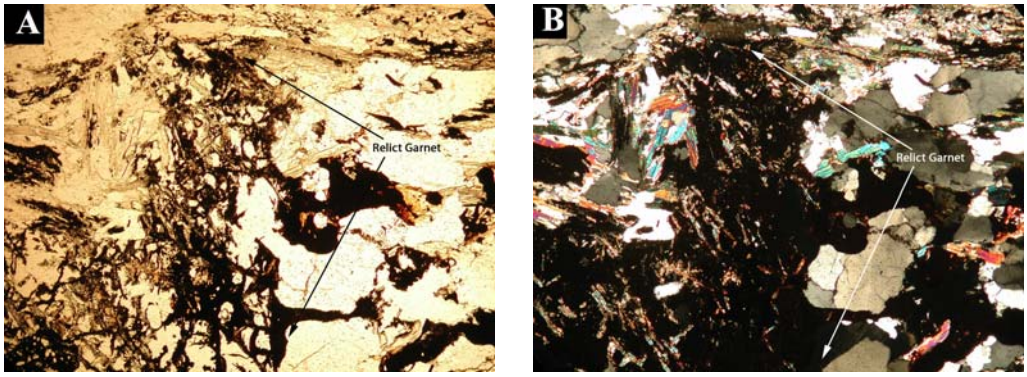

Fig. 27. Garnet within quartz-muscovite-graphite-garnet schist altered/weathered to iron oxide viewed in plane polarized light (A) and crossed polars (B). CC50C; field of view is 3 mm wide.

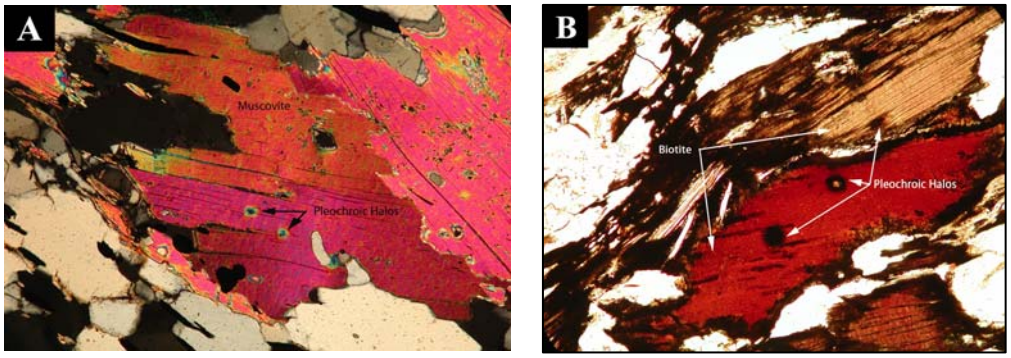

Fig. 28. Pleochroic halos within muscovite (A) and biotite (B) of quartz-muscovite-graphite schist and quartz-biotite-graphite schist, respectively. Photomicrograph A sample CC20E; crossed polarized light. Photomicrograph B sample CC54A; crossed polars; fields of view are 1.5 mm wide.

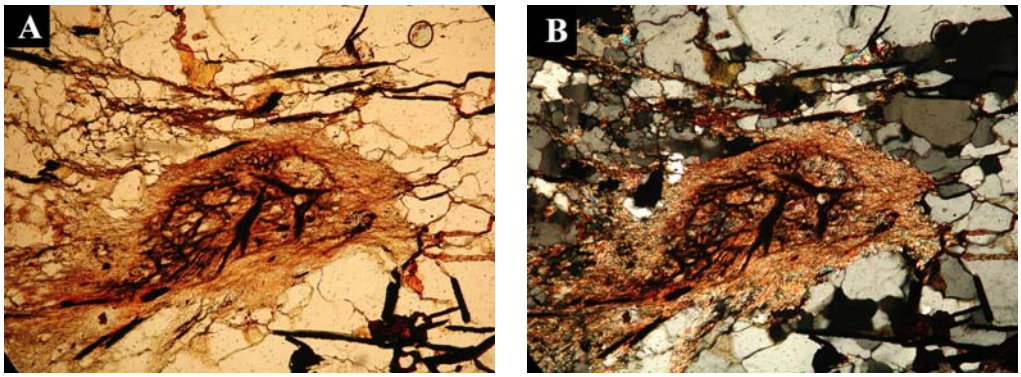

Fig. 29. A mass of altered sericite exhibiting anomalous fracturing within a quartz-muscovite-graphite schist. The fractures inside sericite may be due to radiation damage. Sample CC219; photomicrograph A plane polarized light; photomicrograph B crossed polars; fields of view are 1.5 mm wide.

Microstructures observed within the thin sections include kink bands and undulose extinction in muscovite, biotite and quartz (Fig. 30). Dextral movement is indicated by mica fish, most of which are completely replaced by sericite (Fig. 31). These microstructures help confirm the presence of shear zones, though not specifically mapped, throughout the field area.

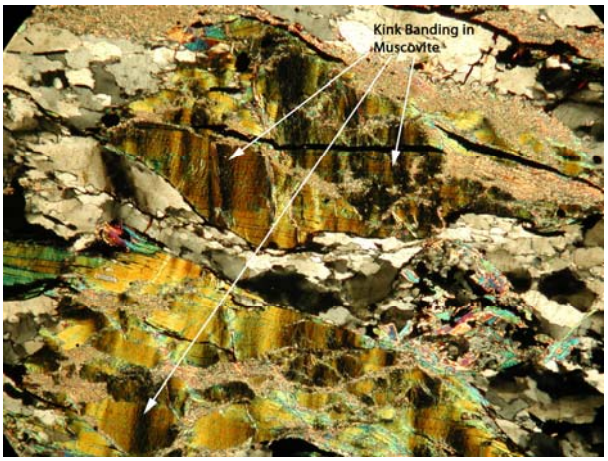

Fig. 30. Kink banding causing undulose extinction in muscovite contained within quartz-muscovite-graphite schist. Sample CC66, crossed polars, field of view is 1.5 mm wide.

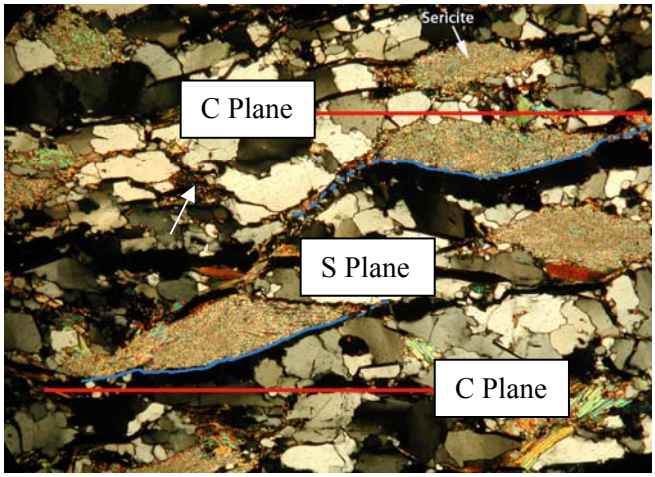

Fig. 31. Mica fish indicating tops-to-the-right dextral shear sense indicators (C and S planes are outlined) contained within non-orientated sample of quartz-muscovite-graphite schist. Sample CC169, crossed polars; field of view is 3 mm wide.

Geochemical Analysis of Rocks and Sediment

Thirty-four rock samples and two sediment samples were selected for whole-rock and trace-element analyses. Table 3 contains data from the whole-rock and trace-element analyses; table 4 contains statistical data for the samples. Complete geochemical data are appended and can be found on the accompanying CD.

Whole-rock data reflect the siliceous nature of the samples; the mean silica content is 71.54 percent and the lowest silica content is 28.80 percent. Mean aluminum oxide, potassium oxide and sodium oxide contents are 9.07, 1.80 and 0.23 percent, respectively. The maximum values determined for aluminum oxide, potassium oxide and silica oxide are 23.30, 4.81 and 89.40 percent, respectively.

A Pearson correlation matrix was produced using the total geochemical dataset (accompanying CD). Only correlations above 0.5 (r) were considered significant. Uranium correlated positively with sulfur (0.52). Barium correlated positively with molybdenum (0.67) and thallium (0.51). However, uranium correlates only weakly at 0.32 and 0.17 with barium and carbon, respectively. Uranium has a weak negative correlation with vanadium (-0.12). Scatter plots indicate a positive linear correlation between uranium and barium (Fig. 32), a weak negative correlation between uranium and vanadium (Fig. 33), and a positive correlation between uranium and carbon (Fig. 34). Vanadium did not correlate strongly with any elements; however, it did positively correlate weakly at values of 0.28, 0.22, 0.26, and 0.19 with carbon, chromium, molybdenum, and zinc, respectively. The carbon-vanadium correlation is consistent with the presence of the anomalously green mica in rocks that also contain graphite, as described by Pallister and Thoenen, (1948).

Table 3. Whole-Rock and Trace-Element Rock Sample Data

Sample Number	Ba	U	V
CC11	>10,000.00* ppm	4.96 ppm	191.00 ppm
CC20A	2,713.09 ppm	3.63 ppm	883.00 ppm
CC20E	2,518.52 ppm	2.98 ppm	959.00 ppm
CC21	3,047.23 ppm	4.10 ppm	1,030.00 ppm
CC34A	3,022.23 ppm	10.10 ppm	242.00 ppm
CC43A	1,052.41 ppm	3.59 ppm	124.00 ppm
CC43B	2,169.39 ppm	9.16 ppm	17.00 ppm
CC45	2,628.52 ppm	3.24 ppm	466.00 ppm
CC48	728.27 ppm	3.64 ppm	183.00 ppm
CC50A	2,061.82 ppm	3.18 ppm	1,180.00 ppm
CC50C	6,513.60 ppm	4.67 ppm	134.00 ppm
CC54A	1,930.25 ppm	2.82 ppm	182.00 ppm
CC54B	1,541.11 ppm	3.19 ppm	177.00 ppm
CC59	>10,000.00* ppm	3.91 ppm	315.00 ppm
CC66	2,104.82 ppm	8.45 ppm	338.00 ppm
CC73C	5,675.32 ppm	4.21 ppm	348.00 ppm
CC77	1,747.68 ppm	20.60 ppm	497.00 ppm
CC78	5,755.32 ppm	17.55 ppm	751.00 ppm
CC83	>10,000.00* ppm	31.70 ppm	145.00 ppm
CC84	559.70 ppm	2.95 ppm	86.00 ppm
CC90	2,693.09 ppm	9.70 ppm	140.00 ppm
CC95	5,466.19 ppm	7.10 ppm	223.00 ppm
CC110	2,289.39 ppm	7.94 ppm	1,010.00 ppm
CC124	8,857.98 ppm	4.43 ppm	195.00 ppm
CC169	3,142.23 ppm	3.54 ppm	847.00 ppm
CC173	685.27 ppm	0.41 ppm	294.00 ppm
CC176A	4,049.64 ppm	10.05 ppm	231.00 ppm
CC177	5,207.05 ppm	21.30 ppm	322.00 ppm
CC178	6,214.03 ppm	4.81 ppm	479.00 ppm
CC180	2,418.96 ppm	5.43 ppm	859.00 ppm
CC186	5,166.62 ppm	9.87 ppm	910.00 ppm
CC191	5,665.75 ppm	6.82 ppm	190.00 ppm
CC207	3,241.80 ppm	10.80 ppm	558.00 ppm
CC219	3,900.07 ppm	4.47 ppm	1,200.00 ppm

*10,000 ppm is the upper detection limit

Table 4. Statistical Data for Whole-Rock and Trace-Element Analyses of Rock Samples

	Barium	Uranium	Vanadium
Minimum Value	559.70 ppm	0.41 ppm	17.00 ppm
Maximum Value	>10,000* ppm	31.70 ppm	1,200.00 ppm
Median	3,034.73 ppm	4.74 ppm	318.50 ppm
Mean	3,963.75 ppm	7.51 ppm	461.94 ppm
Standard Deviation	2,701.16 ppm	6.51 ppm	356.18 ppm
1-Sigma Threshold	6,664.90 ppm	14.02 ppm	818.12 ppm
2-Sigma Threshold	8,366.06 ppm	20.52 ppm	1,174.29 ppm

*10,000 ppm is the upper detection limit

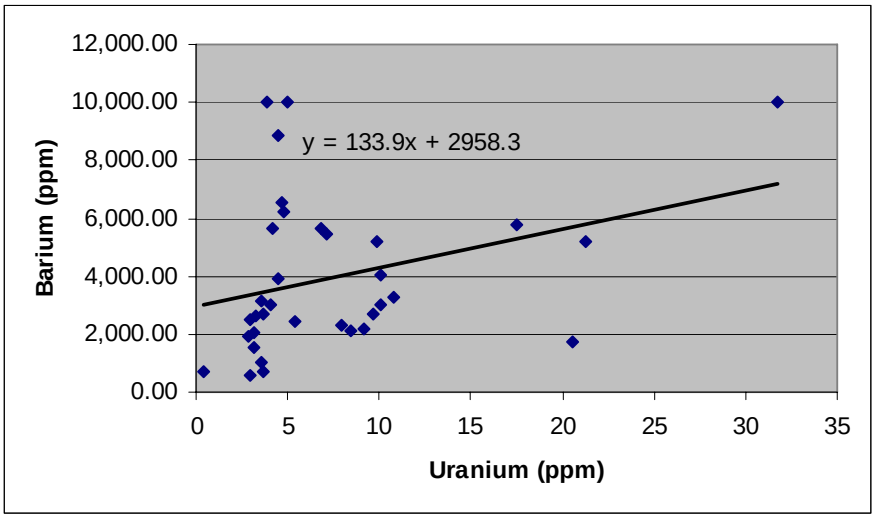

Fig. 32. Uranium and barium correlation within rock samples.

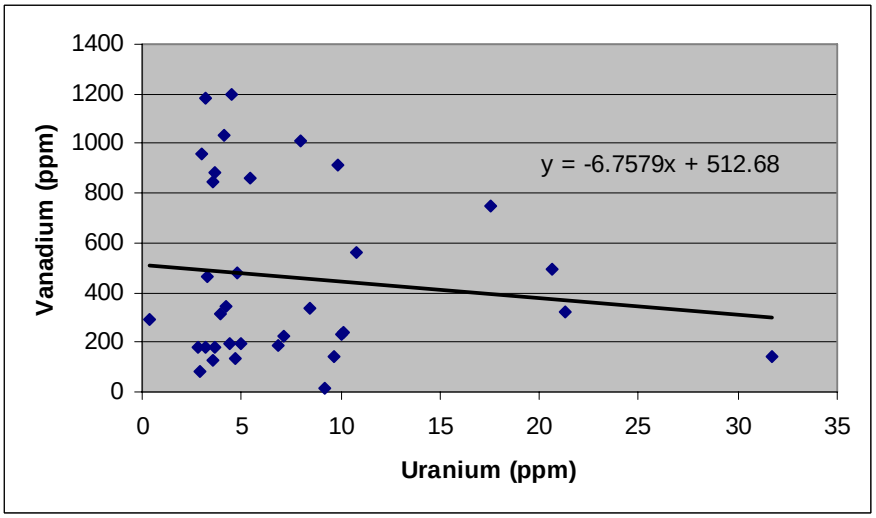

Fig. 33. Uranium and vanadium correlation within rock samples.

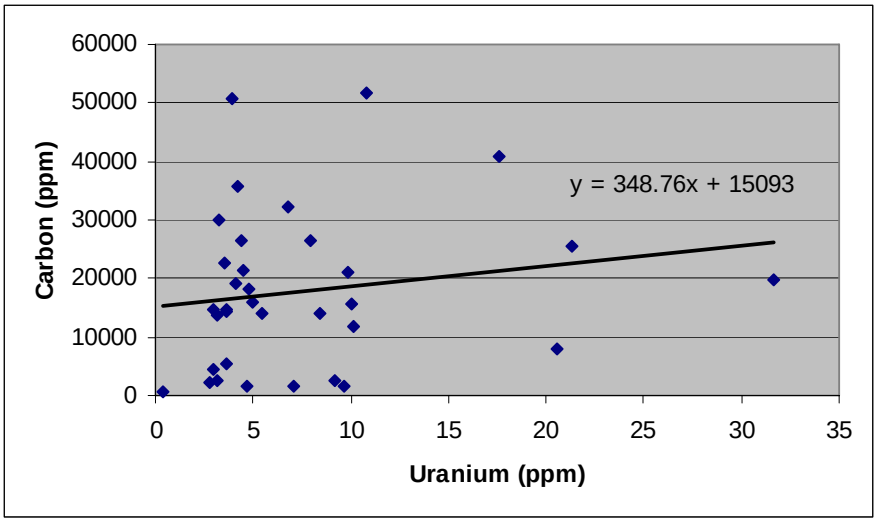

Fig. 34. Uranium and carbon correlations within rock samples.

Geochemical Analysis of Micas

Ten samples of anomalously green, handpicked mica were selected for trace-element analysis (Table 5). Table 6 presents statistical data for the samples.

Calculated Pearson Correlation Matrices indicate uranium correlates with thallium (0.59), zinc (0.61), silver (0.69), gallium (0.71) and vanadium (0.79). Vanadium correlates with chromium (0.64), rubidium (0.69), thallium (0.69), lead (0.70), tungsten (0.72), copper (0.79), uranium (0.79) and gallium (0.89). Barium correlates with hafnium (0.50), strontium (0.51), tantalum (0.67) and niobium (0.67). Scatter plots reflect positive correlation of uranium and vanadium (Fig. 35).

Table 5. Results From Trace-Element Analyses of Micas

Sample	Ba	U	V
CC20E	5,300.00 ppm	5.01 ppm	5,420.00 ppm
CC21	7,730.00 ppm	6.75 ppm	6,370.00 ppm
CC50A	2,500.00 ppm	3.66 ppm	4,290.00 ppm
CC50C	9,630.00 ppm	2.10 ppm	337.00 ppm
CC54B	565.00 ppm	3.50 ppm	158.00 ppm
CC59	>10,000.00* ppm	3.98 ppm	446.00 ppm
CC66	4,160.00 ppm	2.79 ppm	2,800.00 ppm
CC169	8,150.00 ppm	5.09 ppm	2,900.00 ppm
CC180	5,090.00 ppm	9.16 ppm	6,290.00 ppm
CC219	5,820.00 ppm	6.87 ppm	5,690.00 ppm

*10,000 ppm is the upper detection limit

Table 6. Statistical Data for Trace-Elements in Handpicked Mica Grains

	Ba	U	V
Low	565.00 ppm	2.10 ppm	158.00 ppm
High	>10,000.00* ppm	9.16 ppm	6,370.00 ppm
Median	5,560.00 ppm	4.50 ppm	3,595.00 ppm
Mean	5,894.50 ppm	4.89 ppm	3,470.10 ppm
Standard Deviation	3,040.58 ppm	2.16 ppm	2,504.86 ppm
1σ Threshold	8,935.08 ppm	7.05 ppm	5,974.96 ppm
2σ Threshold	11,975.67 ppm	9.22 ppm	8,479.83 ppm

*10,000 ppm is the upper detection limit

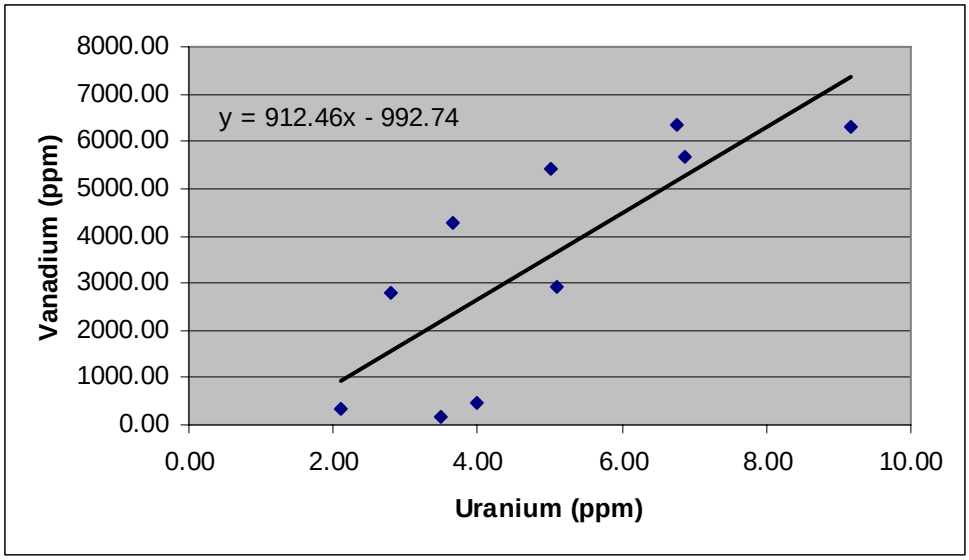

Fig. 35. Uranium and vanadium correlation within handpicked mica samples.

Microprobe Data

Ten grains of mica, including the green 'roscoelite', were chosen from four polished thin sections for microprobe analysis. Photomicrographs of the locations of the probed grains are in Appendix IV. Statistical information based on the microprobe analyses are summarized in Tables 7 and 8. Data from the unaltered and altered micas can be found in Table 9. The full dataset can be found on the accompanying CD and within appendix IV. Results from microprobe analyses show that the green micas are not true roscoelite, but are vanadium-barium-uranium-rich micas. True roscoelite contains between 17 and 19 percent V_2O_5; micas within the study area contain much less V_2O_5 (between 0.093 and 1.393 weight percent) (Green et al., 1986). Muscovite formulas for those probed can be found within Appendix IV**.**

Table 7. Statistical Data for Microprobe Analyses of Unaltered Mica

	U wt.%	**V wt.%**
Low	0.41	0.48
High	1.82	1.40
Median	1.59	0.92
Mean	1.50	0.92
Standard Deviation	0.29	0.25
1σ Threshold	1.79	1.17
2σ Threshold	2.08	1.42

Table 8. Statistical Data for Microprobe Analyses of Altered Mica

	U wt.%	**V wt.%**
Low	0.23	0.00
High	1.80	0.83
Median	1.07	0.23
Mean	1.07	0.27
Standard Deviation	0.45	0.19
1σ Threshold	1.52	0.47
2σ Threshold	1.97	0.66

Table 9. Results From Microprobe Analyses of Unaltered and Altered Micas

Label	BaO	U_3O_8	V_2O_5
CC219A.1a	0.3802	0.7876	0.2083
CC219A.1b	0.6206	1.0821	0.2239
CC219A.1c	0.5447	0.6698	0.1938
CC219A.1d	0.6688	0.7875	0.2275
CC219A.1e	1.4983	1.5305	0.1947
CC219A.1f	1.2157	1.3266	0.0930
CC219A.1g	1.0944	1.0646	0.1082
CC219A.1h	1.9334	1.4201	0.0000
CC219A.2a	0.3967	0.4438	0.1873
CC219A.2b	0.9431	1.2530	0.2254
CC219A.2c	0.3248	0.2290	0.1980
*CC219A.2d	0.8609	1.5	0.6826
*CC219A.2e	0.7745	1.6486	0.6917
CC219A.2f	0.2943	0.2696	0.2332
CC219A.2g	0.7647	0.9723	0.1922
CC219A.2h	0.3086	0.6354	0.2662
*CC219A.4a	0.662	1.6217	0.6675
*CC219A.4b	0.657	1.6835	0.7405
*CC219A.4c	0.6616	1.724	0.7192
CC219A.4d	0.7310	1.7785	0.7856
*CC180.1a	0.6251	1.7194	0.6874
*CC180.1b	0.6991	1.6082	0.7326
*CC180.2a	0.3609	0.4103	0.4808
*CC180.2b	0.7149	1.4382	0.8668
*CC180.2c	0.6758	1.506	0.7892
CC180.2d	0.6503	1.6703	0.8322
CC180.2e	0.4147	1.1806	0.2369
*CC180.4a	0.7722	1.6343	0.9181
*CC180.4b	0.71	1.6151	0.9199
CC169.1a	0.4554	1.3013	0.2768
*CC169.1b	0.4727	1.0856	1.234
*CC169.1c	0.5321	1.6305	1.1428
CC169.1e	0.5684	1.7992	0.4284
*CC20E.1a	0.6226	1.2819	0.9119
CC20E.1b	0.5332	1.3705	0.3588
*CC20E.1c	0.6502	1.4515	1.1205
*CC20E.4a	0.6083	1.5871	1.363
*CC20E.4b	0.6571	1.5764	1.3993
*CC20E.4b	0.701	1.332	1.2288
*CC20E.4d	0.608	1.819	1.111
CC20E.5a	0.2740	1.0350	0.3018
*CC20E.5b	0.7311	1.6023	0.9619
CC20E.5c	0.3065	0.9540	0.2481
*CC20E.5d	0.7383	1.48	0.9674

* Denotes unaltered mica

Microprobe data also show that there is a higher uranium and vanadium content within the "unaltered" micas than the "altered" micas, suggesting mobilization of these elements by retrograde-like alteration. Mean uranium content of the unaltered and altered micas are 1.76 and 1.20 weight percent, respectively. Mean vanadium content within unaltered and altered micas were 1.69 and 0.49 weight percent, respectively. Using the mean values, uranium decreased by 31 percent through alteration. Similarly, vanadium content decreased by 71 percent as a result of alteration.

Although the dataset is small, a Pearson correlation analysis was preformed on the unaltered and altered micas. Uranium and vanadium correlated at 0.60 and 0.48 for the unaltered and altered micas, respectively. Uranium and barium correlations did not change significantly between the unaltered (0.62) and altered micas (0.60).

Scatter plots also confirm the correlation of the elements. Comparison of uranium and vanadium between the unaltered and altered sections of green mica indicates a positive linear correlation (Fig. 36). The unaltered mica data plots as a loosely scattered group, without any strong trend, indicating the initial uptake of both uranium and vanadium into the mica structure. The altered micas have a linear correlation between the uranium and vanadium, which is representative of a continuum of alteration. Mica grains plotting on the left of the graph stayed within the temperature range for uranium and vanadium mobilization for a longer period of time, allowing for more of the elements to diffuse from the crystal structure. These same observations hold true for the correlations between uranium and barium (Fig. 37). The unaltered data plots as a loosely scattered group, without any trend. The altered micas plot in a linear fashion. Data to the left staying within the temperature range for diffusion for a longer period of time.

The microprobe data from the altered and unaltered micas corroborates the observations made from thin-section analysis. In thin-section analysis, the altered grains of mica were altered mainly by seritization. This alteration can be seen in the strong trend lines among altered mica analyses. Data obtained from sample sites appearing to be unaltered did not show a trend, but grouped to the right in both sets of correlation, indicating that they had not been subjected to alteration leading to diffusion.

Microprobe data were also used to analyze the interactions and relationships between other elements within the mica. Figure 38 graphs the analysis of uranium and total aluminum and figure 39 illustrates the similar relationship between vanadium and aluminum, and again indicates substitution during metamorphism. An increase in sodium is shown in the altered micas, suggesting sodium metasomatism (figs. 40 and 41). All figures show two different generations of mica, shown best in figure 42.

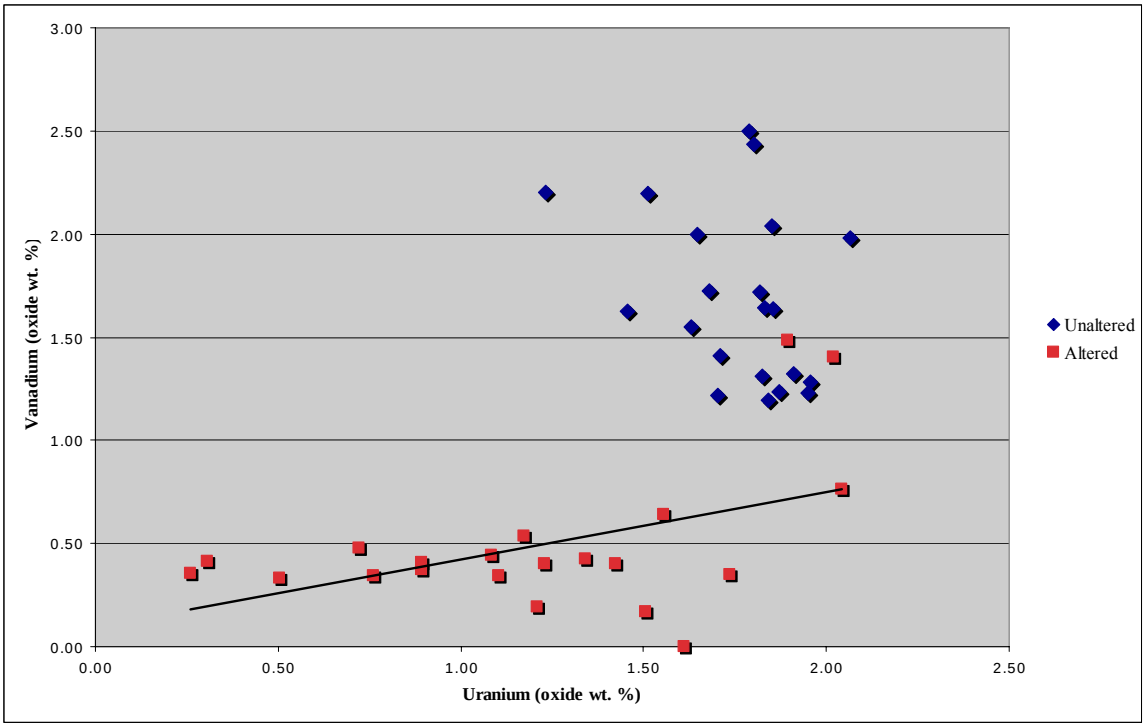

Fig. 36. Correlation plots of uranium and vanadium in unaltered mica and altered mica.

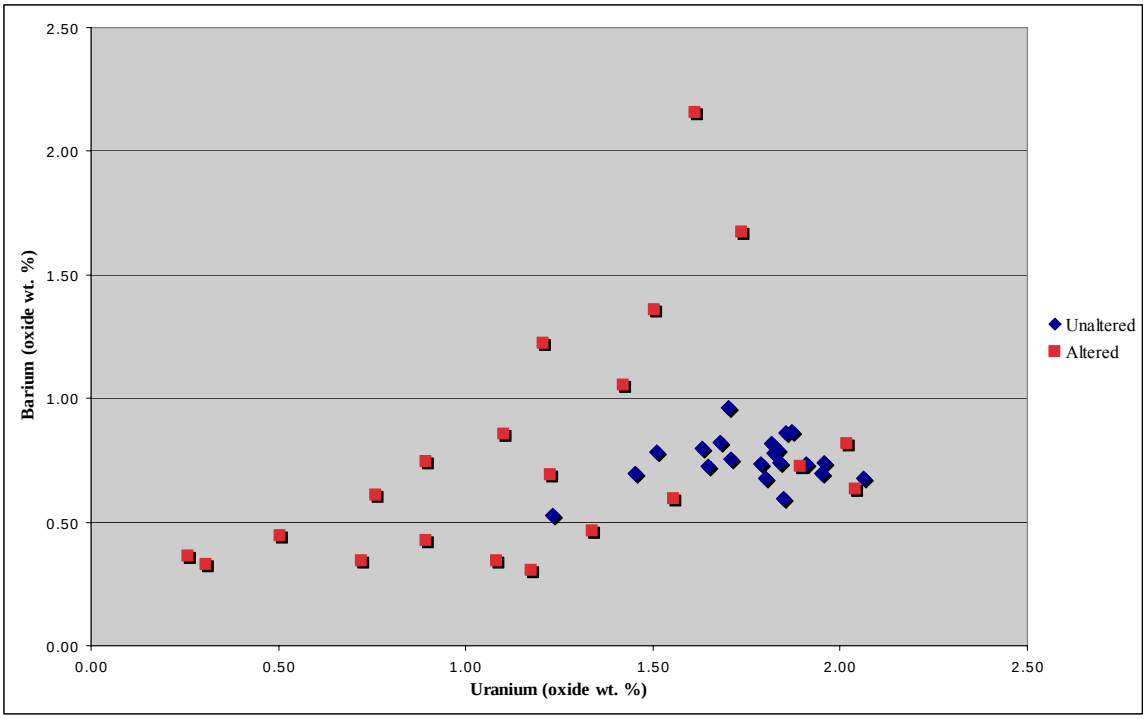

Fig. 37. Correlation plots of uranium and barium in unaltered mica and altered mica.

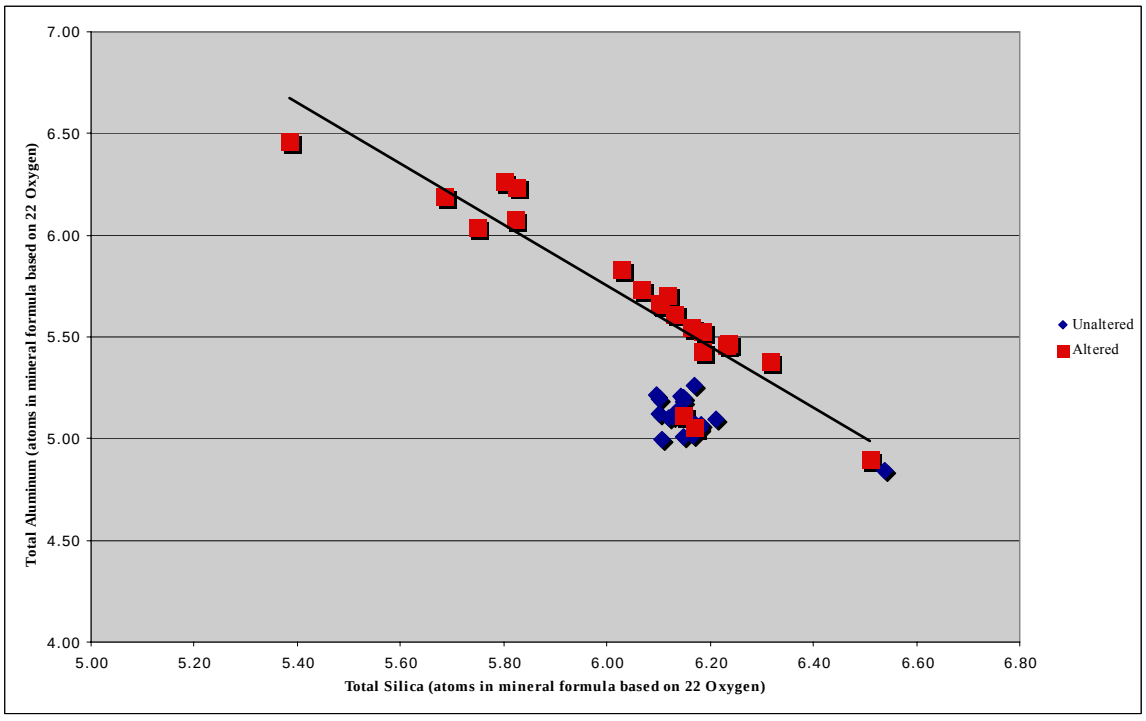

Fg. 38. Correlation between uranium and total aluminum in unaltered and altered micas.

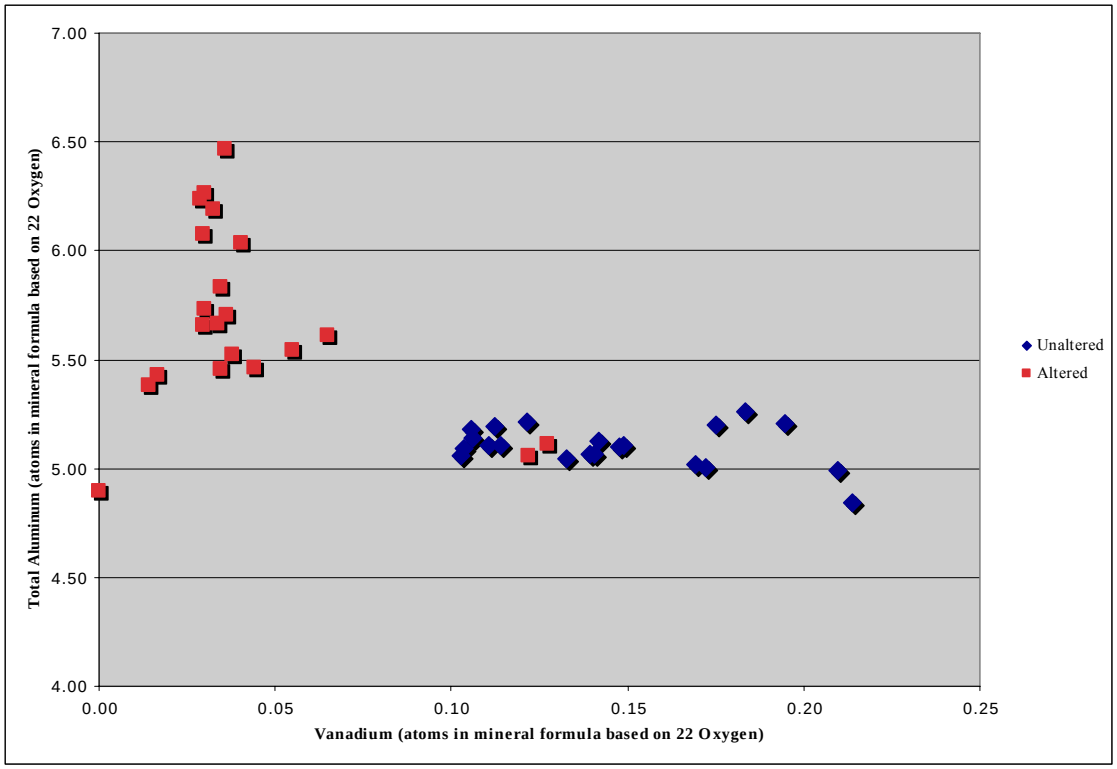

Fig. 39. Correlation between vanadium and total aluminum in unaltered and altered micas.

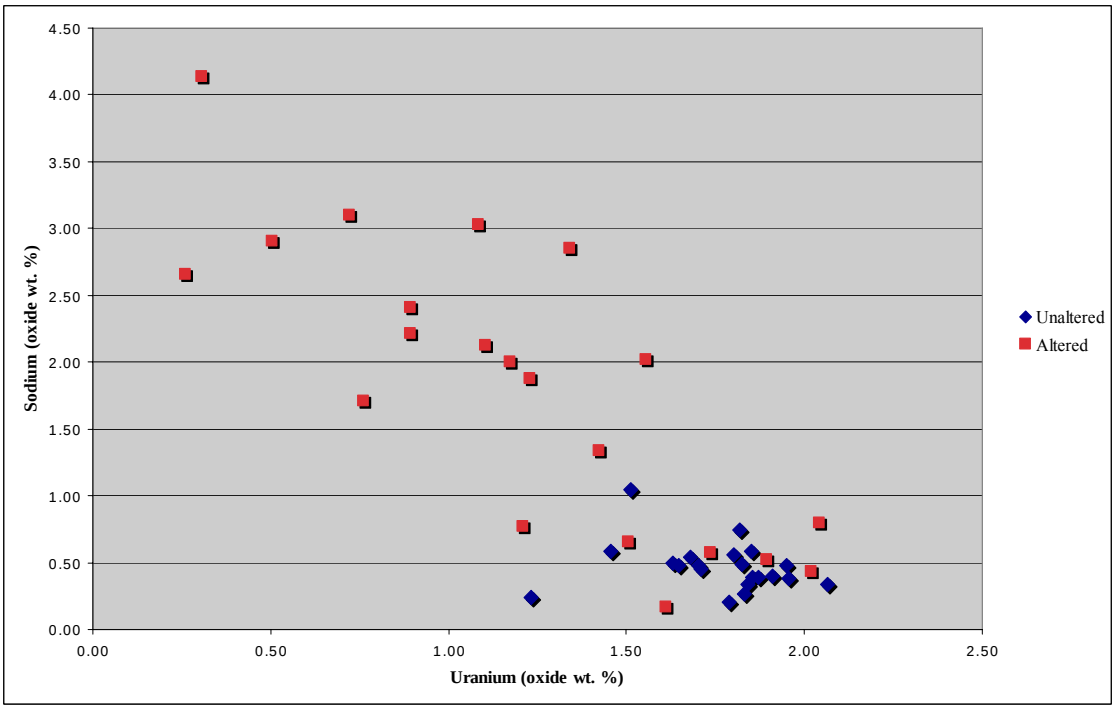

Fig. 40. Correlation between uranium and sodium in unaltered and altered micas.

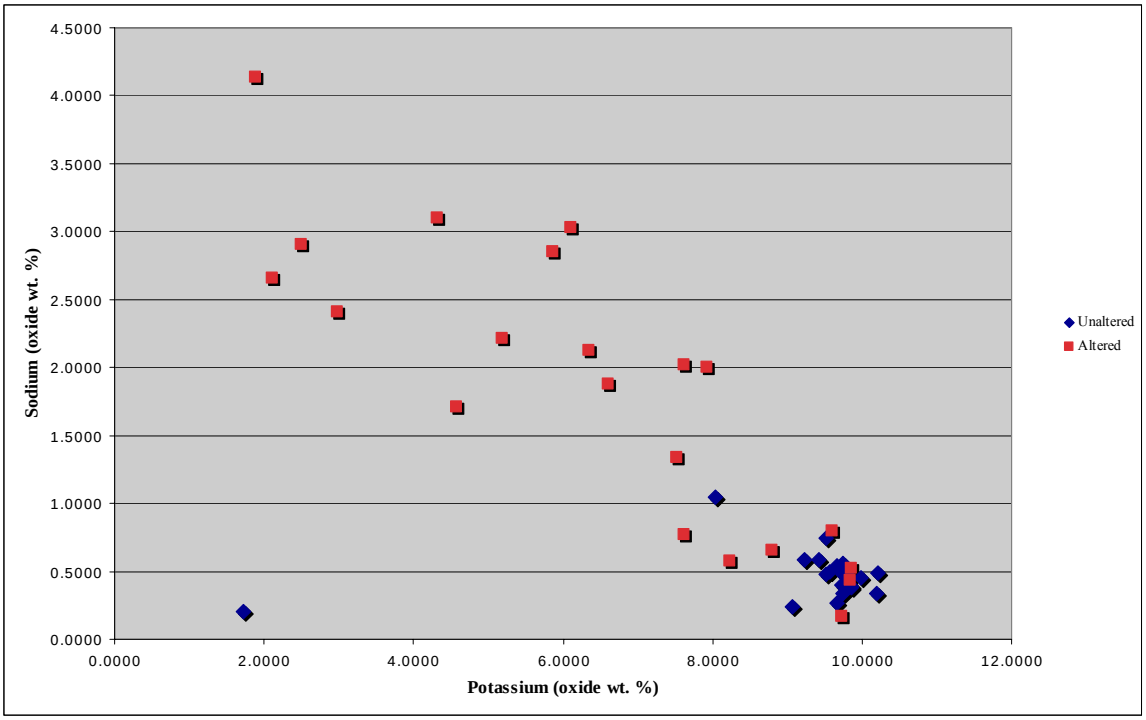

Fig. 41. Correlation between potassium and sodium in unaltered and altered micas.

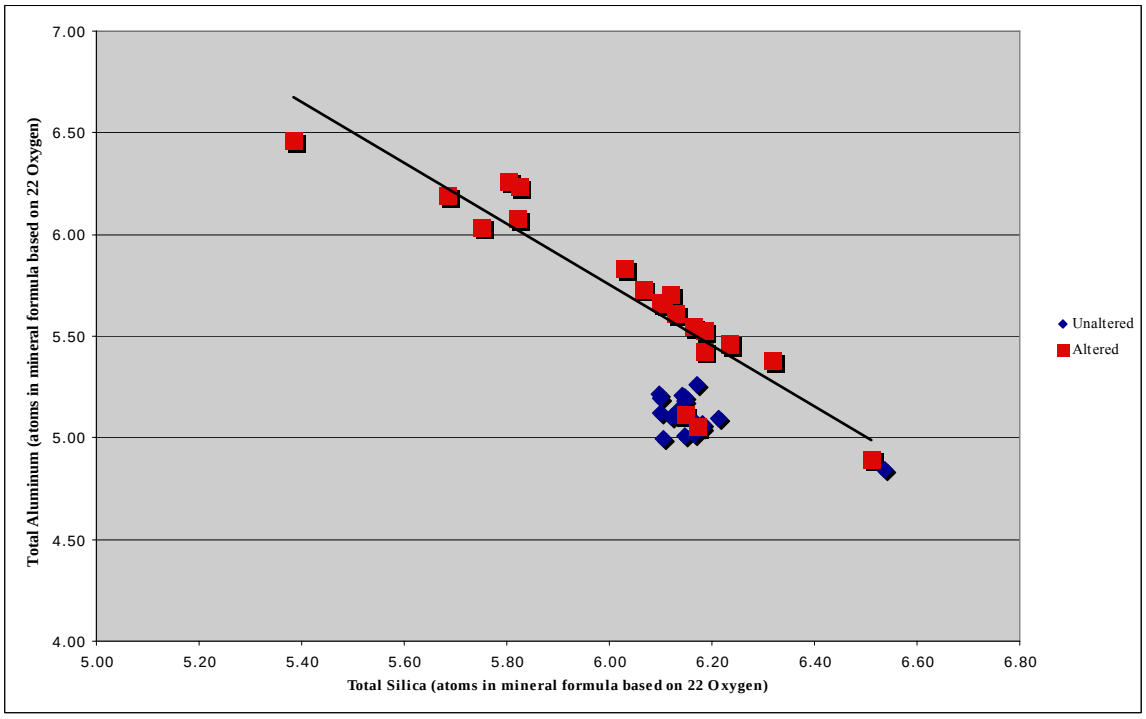

Fig. 42. Correlation between total silica and total aluminum in unaltered and altered micas.

GIS Data Synthesis

Figure 43 shows the distribution of uranium, vanadium and barium which have a northeastern trend of anomalous values. Samples containing anomalous uranium cluster near each other in section 30 and on the boundary between sections 19 and 20.

With respect to the rock samples collected for this investigation, three of the anomalous uranium samples occur near anomalous vanadium and barium sample sites; these same areas of anomalies correspond to those reported by Cook et al. (1982). Sample CC78 has anomalous uranium and vanadium, and sample CC83 has anomalous uranium and barium. Most of the anomalous vanadium sample sites occur on or near the prominent northeast-trending ridge.

Within the group of hand-picked mica samples, four are anomalous (CC50C, CC59, CC 21, CC180) (Fig. 44). Sample CC180 is anomalous in both uranium and vanadium. Samples containing anomalous values occur in a northeastern trend following the prominent ridge within the quadrangle.

Samples of saprolite/soil from Cook et al. (1982) and UNAREZ U.S.A. Inc. contain anomalous uranium (Fig. 45). Though the majority of these anomalies occur within or near the ridge, sample CS76, from Cook et al. (1982), was collected southwest of the ridge.

Anomalous uranium values also were recorded within the stream-sediment samples of Cook et al. (1982) (Fig. 46). Sample CA57 (Cook et al., 1982) was anomalous for both uranium and barium. Comparison of the various geochemical datasets documents that most of the anomalous samples cluster around one another, with uranium and barium concentrated in Section 30 (Fig. 47). Three anomalous uranium samples are from near

the border of Sections 30 and 31 and two are near the center of Section 31. Within Sections 20 and 29, seven anomalous uranium outliers occur. Vanadium anomalies are spread throughout the area and tend to be found on or near the ridge.

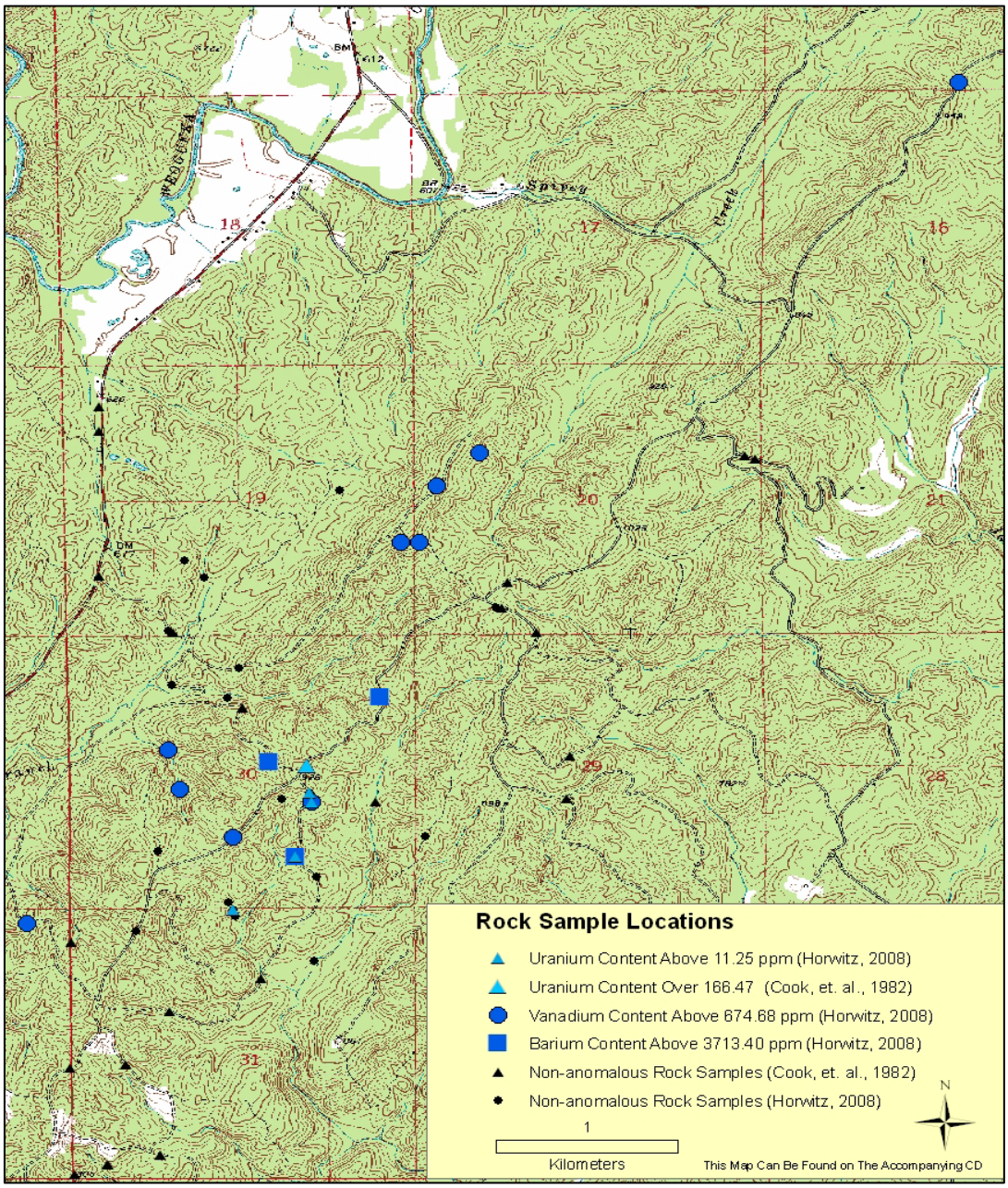

Fig. 43. Distribution of rock samples and those values meeting or exceeding anomalous threshold (sections 19, 20, 29, 30, 31 T. 23 N., R. 18 E.) (*modified from* United States Geological Survey, 1971). The number given in the legend is the 1-Sigma threshold for each dataset.

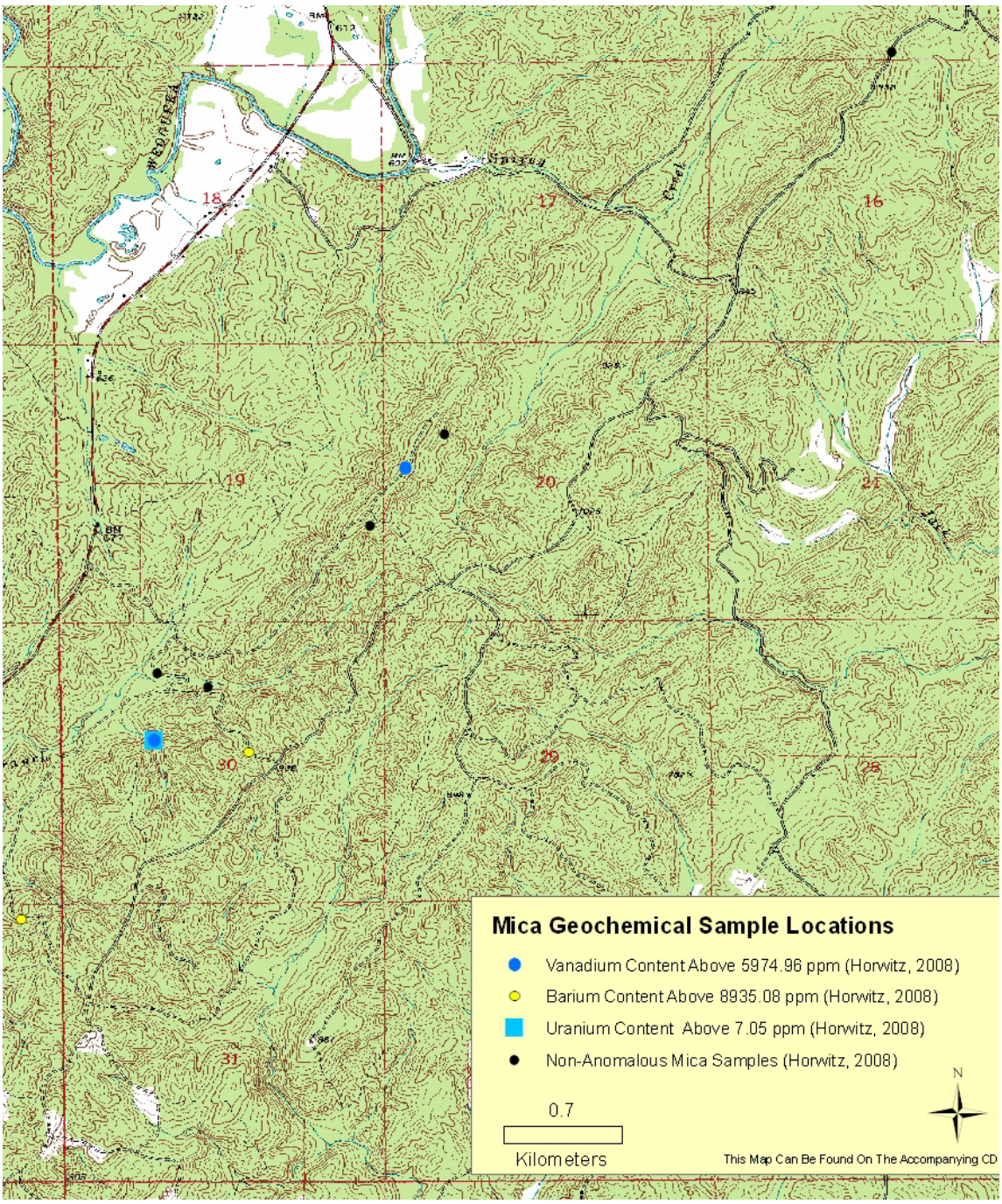

Fig. 44. Distribution of analyzed handpicked mica samples (sections 9, 19, 20, 29, 30, and 31 T. 23 N., R. 18 E.) (*modified from* United States Geological Survey, 1971). The numbers given in the legend are the 1-Sigma threshold for each dataset.

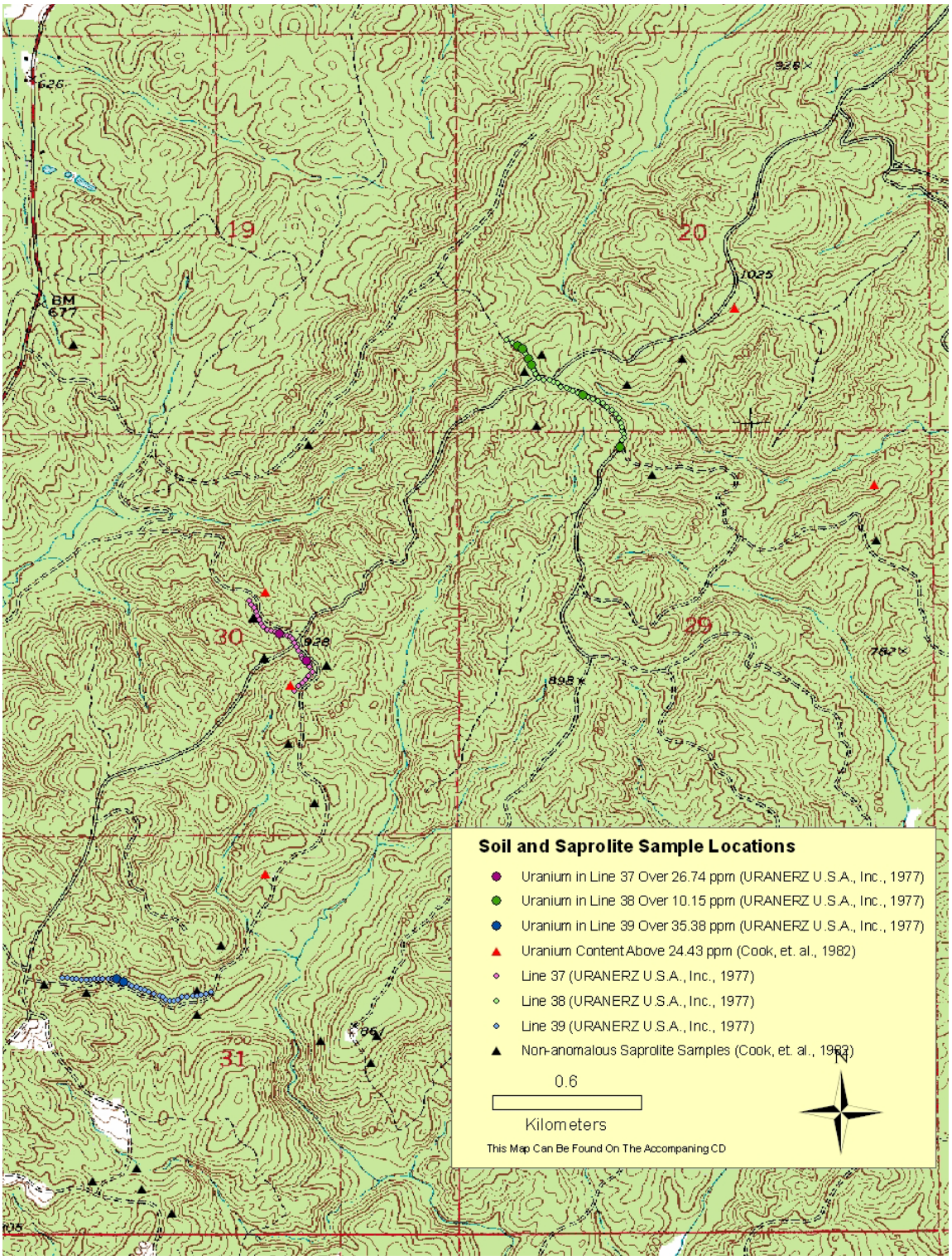

Fig. 45. Distribution of soil and saprolite samples for which geochemical analyses were performed by others (sections 19, 20, 29, 30, and 31 T. 23 N., R. 18 E.) (*modified from* United States Geological Survey, 1971). The number given in the legend are the 1-Sigma threshold for each dataset.

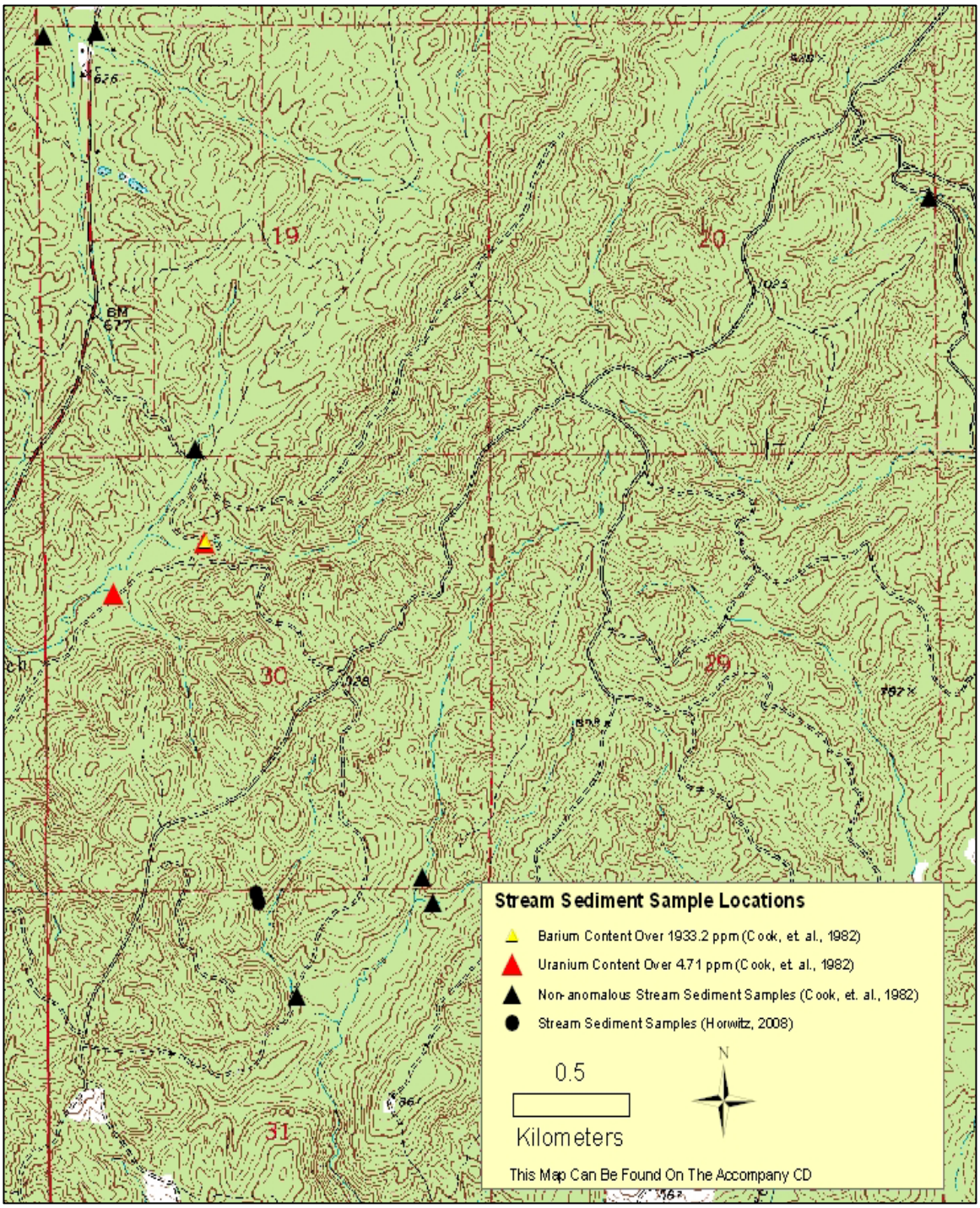

Fig. 46. Distribution of stream-sediment geochemical data (sections 19, 20, 29, 30, and 31 T. 23 N., R. 18 E.) (*modified from* United States Geological Survey, 1971). The numbers given in the legend are the 1-Sigma threshold for each dataset.

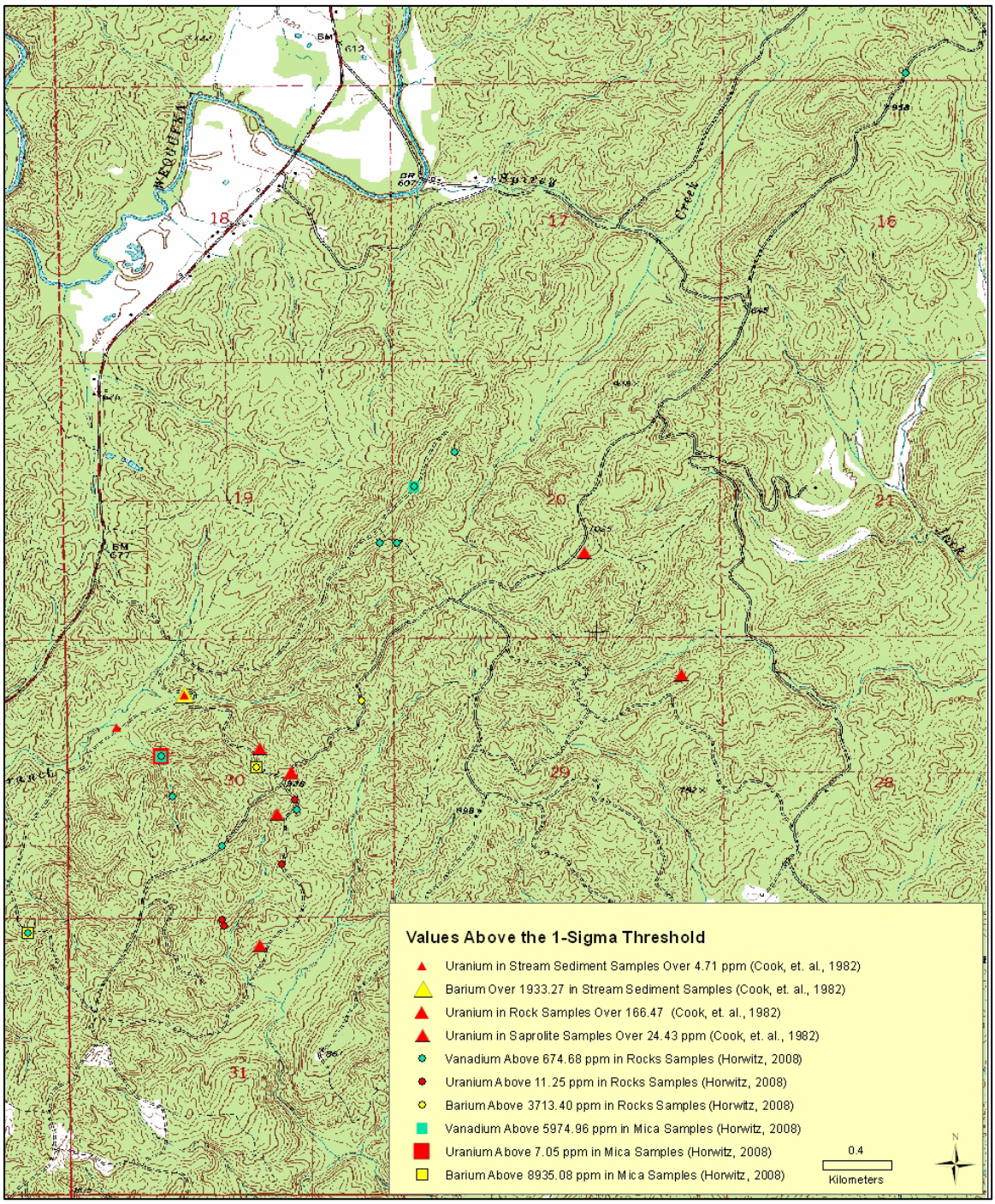

Fig. 47. Distribution of all sample types containing uranium, vanadium, or barium above the 1-Sigma threshold (sections 9, 19, 20, 29, 30, and 31 T. 23 N., R. 18 E.) (*modified from* United States Geological Survey, 1971). The map in expandable form can be found on the accompanying CD.

DISCUSSION

In order for the results from this investigation to be meaningful, they must be integrated with results from other studies. If the results are consistent and correlate positively, then data from this investigation can be used to define a deposit model for the Coosa County uranium occurrences and their prototype.

Geology

Strike and dip of foliation planes taken by this author were similar to those recorded by other investigators. Strike is to the northeast, and dip varies from 18 to 83 degrees typically to the southeast. Shear zones are accompanied locally by fault gouge indicating brittle deformation; these zones were noted throughout the field area. Crystal plastic deformation is evident from microstructural observations of thin sections from some shear zone rocks indicating high temperature (amphibolite facies, ~ 525°C) conditions for deformation. Several authors discuss similar shear zones within the greater Northern Piedmont (Steltenpohl and Moore, 1988; Guthrie and Lesher, 1994; Steltenpohl, 2005).

Joints within the field area were often filled with iron oxide and had a rough surface texture. The joints were anastomosing and formed both along and across strike. Uranium is possibly contained within the joints, as scintillometer readings from this study were highest in areas containing pyrite and fracture zones filled with iron oxide. This observation is supported by a 1979 report from the Drummond Company, and Cook et al.

(1982) who noted, “locally intense ground radiation exceeding 2,000 cps occurs in aerially restricted zones characterized by abundant iron oxide-filled joints and shear zones.” The Drummond Company report also reported that filled joints contained both secondary copper minerals and the vanadium minerals (Cook and Mallette, 1979).

Higgins Ferry Group schists and quartzites are thinly interbedded with amphibolites interpreted as mafic metavolcanics (Neathery and Tull, 1975; Tull and Stow, 1980; Cook et al. 1982; Stow et al., 1984). Within the schists and quartzite, graphite is locally abundant (Pallister and Thoenen, 1948; Neathery and Tull, 1975, Cook et al., 1982). The graphite-rich rocks are locally associated with the anomalously green mica, as Pallister and Thoenen (1948) and Cook et al. (1982) noted. Thin section analysis confirms the general character of these schists and quartzites as containing varying amounts of muscovite, graphite, garnet and sillimanite.

Soil changes within the area are visible on satellite images taken from Google Earth™. The anomalous green mica and rocks of the Higgins Ferry Group crop out within the dominant red soil unit. Soil variation coupled with radiometrics could be used to explore for uranium occurrences within this area.

Petrography

Pleochroic halos surrounding monazite or zircon crystals within muscovite and biotite grains give evidence that uranium- and thorium-bearing minerals are found within the rocks, although it is not likely that these refractory minerals are related to the uranium and vanadium occurrences of interest in this study. According to Gentry (1970), pleochroic halos formed from thorium and uranium are between 12 and 42 μm when they

are contained within micas, and halos in the thin sections examined during the present study fall within this range. This fact is also corroborated in the thin section from sample CC219. In this rock, there are several masses of sericite containing severe cracking possibly due to radiation damage. These severely cracked sericite masses contain no monazite or zircon.

Continuous metamorphic foliation and compositional banding were seen. Compositional banding is likely related to bedding or compositional layers that were originally within the protolith, or to wholesale reorganization during high-grade regional metamorphism.

Microstructures such as kink bands were seen in several thin sections. The preservation of these structures reflects the deformational history of rocks of the region and its relatively high metamorphic grade. Neathery and Tull (1975) state that there are kinks, breaks and shears within phyllosilicates that were likely produced by a retrograde event, which also caused the growth of sericite.

Geochemical Analysis of Rock, Sediment and Soil/Saprolite

Geochemical analysis of rocks, sediment and soil/saprolite from the present study give a mean uranium value of 7.51 ppm. This is much lower than that obtained by Cook et al. (1982). On average, rocks in the Cook et al. (1982) study contained 65.67 ppm total uranium and 22.72 ppm HNO-extractable uranium. Only one sample from the present study was above the average values recorded for the HNO-extractable uranium (31.70 ppm), and only two others were close to that value (20.6 and 21.3 ppm). The reason that the values obtained in this study are so much lower than those reported in Cook et al.

(1982) may be because data are not total uranium (not all of the uranium was extracted from the rocks during the sample preparation) or the result of selective sampling of anomalously radioactive outcrops by Cook et al. (1982). Although the numbers for the present study are relatively low, they do reflect anomalies within the data population.

When both new and previous geochemical data from rock samples are plotted on the base topographic map, most anomalous sample sites fall within Section 30, T. 23 N., R. 18 E. (Fig. 43). The majority of the samples containing anomalous vanadium occur on the dominant northeast-trending ridge and most of the uranium and barium anomalies are on the southeastern flank. Soil and saprolite samples have anomalous uranium values along the northeastern ridge throughout the study area (Fig. 45). Geochemical data from sediment samples have anomalous uranium and barium from streams draining the ridge (Fig. 46).

The geochemical data correspond to radon anomalies documented in a map produced by URANERZ U.S.A., Inc. in 1977 that was generated by measuring radon with alpha meters. The radiometric contours trend northeast and follow the prominent ridge within the field area. Most of the anomalous uranium values occur within or near the contoured highs (Fig. 48). Correspondence of the radiometric contour map and the anomalous uranium, vanadium and barium sample sites, and near the prominent ridge implies a lithostratographic and/or structural control of the Coosa County occurrences.

All of the anomalous samples sites occur within the Higgins Ferry Group, particularly within the pyrititic quartzose roscoelite schists (Cook et al., 1982). Neathery et al. (1976) noted that the Hollins Line fault is the boundary with the high-grade metamorphic rocks, which have a higher level of radioactivity than the lower-grade rocks; there are no

radiometric anomalies north of the Hollins Line.

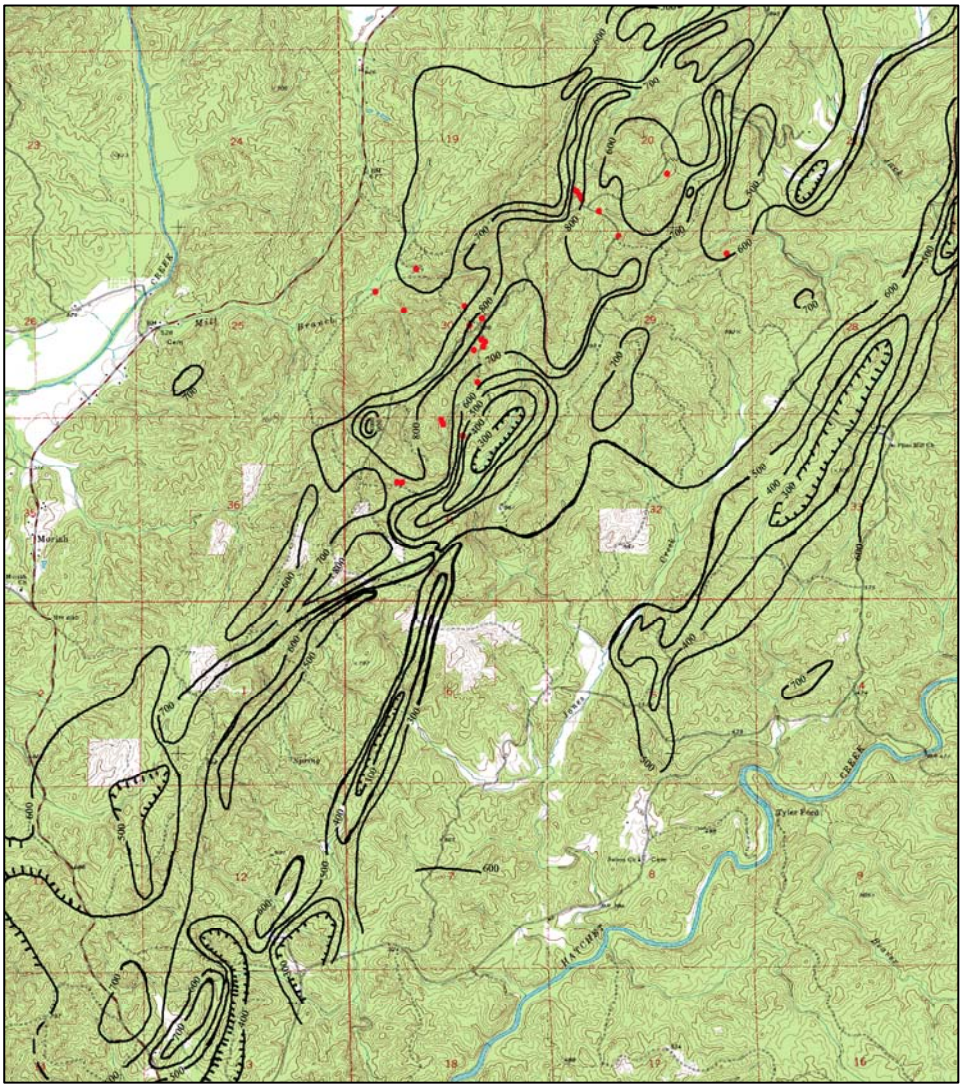

Fig. 48. Ground radiometric contour map using alpha-meter radon data plotted with location of anomalous uranium samples from all the studies (red circles) (*modified from* URANERZ U.S.A., Inc., 1977).

Geochemical Analysis of Handpicked Micas

As expected, results from the geochemical analyses of the micas are slightly different than the results of the geochemical analyses of the rocks. Within the mica samples, uranium, vanadium and barium all correlated with several elements. Uranium strongly

correlates with thallium, zinc, silver, gallium and vanadium. Vanadium correlates with chromium, rubidium, thallium, lead, tungsten, copper, uranium and gallium. Barium correlates with hafnium, strontium, tantalum and niobium. Unlike the results from the rock analyses, barium and uranium correlated very weakly within the mica, giving a correlation of 0.02. It is important to keep in mind that the data are from these handpicked micas are from a small population (n=10), possibly explaining the large degree of variance.

Handpicked green micas containing the anomalous uranium and vanadium were generally restricted to the dominant ridge. Barium-rich micas were found in samples from the southeast flank of the ridge (Fig. 44).

Microprobe Data

Microprobe analyses reveal varying total amounts of uranium, vanadium and barium within the "altered" and "unaltered" mica. Uranium and vanadium contents decrease with progressive alteration. Using the mean values, uranium decreased 31 percent. Vanadium mean values declined 71 percent, suggesting that both uranium and vanadium are mobile and migrated from the grains during "alteration." Figures 36 and 37 suggest the loss and mobility of barium, uranium and vanadium during "alteration." In Figure 36, uranium and vanadium contained in "unaltered" and "altered" micas indicate a change in the dispersion pattern. In the "unaltered" micas, most data points plot in the upper right corner, suggesting a relatively homogenous population. The "altered" micas suggest a heterogeneous population, with data points spread throughout the trend line of the graph indicating varying levels of alteration.

Correlation between uranium and barium in microprobe analyses of micas (Fig. 37) is very similar to that of uranium and vanadium. In the "unaltered" micas, the data points plot as a cohesive group in the upper right corner, and the "altered" micas data points are laid out all along the trendline.

The microprobe data demonstrate that the anomalously green micas are not technically roscoelite. The maximum vanadium content in the "unaltered" mica is 1.14 weight percent. This value is in accordance with Green et al. (1986), who found the amount of vanadium within muscovites of the Higgins Ferry Group to be between 0.86 and 1.12 weight percent V_2O_5. True roscoelite contains 17-19 percent V_2O_5, which means the anomalously green micas are not roscoelite, but rather an unusual vanadium-uranium-barium-rich muscovite. Green et al. (1986) also report that the micas contain barium.

Figures 40 and 41 demonstrate the effects of sodium metasomatism by plotting sodium against uranium and potassium, respectively. In both graphs the sodium has a wide dispersion pattern and shows an increase over the unaltered micas. This increase is typical of rocks which have undergone sodium metasomatism. Drummond et al. (1981) explains how sodium rich fluids enriched the Rockford Granite transforming it to a trondhjemite though substitution of potassium with sodium. As seen in figure 41, the sodium is substituted for potassium, both within rocks of the field area and in the area studied by Drummond which suggests sodium metasomatism occurred at a regional scale. This process allows for the reorganization of uranium and vanadium within the host micas during retrograde metamorphism.

Locations of Anomalous Barium, Vanadium and Uranium

Based on the barium content within whole rocks and within the anomalously green micas, barium is likely to be hosted within the anomalously green mica of the Higgins Ferry Group. Mean barium content within the rocks is 3,963 ppm, and within the micas is 5,894 ppm. Using these mean contents, the micas have on average 1,930 ppm more barium than the rocks as a whole, suggesting that the barium is hosted within the micas which is confirmed by the microprobe data. More anomalous barium was found in the southeastern parts of the study area, away from those rocks containing vanadium. This suggests that the rocks hosting the barium and vanadium differ in their chemical make-up and distribution.

Vanadium within the rocks of the Higgins Ferry Group is clearly sited within the anomalously green micas. Average vanadium content within all the rocks selected for geochemical analysis is 462 ppm. The vanadium content of rocks containing the micas that were picked and separated contain on average >764 ppm vanadium. As previously mentioned, anomalous vanadium is found predominately in the rocks along the ridge and is not associated with sites containing anomalous barium.

The location of uranium within the rocks of the Higgins Ferry Group is complex. Comparison of the whole-rock uranium content with that of micas analyzed for this study indicates that the rocks have on average 2.62 ppm more uranium than do the micas; however, the micas do contain uranium averaging 4.89 ppm. Values obtained from rocks analyzed by Cook et al. (1982) were much higher, averaging 65.67 ppm total uranium and 22.72 ppm HNO-extractable uranium. Only one sample from this study was above the average values recorded for the HNO_3-extractable uranium (31.70 ppm), and only two

others were close to that value (20.6 and 21.3 ppm).

Microprobe analyses of "unaltered" and "altered" micas document that uranium moved out of the micas as they were "altered". Petrographic observations suggest that this alteration is mostly due to retrograde metamorphism, which mobilized fluids and allowed the uranium to redistribute throughout the rock. "Unaltered" micas had 1.498 percent uranium versus 1.071 percent uranium in "altered" micas.

Uranium is known to be mobile during metamorphism, especially when partial melting of the host rocks occurs. According to Heier (1979), uranium will move through rocks during greenschist, amphibolite and granulite facies metamorphism. Uranium dioxide's solubility is at a maximum at about 260°C and decreases at temperatures below 200°C and above 300°C (Rich et al., 1977). Crystal plastic deformation of quartz indicates a prograde amphibolite-facies metamorphism. Brittle deformation of quartz and alteration of micas to sericite indicate a retrograde greenschist-facies event. In thin sections, mica crystals are kinked and recrystallized which implies temperatures above 400°C (Passchier, and Trow, 1998). Brittle fractures observed in quartz indicate temperatures less than 300°C. Temperatures during the peak amphibolite-facies metamorphism would be too high for optimum transport of uranium, but lower greenschist-facies temperatures during greenschist retrogression, therefore, appear appropriate for uranium mobilization. It is very likely that uranium was mobilized during the retrograde event. If uranium moved into other sites, any economic occurrences within Coosa County were likely produced under retrograde metamorphic conditions, and thus may be related to structures produced by this event.

Folding and kinking in muscovite is consistent with the movement of uranium out of

micas and into other minerals within the rock. Wilson (1977) reports that uranium diffusion in micaceous schists occurs along grain boundaries of the deformed micas where uranium content was variable. Wilson (1977) suggested that deformation, along with hydrothermal or metamorphic fluids, is able to relocate the uranium within micas. If deformation during retrograde metamorphism did redistribute the uranium, then this relocation would slightly postdate the formation of the deformed micas. Microprobe analyses reported in the present study document that the retrograded micas contain less uranium than the unaltered ones, compatible with the interpretation for late-stage transport of the uranium.

Interpretation of the Coosa County Occurrences

The presence of graphitic aluminous schists and oxide filled joints within the field area suggest that the Coosa County uranium occurrences are either metamorphosed sediment-hosted or non-granitic vein-type deposits. Following are brief descriptions of examples of the most likely deposit types for the Coosa County occurrences. From there a prototype for the Coosa County occurrences is hypothesized.

Non-Granite, Metamorphic-Hosted Uranium Vein-Type Deposits: The Schwartzwalder deposit in Colorado is a non-granite related, simple vein-type uranium deposit occurring in a metamorphosed sequence of shallow-water sandstone, shale and carbonate deposited during the Paleozoic Era. These rocks were plastically deformed under amphibolite-facies conditions. The Schwartzwalder deposit has characteristic 'horsetail' veins rich in uranium in the hanging wall, which are associated with the steeply dipping (75°) Illinois fault, which is bordered on each side by the East and West

Rogers faults (Nash, 1981; Young, 1985; Dahlkamp, 1993). The vein system is hosted within the Idaho Springs Formation that comprises garnet-biotite gneiss and quartzite within 5-10 km of the contact between Proterozoic and Paleozoic rocks. Within the metamorphic rocks are compositional layers of the original sedimentary bedding. Graphite occurs within sulfide-rich layers of the gneiss (Wallace and Karlson, 1985). This high-grade deposit has been exploited by mining companies as a source of uranium for almost 50 years and it has been used as an exploration model elsewhere.

Sedimentary Uranium Deposits: Within the United States are many sandstone-hosted uranium deposits. The Colorado Plateau comprises several uranium districts in New Mexico, Colorado, Utah and Arizona. Two of the most well-know districts are in the Uravan mineral belt and those in the Grants, New Mexico area (Chenoweth and McLemore, 1989; Finch, 1996).

According to Chenoweth and McLemore (1989), most of the uranium occurs within horizontal fluvial Jurassic and Triassic sandstones, conglomerates and mudstones. Limestones and marginal marine sandstones also host minor uranium occurrences (Chenoweth and McLemore, 1989).

Sandstone-hosted uranium deposits in Colorado occur within the Morrison Formation. The eastern Paradox basin hosts the Uravan mineral belt, an area dominated by uranium-vanadium deposits that are tabular and concordant with bedding. Vanadium to uranium ratios range from 3:1 to 10:1 and have an average ratio of 5:1 (Chenoweth and McLemore, 1989).

New Mexico contains the Grants uranium districts, which contain ore hosted mainly within the Morrison Formation. Ore bodies are lenticular, tabular masses of sediment

containing uranium and organic compounds that form parallel trends. Between the mineralized zones are barren fine-grained sandstones. The deposits, which likely formed prior to the Cretaceous Dakota Sandstone, are less than 2.4 m thick. These deposits average more than 0.20% U_3O_8 and are low in vanadium. Some of the uranium from the Morrison Formation have been remobilized and distributed within the Dakota Sandstone. These later deposits are also tabular in shape (Chenoweth and McLemore, 1989).

Besides the well-known Colorado Plateau deposits, uranium occurs in the Pennsylvanian Mauch Chunk Formation, which is immediately below the Pottsville Formation in Pennsylvania. The Pottsville Formation stretches into the Southern Appalachians as far as Alabama. The Mauch Chunk Formation hosts the Mount Pisgah, Mauch Chunk Ridge, and Butcher Hollow uranium deposits (Wherry, 1915; Dyson, 1954; Klemic and Baker, 1954; Klemic, 1958). According to Klemic (1958), the uranium is syngenetic within the host formation and was locally concentrated epigenetically, creating roll-front type-deposits similar to those of the Western United States. The grades of the deposits range from 0.05-0.02 percent U_3O_8. One area contains a higher uranium content that locally reaches 2.6 percent. The vanadium content is much higher than the uranium (1.3 percent V_2O_5) (Rose, 1999). This deposit is considered analogous with the deposits of the Morrison Formation within Colorado and Utah (Klemic et al., 1963; Rose, 1999).

The Pottsville Formation is comprised of quartz conglomerates, thin beds of coal and red, gray and tan shales. The basal member of the unit consists of coarse greywacke, conglomerate and sandstone. The basal conglomerate is different from others higher in the unit in that it has a dark matrix. The lithology of the Pottsville is not laterally uniform

and the shales and conglomerates thicken and thin throughout the unit. The underlying Mauch Chunk Formation is comprised of sandstone, siltstone and shale, and can be considered generally a low-rank greywacke (Wherry, 1915; Dyson, 1954; Klemic et al., 1963). The red shales within the Pottsville Formation are sometimes mistaken for those in the Mauch Chunk, and there has been disagreement by workers on the contact between the formations. Trace copper is contained within the Mauch Chunk as evidenced by malachite and azurite (Klemic et al., 1963).

Likely Deposit Type and Prototype of the Coosa County Occurrences

Although the uranium anomalies in Coosa County occur within metamorphic rock, some features are at odds with conceptualized models of metamorphic uranium deposits. The present conceptual deposit models also do not explain the possible importance of the significant retrogression seen within the rocks of the Coosa County occurrences. The most reasonable hypothesis is that the Coosa County occurrences were originally low-grade sandstone-hosted, uranium-vanadium deposits, which were then metamorphosed to amphibolite-facies and later retrograded. Then, if this is the case, it could be expected that the uranium would be hosted in a quartz-rich schist or quartzite, and that there would be an intimate association with vanadium. The anomalous rocks of the Higgins Ferry Group are indeed quartz-rich schists and quartzites that contain vanadium-rich micas, graphite, and locally anomalous uranium and copper.

Even though this seems a reasonable hypothesis for the prototype of the Coosa County occurrences, there is still the question of what any significant deposits would be classified. Since, in the absence of definitive roll-fronts or veins, the weak mineralization

seen at the surface does not closely match any current deposit models. If retrograde metamorphism was removed from the picture, it is possible that uranium would be far more dispersed and the occurrences classified simply as geochemicaly anomalous metasediments.

The rocks hosting non-granitic vein-type deposits, such as the Schwartzwalder deposit, occur within schists and/or quartzite, both of which are similar to the host rocks for the Coosa County occurrences. If the ultimate Coosa County deposit type is a non-granitic deposit, tabular concentrations of mineralization would be seen. Though no primary uranium mineralization is documented within rocks of the field area, there is indication that it occurs within fractures infilled with sulfides that are weathered to iron oxide at the surface. These fractures could have been filled with uranium-bearing minerals below the present water table and could in general represent either simple or complex vein-type deposits. Finally, rocks of the study area are locally sheared, another common feature closely associated with non-granitic vein-type deposits (Elevatoriski, 1979; Nash, 1981; Dahlkamp, 1993). Graphite, seen throughout the study area, is also found within sulfide-rich layers of gneiss at the Schwartzwalder vein-type deposit (Wallace and Karlson, 1985).

Now that a likely sedimentary protolith is recognized, a depositional model for the Coosa County occurrences can be formulated. A sandstone protolith analogous to the Mauch Chunk Formation was the likely original host for the Coosa County uranium-vanadium. Closely associated graphitic rocks are likely the metamorphic product of carbonaceous shales, analogous to those in the Mauch Chunk.

Although there are no known sandstone-hosted uranium deposits in Alabama, the

Pottsville Formation is found throughout the Appalachians and as near to Coosa County as the Cahaba basin. The Cahaba Basin is an Appalachian foreland thrust basin containing deltaic sands, silts and muds rich in carbonaceous material (Rodgers, 1987; Robinson and Prave, 1995). Beneath the Pottsville in the Cahaba Basin, are the Bangor Limestone, Parkwood and Pennington Formations. The contact between the Pottsville and the Bangor contains a carbonaceous claystone, and a carbonaceous, argillaceous sandstone, both of which would become graphitic units at moderate rank regional metamorphism. Both the upper Parkwood and Pennington also contain carbonaceous material (Thomas, 1972) which would likely become graphite such as that seen within the Coosa County schists and quartzites, if they were to become metamorphosed.

The nearest mapped occurrence of the Pottsville Formation to the Coosa County uranium occurrences is about 40 miles northwest of the study area, across several major tectonic boundaries. However, Mississippian carbonaceous units such as the Erin Shale and associated metasediments are contained in the tectonic block hosting the Coosa County occurrences.

It should be noted that there has been a report of anomalous radiation within units of the Lay Dam Formation of the Talladega belt (Tull, 1978; Guthrie, 1994). These anomalies were first noted during an aero-radiometric survey. It was reported that finely laminated and darker slates had a higher observed radioactivity (Beg, 1980). Though not stated in the report (Beg, 1980), the darker slate is most likely the Erin Slate, a member of the Lay Dam Formation of Mississippian Age (Gastaldo et al., 1993), which is located structurally beneath the Hollins Line fault. It is likely that the high content of carbonaceous material in the unit is responsible for the anomalous radioactivity. It is

believed that the Erin Slate would not have contributed to the Coosa County occurrence due to the fact that the Hollins Line fault would be a barrier to any fluids migrating upwards into the Coosa Block. However, the thrust stack models of Higgins et al. (1988) would allow repetition of this and similar related carbonaceous units to occur within the Coosa Block.

Method of Emplacement

A hypothesis for how the Coosa County uranium occurrences evolved can be formulated using the deposits found within the Mauch Chunk as a guide. The Southern Appalachians have been interpreted by some (Higgins et al., 1988) as having formed by the stacking of thrust sheets. Within Alabama, there are three stacks of folded thrust sheets, one of which is the Georgiabama stack. The Georgiabama stack's basal unit is the Bill Arp sheet, which is found within the field area. The Bill Arp sheet locally comprises Grenville aged basement rock and late Precambrian to early Paleozic non-volcanic, clastic, and poorly sorted metasedimentary rocks. Prior to the Taconic Orogeny (460-420 Ma), these sediment,s which are lithologically similar to the basal unit of the Pottsville Formation, would have been deposited in one or more shallow basins. These rocks would contain quartz sandstones that included carbonaceous material. Uranium and vanadium were concentrated in the rocks by normal groundwater to form rollfront-type deposits.

During the Taconic Orogeny, the Georgiabama stack was emplaced within Georgia and Alabama (Higgins et al., 1988). Outcrops of the Bill Arp sheet are found within tectonic windows and at the boundary of Blue Ridge and Valley and Ridge province

rocks. This sheet, which contains metamorphosed carbonate rocks and clastic sediments consistent with shallow water deposition, is enriched in titanium, barium and graphite (Higgins et al., 1988).

The dominant prograde metamorphic event impacting these units occurred during the Acadian Orogeny (390-360 Ma). During this metamorphic event, (and perhaps secondarily during thrust sheet emplacement) the uranium and vanadium from the original sedimentary accumulations would have been incorporated into the anomalously green micas observed in the Higgins Ferry. Carbonaceous material within the rocks would have been metamorphosed to graphite.

During the Alleghanian Orogeny (330-285 Ma), metamorphic fluids mobilized elements from the micas into the surrounding rocks. During this time, the Mitchell Dam Amphibolite, then a tholeiitic basalt, was folded into what is now the Higgins Ferry Group. According to $^{40}Ar/^{39}Ar$ dating, Blue Ridge rocks would have been elevated above ~500°C (amphibolite-facies), possibly as late as 330 Ma (Steltenpohl and Kunk, 1993). This would have allowed for the metamorphism of the tholeiitic basalt into the current Mitchell Dam Amphibolite. The muscovite containing vanadium, uranium and barium became depleted in these elements, and the geochemically complex muscovite was altered. This alteration allowed for the possible movement and fixation of uranium within fractures in the rocks. Vein-type deposits could have been produced during this second event, although there is little supporting evidence exposed at the surface today for these types of deposits. Vein-type deposits, if they ever existed, are either still at depth or have been eroded away, leaving only weak geochemical traces (anomalies) at the surface today.

CONCLUSIONS

Based on petrography of rocks of the Higgins Ferry Group, retrograde sericite has been derived from several minerals including feldspars, muscovite and aluminosilicates. Microstructures observed in thin sections record compression and right-slip shearing at greenschist-facies conditions within the ductile-brittle transition. Brittle fractures within quartz indicate temperatures lower than 300°C, and recrystalized micas, quartz and feldspars indicate temperatures of about 400°C.

Geochemical map trends in the study document that most of the anomalous uranium occurs within Section 30 T. 23 N, R. 18 E. The anomalies overlap radiometric contour highs reported in surveys conducted during the 1970's.

Microprobe analyses document variation of elemental content in the unaltered and altered micas. Uranium and vanadium contents decrease with increasing alteration of mica suggesting that uranium has been removed from micas during alteration. Calculated mica compositions infer sodium metasomatism as described for Coosa County by Drummond (1986, 1987a, 1987b; Drummond et al., 1986; Drummond and Allison, 1987).

Geochemical analyses document that barium and vanadium are concentrated within the anomalously green mica. These micas traditionally have been referred to as 'roscoelite' but concentration levels of barium and uranium make them better described as complex vanadium-uranium-barium muscovites. Uranium is present in small

quantities within the anomalously green mica but higher abundances are documented in individual whole rock samples, a further indication of mobilization during alteration.

Taking all of the data into consideration, the two most likely prototypes for the Coosa County uranium occurrences are metamorphosed sandstone-hosted or unrecognized non-granitic vein-type deposits. The model that best fits the observations reported within this study is the metamorphosed sandstone-hosted, uranium-type deposit, similar to either the Colorado Plateau or Mauch Chunk Formation occurrences. In this model, prior to the Taconic Orogeny, quartz-rich sandstones containing carbonaceous material were deposited and uranium and vanadium contained in these rocks migrated through normal groundwater processes to form rollfront-type deposits. The deposit(s) was then metamorphosed to sillimanite grade during the Acadian Orogeny during which the uranium and vanadium were mobilized from the original sandstone-hosted deposits and incorporated into the green micas; the carbonaceous material underwent crystallization into graphite. These rocks then underwent retrograde metamorphism during the Alleghanian Orogeny, at which time the uranium and vanadium were released from the muscovites to migrate into other unidentified sites (such as minor shear zones) within the host rock. If vein-type deposits were formed during the retrograde metamorphic event, they have been eroded away or are still at depth.

REFRENCES

Adams, G. I., 1926, Geology of Alabama; the crystalline rocks: Geological Survey of Alabama Special Report 14, 40 p.

Adams, G. I., 1930, Gold deposits of Alabama and occurrences of copper, pyrite, arsenic and tin: Geological Survey of Alabama Bulletin 40, 91 p.

Adams, S. S. and Harshman, E. N., 1981, Geology and Recognition Criteria for Roll Type Uranium Deposits in Continental Sandstones – Final Report: Department of Energy, Report GJBX-1(81), 185 p.

Armstrong J.T., 1988, Quantitative analysis of silicate and oxide materials: comparison of Monte Carlo, ZAF, and f(rZ) procedures, in Newbury, D.E., ed., Microbeam Analysis, p. 239-246.

Beg, M. A., 1980, Assessment of uranium resources in three selected radiometric anomalies in the Northern Alabama Piedmont (unpublished): Geological Survey of Alabama, 37 p.

Burns, P. C. and Finch, R., 1999, Uranium: Mineralogy, Geochemistry, and the Environment: Washington DC, The Mineralogical Society of America, 679 p.

Cameron, E. N. and Weis, P.L., 1960, Strategic graphite a survey, An appraisal of domestic resources: United States Geological Survey Bulletin 1082-E, p. 201-321.

Chenoweth, W. and McLemore, V.T., 1989, Uranium resources of the Colorado Plateau: Energy Frontiers in the Rockies, p. 153-165.

Clark, G. H., 1921, Mica deposits of Alabama: Geological Survey of Alabama, Bulletin 24, 115 p.

Cook, R. B. and Mallette, R. E., 1979, Reconnaissance uranium exploration in Coosa and Clay Counties, Alabama: Birmingham, Reese E. Mallette Associates Inc., 21 p.

Cook, R. B., Hicks, B. K. and Beg, M. A., 1982, Reconnaissance uranium exploration in Coosa and Clay Counties, Alabama: Geological Survey of Alabama, Circular 107, 27 p.

Cook, R. B., Dean, L. D. and Foord, E.E., 1987, Tin-Tantalum mineralization associated with the Rockford Granites, Coosa County, Alabama *in* Drummond, M., and Green, N., eds., Granites of Alabama: Geological Survey of Alabama, p. 209-220.

Dahlkamp, F., J., 1993, Uranium Ore Deposits: Springer-Verlag, Berlin, Federal Republic of Germany, 460 p.

Dean, L.S. and Cook, R. B., 1987, Some geochemical aspects of tin mineralization related to granitic rocks of the Northern Alabama Piedmont Granites of Alabama: *in* Drummond, M., and Green, N., eds., Granites of Alabama: Geological Survey of Alabama, p.199-207.

Dean, L. S., 1989, A review of gold mining and exploration in Alabama, *in* Lesher, C. M., Cook, R. B., and Dean, L. S., Gold deposits of Alabama: Geological Survey of Alabama Bulletin 136, p. 1-7.

Dean, L.S., 2007, Minerals in the economy of Alabama, 2007: Geological Survey of Alabama Information Series 64R, 23 p.

DeVoto, R. H., 1978, Uranium Geology and Exploration: Short course lecture notes and references, Colorado School of Mines, 396 p.

Drummond, M.S., 1986, Igneous, metamorphic, and structural history of the Alabama tin belt, Coosa County, Alabama, [Ph.D. dissertation]: Florida State University, Tallahassee, Florida, 411 p.

Drummond, M., 1987a, Rockford Granite, Coosa County, Alabama; Alkali metasomatism and trondhjemite genesis, *in* Drummond, M. and Green, N., eds., Granites of Alabama: Alabama Geological Survey, p. 117-130.

Drummond, M., 1987b, Rockford Granite, Coosa County, Alabama; I. Geologic setting, occurrence, petrography and mineral chemistry, *in* Drummond, M. and Green, N., eds., Granites of Alabama: Geological Survey of Alabama, p. 131-153.

Drummond, M., and Allison, D. T., 1987, Rockford Granite, Coosa County, Alabama; III, Igneous petrogenesis and tectonic setting, *in* Drummond, M. and Green, N., eds., Granites of Alabama: Geological Survey of Alabama, p. 154-182.

Drummond, M. S., Ragland, P. C., Wesolowski, D., 1986, An example of trondhjemite genesis by means of alkali metasomatism: Rockford Granite, Alabama Appalachians: Contributions to Mineralology and Petrology, v. 93, p. 98-113.

Dyson, J. L., 1954, Relation of stratigraphy and structure to uranium occurrences near Mauch Chunk, Pennsylvania: Proceedings of the Pennsylvania Academy of Science, vol. 28, pp. 124-134.

Epperson, R. S., Rheams, K. F., 1984, Mica in Alabama: Geological Survey of Alabama, Atlas 18, 63 p.

Elevatorski, E. A., 1979, Uranium Deposits in Metamorphic Environments: Dana Point, MINOBRAS, 158 p.

Finch, W. I., 1967, Geology of Epigenetic Uranium Deposits in Sandstone in the United State: U. S. Geological Society Professional Paper P-0538, 121 p.

Finch, W. I., 1996, Uranium provinces of North America-Their definition, distribution and models: United States Geological Survey Bulletin 2141, 18 p.

Foord, E.E. and Cook, R.B., 1989, Mineralogy and Paragenesis of the McAllister Sn-Ta bearing pegmatite, Coosa County, Alabama: Canadian Mineralogist, v. 27, p. 93-105.

Frinak, T.R., 1984, The geology of a part of northeast Coosa County, [Master's thesis]: Auburn University, Auburn, Alabama 173 p.

Gastaldo, R. A., Gutherie, G. M., Steltenpohl, M. G., 1993, Mississippian fossils from Southern Appalachian metamorphic rocks and their implications for Late Paleozoic tectonic evolution: Science, v. 262, no. 5134, p. 732-734.

Gentry, R. V., 1970, Giant radioactive halos; indicators of unknown radioactivity?: Science, v. 169, p. 670-673.

Gabelman, J.W., 1988, Representative uranium deposits and occurrences exclusive of sandstone impregnations and quartz conglomerates: Ore Geology Reviews, v. 3, p. 31-159.

Goldstein, J. I., Yakowitz, H., Newbury, D. E., Lifshin, E., Colby, J. W. and Coleman, J. R., 1975, Practical scanning electron microscopy; electron and ion microprobe analysis: Plenum Press, New York, N.Y., 582 p.

Guthrie, G. M. and Lesher, C. M., 1989, Geologic setting of lode gold deposits in the Northern Piedmont and Brevard Zone, Alabama, *in* Lesher, C. M., Cook, R. B., Dean, L. S., Gold deposits of Alabama: Geological Survey of Alabama Bulletin 136, p. 11-32.

Guthrie, G. M., 1994, Geology of the Columbiana Area, Chilton, Coosa and Shelby Counties, Alabama: Geological Survey of Alabama Bulletin 151, 80 p.

Green, N.L., Usdansky, S. I., Atwood, J. L. and Dechter, J. J., 1986, Occurrence and characterization of barium-vanadium muscovite from the Higgins Ferry Formation, northern Alabama Piedmont: Abstracts with Programs-Geological Society of America, v. 18, no. 3, 224 p.

Heier, K. S., 1979, Movement of uranium during higher grade metamorphic processes: Philosophical Transactions of the Royal Society of London, Series A: Mathematical and Physical Sciences, v. 291, p. 413-421.

Hicks, B. K., 1981, Geology of a portion of the Rockford, Alabama 7 1/2' Quadrangle, Coosa County, Alabama, [unpublished Master's thesis]: Auburn University, Auburn, Alabama, 130 p.

Higgins, M. W., Atkins, R. I., Crawford, T. J., Crawford III, R. F., Brooks, R. and Cook, R. B., 1988, The structure, stratigraphy, and evolution of the Southernmost part of the Appalachian Orogen: United States Geological Survey Professional Paper 1475, 173 p.

Hunter, F. R., 1944, Geology of the Alabama Tin belt: Geological Survey of Alabama Bulletin 54, 61 p.

International Atomic Energy Agency, 2009, World distribution of uranium deposits (UDEPO) with uranium deposit classification: Technical Document 1629, 126 p.

Jones, W.B., 1929, Summary Report on Graphite in Alabama: Geological Survey of Alabama Circular 9, 27 p.

Klemic, H., 1958, Mauch Chunk, Pennsylvania: U. S. Atomic Energy Commission Trace Element Investigation Report TEI 0740, p. 121-126.

Klemic, H. and Baker, H.C., 1954, Occurrences of uranium in Carbon County, Pennsylvania: United States Geological Survey Circular 350, 8 p.

Klemic, H., Warren, J.C. and Taylor, A. R., 1963, Geology and uranium occurrences of the northern half of the Leighton Pennsylvania quadrangle and adjoining areas: United States Geological Survey Bulletin 1138, 93 p.

Lentz, D., 1996, U, Mo, and REE mineralization in late-tectonic granitic pegmatites, southwestern Greenville Province, Canada: Ore Geology Reviews, v. 11, p. 197-227.

Marmont, S., 1987, Ore Deposit models; Unconformity-type uranium deposits: Geoscience Canada, v. 14, p. 219-229.

McMillan, R. H., 1998, Unconformity-associated U, geological fieldwork 1997: British Columbia Ministry of Employment and Investment Paper 1998-1, p. 24G-1–24G-4.

Nash, J.T., 1981, Geology and genesis of major world hard rock uranium deposits –An overview: United States Geological Survey Open-File Report 81-166, 123 p.

Nash, J. T., Granger, H. C., Adams, S.S., 1981, Geology and concepts of genesis of important types of uranium deposits: Economic Geology v. 75, p. 63-116.

Neathery, T. L. and Tull, J. F., 1975, Geologic profiles of the northern Alabama Piedmont: The Alabama Geological Society Annual Field Trip Guide Book, 13, 115 p.

Neathery, T. L., Bentley, R. D., Higgins, M. W. and Zietz, I., 1976, Preliminary interpretation of aeromagnetic and aeroradioactivity maps of the Alabama Piedmont: Geology, v. 4, p. 375-381.

Neathery, T. L., 1977, Mineral resources of Coosa County, Alabama: Geological Survey of Alabama Map 200, 19 p.

Osborne, W. E., Szabo, M.W., Neathery, T.L. and Copeland, C., 1988, Geologic map of Alabama, Northeast Sheet: Tuscaloosa, Geological Survey of Alabama.

Passchier, C. W., and Trouw, R. A. J., 1998, Microtectonics: Springer-Verlag, Berlin, Germany, 289 p.

Pallister, H. D. and Thoenen, J. R., 1948, Flake graphite and vanadium investigation in Clay, Coosa and Chilton Counties, Alabama: U.S. Bureau of Mines Report 4366, 84 p.

Raymond, D. E., Osborne, W. E., Copeland, C. W. and Neathery, T. L., 1988, Alabama Stratigraphy: Geological Survey of Alabama Circular 140, 97 p.

Reed, A. H. Jr., 1950, Investigation of the Coosa tin deposits Coosa County, Ala., U.S. Bureau of Mines Report of Investigations 4704, 33 p.

Rich, R. A., Holland, H. D. and Petersen, U., 1977, Hydrothermal uranium deposits: Amsterdam, Elsevier, 264 p.

Robinson, R. A. and Prave, A. R., 1995, Cratonal contributions to a “classic” molasses: The Carboniferous Pottsville Formation of eastern Pennsylvania revisited: Geology, v. 23, p. 369-372.

Rodgers, J., 1987, The Appalachian-Ouachita orogenic belt: Episodes, v. 10, p. 259-266.

Rose, A., 1999, Uranium, in Shultz, C., ed., The Geology of Pennsylvania: Slippery Rock, Geological Survey of Pennsylvania, p. 549-553.

Russell, G. S., 1978, U-Pb, Rb-Sr, and K-Ar isotopic studies bearing on the tectonic development of the southeastern most Appalachian orogen, Alabama, [Ph.D. dissertation]: Florida State University, Tallahassee, Florida, 209 p.

Ruzicka, V., 1993, Vein Uranium Deposits: Ore Geology Reviews, v. 8, p. 247-276.

Schweitzer, P., 2006, National uranium resource evaluation (NURE) Hydrogeochemical and Stream Sediment Reconnaissance data, USGS.

Simpson, P.R., Brown, G.C., Plant, J. and Ostle, D., 1979, Uranium mineralization and granite magmatism in the British Isles: Philosophical Transactions of the Royal Society of London, Series A: Mathematical and Physical Sciences, v. 291, p. 385-412.

Simpson, T.A. and Neathery, T.L., 1980, Alabama Gold: Geological Society of Alabama Circular 104, 169 p.

Steltenpohl, M. G. and Moore, W. B., 1988, Metamorphism in the Alabama Piedmont: Geological Survey of Alabama Circular 138, 27 p.

Steltenphohl, M. G. and Kunk, M. J., 1993, $^{40}Ar/^{39}Ar$ thermochronology and Alleghanian development of the southernmost Appalachian Piedmont, Alabama and southwest Georgia: Geological Society of America Bulletin, v. 6, p. 819-833.

Steltenpohl, M. G., 2005, A Primer on terrains of the southernmost Appalachians of Alabama and Georgia in Steltenpohl, ed., New perspectives on southernmost Appalachian terrains, Alabama and Georgia: Guidebook for the 42nd Annual Field Trip of the Alabama Geological Society, v. 42, p. 1-18.

Stow, S. H., Neilson, M. J. and Neathery, T. L., 1984, Petrography, geochemistry, and tectonic significance of the amphibolites of the Alabama Piedmont: American Journal of Science, v. 284, p. 414-436.

Thomas, W.A., 1972, Mississippian stratigraphy of Alabama: Geological Survey of Alabama Monograph 12, 121 p.

Tilsley, J. E., 1981, Ore deposit models - 3 genetic considerations relating to some uranium ore deposits: Geoscience Canada, v. 8, p. 3-7.

Tull, J. F., 1978, Structural development of the Alabama Piedmont northwest of the Brevard Zone: American Journal of Science, v. 278, p. 442-460.

Tull, J. F. and Stow, S. H., 1980, The Hillabee Greenstone; a mafic volcanic complex in the Appalachian Piedmont of Alabama: Geological Society of America Bulletin, v. 91, p. 27-36.

Tull, J. F., Barineau, C. I., Mueller, P. A. and Wooden, J. L., 2007, Volcanic arc emplacement onto the southernmost Appalachian Laurentian shelf: Characteristics and constraints: Geological Society of America Bulletin, V. 119, no. 3/4, p. 261-274.

United States Geological Survey, 1971, Flag Mountain, Alabama, 1:24,000. 7.5 Minute Series: United States Geological Survey.

URANERZ U.S.A. Inc., 1977, Geology, sample locations and analysis and alpha-meter radon anomalies in the Weogufka and Moriah Anomaly, unpublished.

Young, E.J., 1985, Summary of the geology, economic aspects, and geochemistry of the Schwartzwalder uranium-bearing area, Ralston Buttes district, Jefferson County, Colorado: Geological Society of America Bulletin, no. 1555, pp. 32.

Wilson, C. J. L., 1977, Combined diffusion-infiltration of uranium in micaceous schists; a study using the fission track method: Contributions to Mineralogy and Petrology, v. 65, p.171-181.

Wallace, A.R. and Karlson, R.C., 1985, The Schwartzwalder Uranium Deposit, I, Geology and structural controls on mineralization: Economic Geology, v. 80, p. 1842-1857.

Wherry, E.T., 1915, Carnotite near Mauch Chunk, Pennsylvania: United States Geological Survey Bulletin B 0580-H, p. 147-151.

APPENDIX I

Petrographic Descriptions

Sample CC20E:

Prograde:

Quartz - 35% Muscovite - 30% Graphite – 15%

Opaque – 5%

Retrograde Weathering:

Sericite – 15%

The sample is a medium- to fine-grained quartz-muscovite-graphitic schist with seriate-polygonal texture. Quartz grains are monocrystalline, anhedral, and slightly undulose. Graphite grains are tabular and occur mainly between quartz grain boundaries, with some occurrences inside muscovite. Graphite occurs parallel to the foliation of the rock. Muscovite grains are found disseminated throughout the rock or as porphyroblasts. Some muscovites have been altered; this is especially true of the porphyroblasts. Alteration begins in the center of the grain, suggesting a chemical change in the rock itself. Some muscovite grains contain accessory monazite, or zircon, which produce pleochroic halos.

Sample CC21:

Prograde:

Quartz - 45% Muscovite - 15% Graphite – 15%

Fibrolite – 10%

Retrograde Weathering:

Sericite – 15%

The sample is a medium- to fine-grained quartz-muscovite-graphitic schist with intragranular-interlobate texture. Quartz grains are polycrystalline, anhedral, and undulose. Graphite grains are tabular and occur mainly between grain boundaries of quartz, with some occurrences inside muscovite. Most of the graphite is randomly oriented throughout the rock. Sericite occurs throughout the rock and some occurs with fibrolite. Muscovite grains often contain shreds of graphite. Accessory monazite and/or zircon are also contained within the muscovite, and pleochroic halos are found surrounding theses accessory grains. Alteration of the micas begins in or near the center of the grain. Parts of the rock have become iron stained.

Sample CC50A:

Prograde: Quartz - 40% Muscovite - 15% Opaque – 15%

Graphite – 5%

Retrograde Weathering:

Sericite – 25%

The sample is a fine-grained quartz-muscovite schist with seriate-polygonal texture. Quartz grains are polycrystalline, anhedral, and undulose. Graphite occurs between quartz grains and is parallel to foliation. Micas are unaltered to very altered. Opaque minerals not identified as graphite are disseminated throughout the rock. Most of the rock appears iron-stained under plane-polarized light.

Sample CC50C:

Prograde:

Quartz - 20% Muscovite - 10% Graphite – 10%

Garnet– 10% Plagioclase – 20%

Retrograde Weathering:

Iron Oxide- 10% Sericite – 20%

The sample is a fine-grained quartz-muscovite-garnet schist having an overall seriate-polygonal texture. Quartz grains are anhedral and undulose. Graphite occurs between quartz grains and is parallel to foliation. Sericite occurs within the rock parallel to the foliation. Potassium feldspars show exsolution lamellae texture. Garnets occur as porphyroblasts that have been weathered to iron oxide.

Sample CC54A:

Prograde:

Quartz – 30% Biotite - 30% Muscovite – 10%

Zircon - 5% Garnet– 10%

Retrograde Weathering:

Iron Oxide – 5% Sericite – 10%

The sample is a fine-grained quartz-biotite-muscovite schist within an overall inequigranular-polygonal texture. Quartz grains are anhedral, undulose, and mostly polycrystalline. Sericite occurs within the rock parallel to foliation; some mica occurs within this 'matrix'. Micas are unaltered. Biotite is reddish brown in plane-polarized light indicating high titanium. Most of the rock appears iron-stained, and most of the garnet has been weathered to iron oxide.

Sample CC54B:

Prograde:

Quartz – 20% Biotite - 20% Fibrolite – 10%

Muscovite – 5%

Retrograde Weathering:

Iron Oxide – 10% Sericite – 25% Calcite – 10%

The sample is a fine-grained quartz-biotite schist. Quartz grains are anhedral, undulose, and polycrystalline. Very fine-grained sericite occurs within the rock parallel to the foliation. Muscovite grains are very small and unaltered. Biotite is reddish brown in plane-polarized light suggesting high titanium. Most of the rock appears iron-stained and much of the garnet has been weathered to iron oxide. Some of the relict garnet also contains calcite.

Sample CC59:

Prograde:

Quartz - 35% Muscovite - 10% Graphite – 15%

Opaque – 10% Fibrolite – 5%

Retrograde Weathering:

Sericite – 20% Iron Oxide – 5%

The sample is a fine-grained quartz-graphite-muscovite schist with an overall seriate-interlobate texture. Quartz grains are monocrystalline, anhedral, and undulose. Graphite occurs between quartz grains and is parallel to foliation. Sericite occurs often with fibrolite. Within the masses of fine-grained mica is an iron-rich mineral, almost isotropic in crossed polars.

Sample CC66:

Prograde:

Quartz - 40% Muscovite - 20% Graphite – 10%

Retrograde Weathering:

Sericite – 30%

The sample is a fine-grained quartz-muscovite-graphite schist with seriate-interlobate texture. Quartz grains are polycrystalline, anhedral, and undulose. Graphite occurs between grain and is parallel to sub-parallel to foliation. The sericite occurs parallel with the foliation. The very-fine grained mica aggregates are possibly altered mica fish and some contain kink-banding. Alteration of mica seems to begin at the edges of the grain.

Sample CC169:

Prograde:

Quartz - 45% Muscovite - 15% Graphite – 10%

Retrograde Weathering:

Sericite – 30%

The sample is a fine-grained quartz-muscovite-graphite schist with seriate-polygonal texture. Quartz grains are monocrystalline, anhedral, and undulose. Graphite occurs between grains and is parallel to sub-parallel to the foliation of the rock. The sericite occurs as porphyroblasts within the foliation, representing altered mica-fish. Some of these mica fish contain unaltered muscovite. Alteration of the micas seem to begin at the edges of the grain.

Sample CC177:

Prograde:

Quartz - 45% Muscovite - 10% Graphite – 15%

Opaque – 10% Sillimanite – 10%

Retrograde Weathering:

Sericite – 10%

The sample is a fine-grained quartz-muscovite-graphite schist with seriate-interlobate

texture. Quartz grains are polycrystalline, anhedral, and undulose. Graphite occurs between grains and is parallel to sub-parallel to the foliation of the rock. Muscovite occurs disseminated throughout the rock and as porphyroblasts with alteration beginning in the center of the grains. The sericite occurs in streaks parallel with foliation. Sillimanite occurs as masses and occurs with sericite.

Sample CC180:

Prograde:

Quartz - 55% Muscovite - 15% Graphite – 10%

Opaque – 5% Fibrolite – 5%

Retrograde Weathering:

Sericite – 10%

The sample is a medium- to fine-grained quartz-muscovite-graphite schist with seriate-interlobate texture. Quartz grains are polycrystalline. Graphite occurs between grains and is parallel to sub-parallel to the foliation of the rock. Muscovite occurs disseminated throughout the rock and as porphyroblasts. Alteration of muscovite to fine-grained mica begins within the muscovite grain. Sericite occurs within foliation planes and is found with fibrolite.

Sample CC219:

Prograde:

Quartz - 60% Muscovite - 15% Graphite – 10%

Opaque – 5% Plagioclase – 10%

Retrograde Weathering:

Sericite – 10%

The sample is a medium- to fine-grained quartz-muscovite-graphitic schist with seriate-

polygonal texture. Quartz grains are monocrystalline and undulose. Graphite occurs between other mineral grains. Muscovite occurs disseminated throughout the rock and as porphyroblasts. The sericite appears to replace the muscovite in several places. In some of the sericite masses, there appear to be fractures within the porphyroblasts that are reminiscent of metamict minerals. Potassium feldspars show exsolution lamellae.

APPENDIX II

Geochemical Data for Rock Samples

Table 10. Whole-Rock and Trace-Element Geochemical Dataset of Rock Samples*

Sample	Ag	Ba	C	Ce	Co	Cr	Cs	Cu	Dy	Er
CC11	0.50	10,000.00	16,100.00	61.70	0.80	120.00	2.84	92.00	3.04	1.42
CC20A	0.50	1,280.00	14,500.00	22.90	0.25	50.00	1.09	11.00	2.63	1.98
CC20E	0.50	1,175.00	14,800.00	20.10	0.25	60.00	1.05	9.00	1.95	1.46
CC21	0.50	1,435.00	19,000.00	29.00	0.60	40.00	1.39	12.00	2.53	1.70
CC34A	0.50	1,410.00	11,800.00	50.30	1.40	50.00	0.72	162.00	4.88	3.19
CC43A	0.50	515.00	5,400.00	63.30	1.10	90.00	0.49	13.00	4.61	2.17
CC43B	0.50	1,005.00	2,600.00	20.30	1.30	5.00	0.52	18.00	1.52	0.92
CC45	0.50	1,285.00	30,100.00	23.80	0.50	40.00	1.65	95.00	2.12	1.24
CC48	0.50	370.00	14,800.00	56.40	0.90	100.00	1.32	31.00	4.04	2.07
CC50A	0.50	987.00	13,600.00	25.80	0.60	130.00	2.10	46.00	4.15	3.06
CC50C	0.50	3,110.00	1,700.00	86.20	3.30	90.00	1.37	27.00	2.46	1.17
CC54A	0.50	945.00	2,100.00	88.60	20.20	100.00	0.55	39.00	5.62	3.31
CC54B	0.50	735.00	2,500.00	97.80	50.80	90.00	3.63	51.00	6.04	3.38
CC59	0.50	5,880.00	50,800.00	46.70	4.20	70.00	2.25	170.00	3.97	2.43
CC66	0.50	1,030.00	14,100.00	37.80	0.70	70.00	1.00	40.00	1.92	0.82
CC73C	0.50	2,630.00	35,800.00	25.30	0.60	60.00	2.34	34.00	3.47	2.62
CC77	0.50	852.00	7,900.00	26.80	2.70	40.00	1.11	32.00	2.46	1.13
CC78	0.50	2,710.00	40,900.00	41.70	1.00	110.00	0.72	251.00	1.64	0.72
CC83	0.50	10,000.00	19,900.00	40.70	2.70	30.00	0.65	92.00	3.08	1.53
CC84	0.50	291.00	4,400.00	71.50	3.10	40.00	0.78	33.00	3.54	1.72
CC90	0.50	1,260.00	1,700.00	44.10	5.60	10.00	0.89	477.00	3.82	2.30
CC95	0.50	2,600.00	1,600.00	115.00	1.60	100.00	5.03	75.00	6.42	3.67
CC110	0.50	1,125.00	26,500.00	38.50	1.20	100.00	2.28	40.00	2.36	1.28
CC124	0.50	4,290.00	26,500.00	13.20	0.70	40.00	2.72	76.00	2.20	1.73
CC169	0.50	1,530.00	22,800.00	23.20	0.05	50.00	1.18	14.00	2.16	1.28
CC173	0.50	327.00	700.00	30.20	42.20	120.00	0.21	52.00	7.40	4.17
CC176A	0.50	1,900.00	15,600.00	14.30	11.10	30.00	1.01	54.00	1.45	0.86
CC177	0.50	2,520.00	25,600.00	49.30	27.30	60.00	3.63	96.00	6.20	3.85
CC178	0.50	2,900.00	18,100.00	96.40	2.30	80.00	2.42	23.00	6.84	3.98
CC180	0.50	1,165.00	13,900.00	21.40	1.90	70.00	1.14	40.00	1.87	1.18
CC186	0.50	2,390.00	21,100.00	66.60	3.00	90.00	1.49	40.00	3.29	1.77
CC191	0.50	2,710.00	32,100.00	31.50	0.80	40.00	1.40	27.00	2.82	1.76
CC207	0.50	1,540.00	51,700.00	49.30	1.70	90.00	1.59	107.00	5.29	2.19
CC219	0.50	1,840.00	21,500.00	28.90	0.90	70.00	1.71	38.00	2.88	1.93

*Data are reported are ppm

Table 10. Whole-Rock and Trace-Element Geochemical Dataset of Rock Samples (cont.)*

Sample	Eu	Ga	Gd	Hf	Ho	La	Lu	Mo	Nb	Nd	Ni
CC11	1.02	27.10	4.47	4.10	0.53	31.90	0.19	56.00	15.30	28.00	2.50
CC20A	0.34	10.60	2.33	2.80	0.61	12.10	0.32	25.00	7.10	10.60	2.50
CC20E	0.32	11.30	1.88	2.50	0.44	10.80	0.22	21.00	7.10	9.40	2.50
CC21	0.61	11.50	2.87	1.70	0.55	15.50	0.25	32.00	7.20	14.40	2.50
CC34A	1.05	20.40	4.94	2.00	1.00	28.10	0.41	41.00	7.10	25.60	2.50
CC43A	1.35	15.70	5.90	10.70	0.81	30.80	0.25	2.00	16.50	29.80	10.00
CC43B	0.34	7.70	1.86	3.80	0.29	7.90	0.13	4.00	4.10	10.00	2.50
CC45	0.48	14.30	2.58	2.90	0.42	13.00	0.17	46.00	6.60	13.10	2.50
CC48	1.17	11.60	5.74	2.30	0.79	28.60	0.26	6.00	8.50	27.10	5.00
CC50A	0.88	15.70	3.74	2.30	0.96	19.50	0.39	25.00	9.10	18.40	2.50
CC50C	0.88	17.60	3.57	8.90	0.40	24.80	0.16	3.00	16.70	19.10	8.00
CC54A	1.10	22.80	7.26	12.40	1.09	43.00	0.45	1.00	23.70	40.00	44.00
CC54B	1.10	24.40	7.85	9.80	1.15	44.90	0.43	1.00	21.60	43.20	37.00
CC59	1.11	21.90	4.17	4.30	0.80	23.40	0.33	80.00	13.30	21.80	5.00
CC66	0.75	9.30	3.47	1.70	0.30	20.40	0.09	9.00	5.80	20.50	2.50
CC73C	0.58	18.30	2.45	3.20	0.82	13.60	0.39	67.00	12.80	10.50	2.50
CC77	0.65	8.70	2.81	1.30	0.43	13.50	0.11	23.00	5.50	14.10	2.50
CC78	0.62	63.70	2.67	2.20	0.24	21.50	0.07	90.00	9.10	17.40	2.50
CC83	0.93	8.80	3.75	2.10	0.53	21.50	0.20	41.00	5.70	19.40	32.00
CC84	0.85	14.20	5.35	13.80	0.61	32.10	0.25	2.00	13.40	29.40	15.00
CC90	1.07	10.10	4.18	0.90	0.72	26.30	0.28	4.00	3.60	19.80	159.00
CC95	1.75	43.10	8.68	6.80	1.26	63.40	0.52	11.00	23.20	49.80	12.00
CC110	0.70	13.00	3.08	2.30	0.45	23.10	0.17	41.00	7.50	17.80	5.00
CC124	0.28	14.20	1.51	2.70	0.54	6.90	0.26	61.00	8.80	5.60	2.50
CC169	0.68	12.70	2.53	1.70	0.45	12.60	0.19	29.00	6.10	12.30	2.50
CC173	2.40	22.60	6.99	4.40	1.48	14.80	0.55	2.00	14.00	22.30	31.00
CC176A	0.32	8.40	1.51	1.10	0.28	7.30	0.12	22.00	4.70	7.30	64.00
CC177	1.39	14.20	6.35	2.90	0.28	24.70	0.54	54.00	11.80	25.90	212.00
CC178	1.30	30.20	8.53	4.60	1.28	47.70	0.49	34.00	67.50	49.80	21.00
CC180	0.40	10.40	2.29	1.50	0.38	12.00	0.18	20.00	5.10	11.10	5.00
CC186	1.01	13.90	4.92	2.60	0.62	42.20	0.25	47.00	9.30	30.90	15.00
CC191	0.45	10.80	3.09	2.60	0.60	16.00	0.22	52.00	8.30	14.70	2.50
CC207	1.41	10.20	7.11	1.80	0.86	31.30	0.16	6.00	5.50	33.30	12.00
CC219	0.53	15.30	3.10	2.60	0.62	16.20	0.28	51.00	9.90	15.60	16.00

*Data are reported are ppm

Table 10. Whole-Rock and Trace-Element Geochemical Dataset of Rock Samples (cont.)*

Sample	Pb	Pr	Rb	S	Sm	Sn	Sr	Ta	Tb	Th	Tl
CC11	28.00	7.52	149.50	200.00	5.60	3.00	42.00	1.10	0.62	13.05	1.40
CC20A	10.00	2.94	55.20	50.00	2.15	1.00	33.50	0.50	0.40	6.43	0.70
CC20E	10.00	2.49	56.40	300.00	1.80	1.00	31.30	0.50	0.30	5.33	0.90
CC21	14.00	3.81	54.40	200.00	2.80	1.00	39.50	0.50	0.41	5.52	0.80
CC34A	9.00	6.78	35.20	500.00	5.02	3.00	143.00	0.80	0.79	6.40	0.25
CC43A	16.00	7.74	26.90	100.00	6.14	1.00	40.90	0.70	0.88	13.85	0.25
CC43B	19.00	2.49	25.70	2,000.00	2.07	1.00	7.70	0.20	0.25	4.52	0.25
CC45	6.00	3.36	80.50	100.00	2.73	1.00	24.30	0.50	0.39	6.30	0.80
CC48	20.00	6.85	46.80	100.00	5.64	2.00	80.10	0.60	0.83	7.19	0.25
CC50A	20.00	4.86	77.00	400.00	3.50	2.00	17.70	0.60	0.62	6.06	0.80
CC50C	13.00	5.20	84.90	400.00	3.74	1.00	96.00	0.90	0.45	13.20	0.50
CC54A	9.00	10.65	141.50	300.00	7.94	2.00	46.00	1.20	1.02	15.90	0.25
CC54B	10.00	11.30	126.00	400.00	8.36	2.00	34.70	1.10	1.12	16.35	0.60
CC59	11.00	5.78	89.30	300.00	4.12	2.00	41.90	0.80	0.63	9.74	1.40
CC66	12.00	5.21	47.50	300.00	3.91	1.00	36.50	0.40	0.42	5.51	0.50
CC73C	11.00	2.96	94.00	100.00	2.18	2.00	47.00	0.80	0.46	7.79	1.60
CC77	10.00	3.61	36.20	200.00	3.00	1.00	30.70	0.30	0.43	3.65	0.60
CC78	14.00	5.01	30.70	700.00	3.36	2.00	14.30	0.50	0.34	8.19	0.25
CC83	11.00	5.16	30.70	8,300.00	4.14	1.00	52.10	0.40	0.54	4.78	0.25
CC84	8.00	7.87	16.00	300.00	5.86	1.00	8.50	0.80	0.73	12.95	0.25
CC90	25.00	5.39	50.00	600.00	4.22	1.00	41.00	0.10	0.57	16.75	0.50
CC95	55.00	14.60	143.50	100.00	9.39	4.00	107.00	1.70	1.26	19.00	1.20
CC110	15.00	5.09	71.40	100.00	3.33	1.00	35.20	0.50	0.45	6.62	0.90
CC124	6.00	1.54	82.00	600.00	1.22	1.00	24.60	0.60	0.30	6.41	1.70
CC169	12.00	3.15	64.10	100.00	2.60	1.00	39.80	0.40	0.38	4.91	1.00
CC173	2.50	5.06	5.20	500.00	6.18	2.00	389.00	1.00	1.25	1.29	0.25
CC176A	10.00	1.89	29.80	7,300.00	1.58	1.00	34.50	0.30	0.24	3.05	0.60
CC177	9.00	6.46	87.90	38,100.00	5.79	1.00	98.70	0.70	0.99	7.96	2.00
CC178	6.00	12.75	154.50	100.00	10.15	2.00	127.00	8.10	1.22	18.40	0.80
CC180	7.00	2.85	49.70	200.00	2.28	1.00	50.10	0.30	0.33	4.48	0.70
CC186	10.00	8.43	72.00	200.00	5.41	2.00	76.40	0.70	0.63	7.10	0.60
CC191	13.00	3.80	51.90	200.00	2.99	1.00	25.90	0.60	0.49	4.54	1.00
CC207	18.00	8.05	67.00	50.00	7.35	1.00	66.90	0.40	1.02	5.00	0.70
CC219	9.00	3.99	78.30	200.00	3.04	1.00	26.40	0.70	0.47	7.02	1.50

*Data are reported are ppm

Table 10. Whole-Rock and Trace-Element Geochemical Dataset of Rock Samples (cont.)*

Sample	Tm	U	V	W	Y	Yb	Zn
CC11	0.19	4.96	191.00	2.00	11.40	1.28	62.00
CC20A	0.30	3.63	883.00	3.00	19.60	1.97	13.00
CC20E	0.21	2.98	959.00	2.00	14.60	1.43	13.00
CC21	0.24	4.10	1,030.00	3.00	17.40	1.65	19.00
CC34A	0.43	10.10	242.00	6.00	26.40	2.76	27.00
CC43A	0.27	3.59	124.00	2.00	19.30	1.64	102.00
CC43B	0.12	9.16	17.00	5.00	7.50	1.04	64.00
CC45	0.17	3.24	466.00	5.00	11.20	1.04	19.00
CC48	0.27	3.64	183.00	4.00	19.70	1.72	19.00
CC50A	0.43	3.18	1,180.00	2.00	29.80	2.82	13.00
CC50C	0.15	4.67	134.00	5.00	9.20	1.08	56.00
CC54A	0.44	2.82	182.00	9.00	27.00	3.14	104.00
CC54B	0.48	3.19	177.00	2.00	28.30	3.14	131.00
CC59	0.32	3.91	315.00	6.00	21.80	2.21	54.00
CC66	0.09	8.45	338.00	3.00	7.80	0.51	29.00
CC73C	0.39	4.21	348.00	3.00	26.50	2.60	16.00
CC77	0.13	20.60	497.00	2.00	9.40	0.84	15.00
CC78	0.07	17.55	751.00	6.00	5.50	0.56	21.00
CC83	0.19	31.70	145.00	5.00	13.00	1.29	117.00
CC84	0.22	2.95	86.00	2.00	15.00	1.62	57.00
CC90	0.29	9.70	140.00	3.00	18.20	1.94	1,410.00
CC95	0.53	7.10	223.00	3.00	28.90	3.46	32.00
CC110	0.17	7.94	1,010.00	8.00	11.50	1.14	25.00
CC124	0.28	4.43	195.00	6.00	16.60	1.74	24.00
CC169	0.18	3.54	847.00	2.00	13.40	1.25	26.00
CC173	0.58	0.41	294.00	5.00	35.00	3.69	114.00
CC176A	0.13	10.05	231.00	2.00	7.80	0.81	177.00
CC177	0.56	21.30	322.00	3.00	40.30	3.66	512.00
CC178	0.55	4.81	479.00	8.00	37.90	3.63	43.00
CC180	0.16	5.43	859.00	2.00	11.90	1.10	242.00
CC186	0.26	9.87	910.00	2.00	18.70	1.61	80.00
CC191	0.24	6.82	190.00	3.00	16.80	1.56	25.00
CC207	0.21	10.80	558.00	8.00	18.50	1.36	44.00
CC219	0.28	4.47	1,200.00	3.00	19.60	1.87	21.00

*Data are reported in ppm

Table 11. Whole-Rock Oxide-Weight Percentage Analytical Data*

Sample	SiO_2	Al_2O_3	Fe_2O_3	CaO	MgO	Na_2O
CC20E	88.70	5.62	0.66	0.01	0.21	0.23
CC21	88.40	5.36	0.80	0.01	0.22	0.16
CC34A	63.00	10.75	17.80	0.13	0.11	1.06
CC43B	28.80	7.90	50.20	0.06	0.11	0.06
CC50A	82.20	7.14	3.04	0.01	0.44	0.15
CC50C	67.90	10.75	10.55	<.01	0.25	0.22
CC54A	64.40	14.35	9.60	0.05	1.03	0.13
CC54B	60.00	15.85	10.55	0.08	0.98	0.11
CC59	60.30	8.29	17.05	<.01	0.44	0.16
CC66	79.80	5.63	7.50	<.01	0.23	0.09
CC73C	75.10	8.99	4.90	<.01	0.50	0.12
CC77	83.80	3.66	7.67	0.05	0.21	0.03
CC78	56.50	3.69	28.10	<.01	0.22	0.05
CC83	41.40	7.21	34.10	0.02	0.24	<.01
CC84	83.40	8.81	3.39	0.01	0.15	0.02
CC90	41.10	11.95	36.00	0.03	0.12	0.10
CC169	84.30	6.29	1.48	<.01	0.26	0.10
CC176A	83.30	3.89	5.60	0.41	0.44	0.04
CC177	71.40	8.47	5.84	0.84	1.10	0.36
CC180	86.80	5.21	0.79	0.12	0.41	0.20
CC191	81.50	5.02	4.35	0.01	0.31	0.06
CC219	79.50	8.19	2.72	0.03	0.37	0.14

*Data are reported in percent

Table 11. Whole-Rock Oxide-Weight Percentage Analytical Data (cont.)*

Sample	K_2O	Cr_2O_3	TiO_2	MnO	P_2O_5	SrO	BaO
CC20E	1.36	0.01	0.38	<.01	<.01	<.01	0.15
CC21	1.37	0.01	0.34	<.01	0.01	<.01	0.18
CC34A	1.08	0.01	0.22	0.01	0.34	0.02	0.18
CC43B	0.73	0.01	0.38	0.02	0.10	<.01	0.13
CC50A	2.07	0.02	0.44	0.01	0.04	<.01	0.12
CC50C	2.36	0.01	0.93	0.03	0.14	0.01	0.38
CC54A	3.29	0.01	1.47	0.05	0.07	0.01	0.11
CC54B	2.83	0.01	1.20	0.08	0.13	<.01	0.09
CC59	2.22	0.01	0.58	0.01	0.06	0.01	0.70
CC66	1.35	0.01	0.31	0.01	0.08	<.01	0.12
CC73C	2.65	0.01	0.57	0.01	0.03	0.01	0.34
CC77	0.82	0.01	0.24	0.01	0.28	<.01	0.10
CC78	0.70	0.02	0.38	0.01	0.37	<.01	0.34
CC83	0.78	0.01	0.28	0.01	0.66	<.01	4.29
CC84	0.38	0.01	0.66	0.01	0.02	<.01	0.03
CC90	1.75	<.01	0.07	0.02	0.12	<.01	0.16
CC169	1.56	0.01	0.30	0.01	0.03	<.01	0.18
CC176A	0.75	<.01	0.20	0.02	0.12	<.01	0.24
CC177	2.07	0.01	0.49	0.02	0.19	0.01	0.30
CC180	1.22	0.01	0.26	0.01	0.06	0.01	0.14
CC191	1.38	<.01	0.33	0.01	0.03	<.01	0.33
CC219	2.04	0.01	0.45	0.01	0.01	<.01	0.23

*Data are reported in ppm

Table 12. Sulfur and Carbon in Rock Samples*

Sample	C	S
CC11	16,100.00	200.00
CC20A	14,500.00	50.00
CC20E	14,800.00	300.00
CC21	19,000.00	200.00
CC34A	11,800.00	500.00
CC43A	5,400.00	100.00
CC43B	2,600.00	2,000.00
CC45	30,100.00	100.00
CC48	14,800.00	100.00
CC50A	13,600.00	400.00
CC50C	1,700.00	400.00
CC54A	2,100.00	300.00
CC54B	2,500.00	400.00
CC59	50,800.00	300.00
CC66	14,100.00	300.00
CC73C	35,800.00	100.00
CC77	7,900.00	200.00
CC78	40,900.00	700.00
CC83	19,900.00	8,300.00
CC84	4,400.00	300.00
CC90	1,700.00	600.00
CC95	1,600.00	100.00
CC110	26,500.00	100.00
CC124	26,500.00	600.00
CC169	22,800.00	100.00
CC173	700.00	500.00
CC176A	15,600.00	7,300.00
CC177	25,600.00	38,100.00
CC178	18,100.00	100.00
CC180	13,900.00	200.00
CC186	21,100.00	200.00
CC191	32,100.00	200.00
CC207	51,700.00	50.00
CC219	21,500.00	200.00

*Data reported in ppm

APPENDIX III

Geochemical Data for "Roscoelite"

Table 13. Trace-Element and Whole-Rock Analyses of Handpicked Micas*

Sample	Ag	Ba	Ce	Co	Cr	Cs	Cu	Dy	Er
CC20E	0.50	5300.00	41.60	0.25	360.00	5.78	15.00	3.43	2.56
CC21	0.50	7730.00	22.80	0.25	220.00	6.61	21.00	7.81	6.68
CC50A	0.50	2500.00	19.30	0.25	360.00	4.92	44.00	5.61	4.47
CC50C	0.50	9630.00	95.10	2.80	120.00	3.95	41.00	1.35	0.62
CC54B	0.50	565.00	89.60	4.60	100.00	1.66	35.00	22.40	15.30
CC59	0.50	10000.00	19.20	0.25	100.00	4.12	188.00	4.27	3.53
CC66	0.50	4160.00	10.90	0.25	400.00	6.35	62.00	0.62	0.38
CC169	0.50	8150.00	49.60	1.30	220.00	4.97	22.00	3.63	2.64
CC180	3.00	5090.00	50.80	0.25	350.00	5.48	58.00	7.24	5.45
CC219	0.50	5820.00	54.80	0.60	210.00	6.49	33.00	6.10	4.47

*Data reported in ppm

Table 13. Trace-Element and Whole-Rock Analyses of Handpicked Micas (cont.)*

Sample	Eu	Ga	Gd	Hf	Ho	La	Lu	Mo	Nb
CC20E	0.72	53.10	3.77	4.00	0.84	23.30	0.41	9.00	11.70
CC21	0.85	61.60	4.32	4.50	1.99	12.60	1.05	15.00	11.40
CC50A	0.88	45.40	3.75	3.20	1.39	13.70	0.62	11.00	17.60
CC50C	0.65	40.60	2.78	11.20	0.22	18.40	0.12	1.00	16.10
CC54B	1.43	45.30	12.30	5.50	5.30	44.20	1.42	1.00	3.40
CC59	0.87	42.40	2.55	4.60	1.06	9.70	0.56	60.00	27.60
CC66	0.40	57.90	0.96	4.50	0.13	7.60	0.11	8.00	8.20
CC169	0.84	54.60	2.92	8.90	0.85	12.40	0.50	8.00	19.20
CC180	0.97	58.60	6.35	5.80	1.71	28.20	0.96	24.00	10.50
CC219	1.04	61.70	6.57	6.90	1.41	30.00	0.72	22.00	15.10

*Data reported in ppm

Table 13. Trace-Element and Whole-Rock Analyses of Handpicked Micas (cont.)*

Sample	Ni	Pb	Pr	Rb	Sm	Sn	Sr	Ta	Tb
CC20E	2.50	18.00	5.24	306.00	3.67	7.00	130.00	0.80	0.58
CC21	2.50	19.00	2.98	319.00	2.86	8.00	107.00	0.70	0.96
CC50A	2.50	11.00	3.33	224.00	2.88	5.00	36.00	1.10	0.71
CC50C	6.00	12.00	4.34	269.00	3.20	6.00	267.00	0.90	0.33
CC54B	12.00	2.50	10.90	81.10	9.05	4.00	82.50	0.20	2.85
CC59	2.50	5.00	2.23	174.00	1.86	4.00	79.60	1.70	0.54
CC66	2.50	9.00	1.62	321.00	0.99	10.00	84.90	0.40	0.13
CC169	2.50	7.00	2.99	306.00	2.56	6.00	178.50	1.30	0.52
CC180	2.50	11.00	6.89	302.00	5.44	6.00	194.00	0.70	1.11
CC219	18.00	10.00	7.29	315.00	5.88	7.00	75.10	1.00	1.01

*Data reported in ppm

Table 13. Trace-Element and Whole-Rock Analyses of Handpicked Micas (cont.)*

Sample	Th	Tl	Tm	U	V	W	Y	Yb	Zn	Zr
CC20E	9.06	4.90	0.36	5.01	5420.00	3.00	27.60	2.56	51.00	133.00
CC21	4.62	4.90	0.99	6.75	6370.00	5.00	73.70	6.80	70.00	145.00
CC50A	4.22	3.00	0.63	3.66	4290.00	2.00	47.00	4.18	21.00	105.00
CC50C	8.01	2.20	0.08	2.10	337.00	1.00	6.30	0.70	60.00	366.00
CC54B	13.25	0.70	1.94	3.50	158.00	1.00	150.50	10.55	52.00	173.00
CC59	5.76	4.20	0.52	3.98	446.00	2.00	35.10	3.47	34.00	146.00
CC66	4.57	3.30	0.07	2.79	2800.00	2.00	4.00	0.56	23.00	155.00
CC169	6.69	4.60	0.41	5.09	2900.00	1.00	28.80	3.02	37.00	297.00
CC180	9.32	3.90	0.85	9.16	6290.00	2.00	58.60	5.71	86.00	193.00
CC219	9.63	6.20	0.65	6.87	5690.00	3.00	47.10	4.48	40.00	232.00

*Data reported in ppm

APPENDIX IV

Microprobe Results

Table 14. Microprobe Analyses of Unaltered Micas*

Oxide Weight Percent	CC219A.2d	CC219A.2e	CC219A.4a	CC219A.4b	CC219A.4c
V2O5	1.22	1.23	1.19	1.32	1.28
SiO2	48.28	47.19	47.38	47.25	47.13
TiO2	1.70	1.82	1.79	1.74	1.78
UO2	1.70	1.87	1.84	1.91	1.96
Al2O3	33.60	33.52	32.90	33.24	33.22
Cr2O3	0.03	0.16	0.08	0.03	0.10
FeO	0.13	0.32	0.17	0.22	0.24
MgO	1.67	1.65	1.94	1.90	1.84
MnO	0.01	0.05	0.05	0.02	0.00
CaO	0.01	0.00	0.00	0.00	0.00
BaO	0.96	0.86	0.74	0.73	0.74
CuO	0.00	0.00	0.01	0.00	0.01
Na2O	0.47	0.39	0.33	0.40	0.38
K20	9.74	9.85	10.20	9.73	9.86
Cl	0.00	0.00	0.01	0.00	0.00
Total	99.52	98.92	98.63	98.50	98.54
Mineral Formulas on Basis of 22 Oxygen					
V	0.10	0.11	0.10	0.11	0.11
Si	6.21	6.14	6.18	6.16	6.15
Ti	0.16	0.18	0.18	0.17	0.17
U	0.05	0.05	0.05	0.06	0.06
iv AL	1.79	1.86	1.82	1.84	1.85
vi AL	3.31	3.27	3.24	3.26	3.25
Cr	0.00	0.02	0.01	0.00	0.01
Fe	0.01	0.04	0.02	0.02	0.03
Mg	0.32	0.32	0.38	0.37	0.36
Mn	0.00	0.01	0.01	0.00	0.00
Ca	0.00	0.00	0.00	0.00	0.00
Ba	0.05	0.04	0.04	0.04	0.04
Cu	0.00	0.00	0.00	0.00	0.00
Na	0.12	0.10	0.08	0.10	0.10
K	1.60	1.63	1.70	1.62	1.64
Si + iv Al	8.00	8.00	8.00	8.00	8.00
Sum vi	3.81	3.81	3.81	3.83	3.81
Na+K+Ca+Ba	1.77	1.78	1.82	1.76	1.78
% Paragonite	0.07	0.06	0.05	0.06	0.05
% Muscovite	0.90	0.92	0.93	0.92	0.92
% Margerite	0.00	0.00	0.00	0.00	0.00
% Ba-Mica	0.03	0.02	0.02	0.02	0.02

*Locations of probe sites are in Appendix V

Table 14. Microprobe Analyses of Unaltered Micas* (cont.)

Oxide Weight Percent	CC180.2b	CC180.2c	CC180.1a	CC180.1b	CC169.1b	CC169.1c
V2O5	1.55	1.41	1.23	1.31	2.20	2.04
SiO2	47.64	46.72	47.17	46.98	48.94	47.36
TiO2	1.78	1.51	1.62	1.62	1.16	1.10
UO2	1.63	1.71	1.95	1.82	1.23	1.85
Al2O3	32.99	33.88	33.71	33.92	35.39	33.99
Cr2O3	0.08	0.09	0.01	0.09	0.09	0.08
FeO	0.09	0.10	0.05	0.07	0.14	0.14
MgO	1.89	1.70	1.74	1.70	1.09	1.12
MnO	0.07	0.08	0.06	0.05	0.00	0.21
CaO	0.02	0.00	0.03	0.02	0.00	0.02
BaO	0.80	0.75	0.70	0.78	0.53	0.59
CuO	0.05	0.00	0.00	0.00	0.08	0.02
Na2O	0.49	0.45	0.48	0.48	0.24	0.59
K20	9.57	9.98	9.53	10.21	9.07	9.24
Cl	0.00	0.01	0.02	0.00	0.00	0.00
Total	98.66	98.40	98.30	99.06	100.17	98.35
Mineral Formulas on Basis of 22 Oxygen						
V	0.13	0.12	0.11	0.11	0.18	0.18
Si	6.18	6.10	6.15	6.10	6.17	6.15
Ti	0.17	0.15	0.16	0.16	0.11	0.11
U	0.05	0.05	0.06	0.05	0.03	0.05
iv AL	1.82	1.90	1.85	1.90	1.83	1.85
vi AL	3.23	3.31	3.33	3.29	3.43	3.35
Cr	0.01	0.01	0.00	0.01	0.01	0.01
Fe	0.01	0.01	0.01	0.01	0.01	0.02
Mg	0.36	0.33	0.34	0.33	0.21	0.22
Mn	0.01	0.01	0.01	0.01	0.00	0.02
Ca	0.00	0.00	0.00	0.00	0.00	0.00
Ba	0.04	0.04	0.04	0.04	0.03	0.03
Cu	0.00	0.00	0.00	0.00	0.01	0.00
Na	0.12	0.12	0.12	0.12	0.06	0.15
K	1.59	1.66	1.58	1.69	1.46	1.53
Si + iv Al	8.00	8.00	8.00	8.00	8.00	8.00
Sum vi	3.78	3.81	3.84	3.79	3.76	3.71
Na+K+Ca+Ba	1.75	1.82	1.75	1.86	1.54	1.71
% Paragonite	0.07	0.06	0.07	0.07	0.04	0.09
% Muscovite	0.90	0.92	0.91	0.91	0.94	0.89
% Margerite	0.00	0.00	0.00	0.00	0.00	0.00
% Ba-Mica	0.02	0.02	0.02	0.02	0.02	0.02

*Locations of probe sites are in Appendix V

Table 14. Microprobe Analyses of Unaltered Micas* (cont.)

Oxide Weight Percent	CC20E.1a	CC20E.1c	CC20E.5b	CC20E.5d	CC20E.4a	CC20E.4b
V2O5	1.63	2.00	1.72	1.73	2.43	2.50
SiO2	47.25	47.17	47.08	46.91	46.78	50.46
TiO2	1.54	1.78	1.65	1.79	1.79	2.00
UO2	1.45	1.65	1.82	1.68	1.80	1.79
Al2O3	32.86	32.59	33.29	33.18	32.46	31.71
Cr2O3	0.22	0.09	0.10	0.00	0.12	0.18
FeO	0.24	0.17	0.13	0.11	0.07	0.11
MgO	1.69	1.88	1.84	1.65	1.85	2.00
MnO	0.08	0.10	0.00	0.02	0.09	0.03
CaO	0.01	0.01	0.00	0.01	0.02	0.01
BaO	0.70	0.73	0.82	0.82	0.68	0.73
CuO	0.03	0.00	0.00	0.06	0.02	0.00
Na2O	0.58	0.48	0.75	0.54	0.56	0.20
K20	9.43	9.79	9.51	9.67	9.74	1.72
Cl	0.01	0.02	0.01	0.01	0.00	0.00
Total	97.71	98.46	98.72	98.19	98.43	93.43
Mineral Formulas on Basis of 22 Oxygen						
V	0.14	0.17	0.15	0.15	0.21	0.21
Si	6.18	6.15	6.12	6.13	6.11	6.54
Ti	0.15	0.17	0.16	0.18	0.18	0.19
U	0.04	0.05	0.05	0.05	0.05	0.05
iv AL	1.82	1.85	1.88	1.87	1.89	1.46
vi AL	3.25	3.16	3.22	3.24	3.10	3.38
Cr	0.02	0.01	0.01	0.00	0.01	0.02
Fe	0.03	0.02	0.01	0.01	0.01	0.01
Mg	0.33	0.37	0.36	0.32	0.36	0.39
Mn	0.01	0.01	0.00	0.00	0.01	0.00
Ca	0.00	0.00	0.00	0.00	0.00	0.00
Ba	0.04	0.04	0.04	0.04	0.03	0.04
Cu	0.00	0.00	0.00	0.01	0.00	0.00
Na	0.15	0.12	0.19	0.14	0.14	0.05
K	1.57	1.63	1.58	1.61	1.62	0.28
Si + iv Al	8.00	8.00	8.00	8.00	8.00	8.00
Sum vi	3.76	3.72	3.75	3.75	3.65	3.97
Na+K+Ca+Ba	1.76	1.79	1.81	1.79	1.80	0.37
% Paragonite	0.08	0.07	0.10	0.08	0.08	0.13
% Muscovite	0.89	0.91	0.87	0.90	0.90	0.76
% Margerite	0.00	0.00	0.00	0.00	0.00	0.00
% Ba-Mica	0.02	0.02	0.02	0.02	0.02	0.10

*Locations of probe sites are in Appendix V

Table 14. Microprobe Analyses of Unaltered Micas* (cont.)

Oxide Weight Percent	CC20E.4b	CC20E.4d	CC180.4a	CC180.4b
V2O5	2.19	1.98	1.64	1.64
SiO2	45.76	47.77	46.57	48.02
TiO2	0.40	1.64	1.80	1.77
UO2	1.51	2.06	1.85	1.83
Al2O3	32.90	32.97	33.18	33.44
Cr2O3	0.17	0.06	0.04	0.05
FeO	0.31	0.22	0.13	0.15
MgO	1.55	1.88	1.86	1.89
MnO	0.02	0.00	0.00	0.06
CaO	0.05	0.01	0.00	0.03
BaO	0.78	0.68	0.86	0.79
CuO	0.04	0.06	0.00	0.00
Na2O	1.04	0.34	0.39	0.27
K20	8.05	9.74	9.80	9.66
Cl	0.00	0.00	0.01	0.00
Total	94.76	99.43	98.13	99.62
Mineral Formulas on Basis of 22 Oxygen				
V	0.19	0.17	0.14	0.14
Si	6.14	6.17	6.10	6.17
Ti	0.04	0.16	0.18	0.17
U	0.05	0.06	0.05	0.05
iv AL	1.86	1.83	1.90	1.83
vi AL	3.35	3.18	3.22	3.24
Cr	0.02	0.01	0.00	0.01
Fe	0.03	0.02	0.01	0.02
Mg	0.31	0.36	0.36	0.36
Mn	0.00	0.00	0.00	0.01
Ca	0.01	0.00	0.00	0.00
Ba	0.04	0.03	0.04	0.04
Cu	0.00	0.01	0.00	0.00
Na	0.27	0.08	0.10	0.07
K	1.38	1.60	1.64	1.58
Si + iv Al	8.00	8.00	8.00	8.00
Sum vi	3.74	3.73	3.78	3.79
Na+K+Ca+Ba	1.70	1.72	1.78	1.69
% Paragonite	0.16	0.05	0.06	0.04
% Muscovite	0.81	0.93	0.92	0.93
% Margerite	0.00	0.00	0.00	0.00
% Ba-Mica	0.02	0.02	0.02	0.02

*Locations of probe sites are in Appendix V

Table 16. Microprobe Analyses of Altered Micas*

Oxide Weight Percent	CC219A.1a	CC219A.1b	CC219A.1c	CC219A.1d	CC219A.1e
V2O5	0.37	0.40	0.35	0.41	0.35
SiO2	43.23	47.64	44.86	46.83	46.66
TiO2	0.08	0.10	0.03	0.04	0.11
UO2	0.89	1.23	0.76	0.89	1.74
Al2O3	39.95	37.53	39.74	38.43	37.39
Cr2O3	0.07	0.13	0.03	0.01	0.10
FeO	0.60	0.52	0.75	1.03	0.12
MgO	0.52	0.87	0.54	0.57	0.76
MnO	0.00	0.06	0.03	0.00	0.02
CaO	3.08	0.56	2.18	0.67	0.32
BaO	0.42	0.69	0.61	0.75	1.67
CuO	0.06	0.00	0.00	0.01	0.09
Na2O	2.41	1.88	1.71	2.22	0.58
K20	2.98	6.60	4.58	5.18	8.24
Cl	0.01	0.03	0.00	0.03	0.01
Total	94.67	98.23	96.14	97.06	98.15
Mineral Formulas on Basis of 22 Oxygen					
V	0.03	0.03	0.03	0.03	0.03
Si	5.68	6.10	5.82	6.03	6.07
Ti	0.01	0.01	0.00	0.00	0.01
U	0.03	0.03	0.02	0.03	0.05
iv AL	2.32	1.90	2.18	1.97	1.93
vi AL	3.88	3.77	3.90	3.86	3.80
Cr	0.01	0.01	0.00	0.00	0.01
Fe	0.07	0.06	0.08	0.11	0.01
Mg	0.10	0.17	0.10	0.11	0.15
Mn	0.00	0.01	0.00	0.00	0.00
Ca	0.43	0.08	0.30	0.09	0.04
Ba	0.02	0.03	0.03	0.04	0.09
Cu	0.01	0.00	0.00	0.00	0.01
Na	0.61	0.47	0.43	0.55	0.15
K	0.50	1.08	0.76	0.85	1.37
Si + iv Al	8.00	8.00	8.00	8.00	8.00
Sum vi	4.05	4.00	4.09	4.09	3.97
Na+K+Ca+Ba	1.57	1.66	1.52	1.53	1.64
% Paragonite	0.39	0.28	0.28	0.36	0.09
% Muscovite	0.32	0.65	0.50	0.55	0.83
% Margerite	0.28	0.05	0.20	0.06	0.03
% Ba-Mica	0.01	0.02	0.02	0.02	0.05

*Locations of probe sites are in Appendix V

Table 16. Microprobe Analyses of Altered Micas* (cont.)

Oxide Weight Percent	CC219A.1f	CC219A.1g	CC219A.1h	CC219A.2a	CC219A.2b
V2O5	0.17	0.19	0.00	0.33	0.40
SiO2	49.42	47.30	51.21	44.88	48.11
TiO2	0.05	0.07	0.16	0.01	0.06
UO2	1.50	1.21	1.61	0.50	1.42
Al2O3	35.71	35.22	32.67	40.78	35.73
Cr2O3	0.10	0.00	0.00	0.00	0.09
FeO	0.31	2.67	0.63	0.08	0.22
MgO	1.25	1.29	2.84	0.21	1.22
MnO	0.06	0.10	0.00	0.00	0.00
CaO	0.03	0.04	0.02	1.76	0.36
BaO	1.36	1.22	2.16	0.44	1.05
CuO	0.00	0.04	0.00	0.04	0.00
Na2O	0.66	0.77	0.17	2.91	1.34
K20	8.79	7.62	9.73	2.49	7.53
Cl	0.00	0.00	0.03	0.00	0.00
Total	99.41	97.74	101.21	94.44	97.54
Mineral Formulas on Basis of 22 Oxygen					
V	0.01	0.02	0.00	0.03	0.03
Si	6.32	6.19	6.51	5.82	6.23
Ti	0.00	0.01	0.01	0.00	0.01
U	0.04	0.04	0.05	0.01	0.04
iv AL	1.68	1.81	1.49	2.18	1.77
vi AL	3.70	3.61	3.40	4.06	3.69
Cr	0.01	0.00	0.00	0.00	0.01
Fe	0.03	0.29	0.07	0.01	0.02
Mg	0.24	0.25	0.54	0.04	0.24
Mn	0.01	0.01	0.00	0.00	0.00
Ca	0.00	0.01	0.00	0.25	0.05
Ba	0.07	0.06	0.11	0.02	0.05
Cu	0.00	0.00	0.00	0.00	0.00
Na	0.16	0.20	0.04	0.73	0.34
K	1.43	1.27	1.58	0.41	1.24
Si + iv Al	8.00	8.00	8.00	8.00	8.00
Sum vi	3.98	4.18	4.02	4.11	3.96
Na+K+Ca+Ba	1.67	1.54	1.73	1.41	1.68
% Paragonite	0.10	0.13	0.02	0.52	0.20
% Muscovite	0.86	0.83	0.91	0.29	0.74
% Margerite	0.00	0.00	0.00	0.17	0.03
% Ba-Mica	0.04	0.04	0.06	0.02	0.03

*Locations of probe sites are in Appendix V

Table 16. Microprobe Analyses of Altered Micas* (cont.)

Oxide Weight Percent	CC219A.2c	CC219A.2f	CC219A.2g	CC219A.2h	CC219A.4d
V2O5	0.35	0.42	0.34	0.48	1.40
SiO2	45.48	41.27	46.91	44.54	46.98
TiO2	0.03	0.03	0.08	0.24	1.72
UO2	0.26	0.31	1.10	0.72	2.02
Al2O3	41.65	42.02	36.90	39.68	32.65
Cr2O3	0.09	0.00	0.13	0.21	0.06
FeO	0.19	0.99	0.20	0.10	0.19
MgO	0.19	0.31	0.90	0.57	1.83
MnO	0.06	0.00	0.00	0.04	0.00
CaO	2.28	3.96	0.62	2.45	0.01
BaO	0.36	0.33	0.85	0.34	0.82
CuO	0.04	0.00	0.08	0.00	0.00
Na2O	2.65	4.14	2.12	3.10	0.44
K20	2.11	1.88	6.35	4.31	9.84
Cl	0.01	0.00	0.01	0.00	0.00
Total	95.75	95.65	96.60	96.79	97.96
Mineral Formulas on Basis of 22 Oxygen					
V	0.03	0.04	0.03	0.04	0.12
Si	5.80	5.39	6.10	5.75	6.17
Ti	0.00	0.00	0.01	0.02	0.17
U	0.01	0.01	0.03	0.02	0.06
iv AL	2.20	2.61	1.90	2.25	1.83
vi AL	4.06	3.85	3.76	3.79	3.23
Cr	0.01	0.00	0.01	0.02	0.01
Fe	0.02	0.11	0.02	0.01	0.02
Mg	0.04	0.06	0.17	0.11	0.36
Mn	0.01	0.00	0.00	0.00	0.00
Ca	0.31	0.55	0.09	0.34	0.00
Ba	0.02	0.02	0.04	0.02	0.04
Cu	0.00	0.00	0.01	0.00	0.00
Na	0.66	1.05	0.54	0.78	0.11
K	0.34	0.31	1.05	0.71	1.65
Si + iv Al	8.00	8.00	8.00	8.00	8.00
Sum vi	4.13	4.02	3.97	3.94	3.77
Na+K+Ca+Ba	1.33	1.93	1.72	1.84	1.80
% Paragonite	0.49	0.54	0.31	0.42	0.06
% Muscovite	0.26	0.16	0.61	0.39	0.91
% Margerite	0.23	0.29	0.05	0.18	0.00
% Ba-Mica	0.01	0.01	0.03	0.01	0.02

*Locations of probe sites are in Appendix V

Table 16. Microprobe Analyses of Altered Micas* (cont.)

Oxide Weight Percent	CC180.2d	CC180.2e	CC169.1e	CC20E.1b	CC20E.5a	CC20E.5c
V2O5	1.49	0.42	0.76	0.64	0.54	0.44
SiO2	47.49	47.49	47.60	47.60	50.12	47.92
TiO2	1.63	0.03	0.01	0.09	0.32	0.18
UO2	1.89	1.34	2.04	1.55	1.17	1.08
Al2O3	33.52	37.58	36.96	36.34	37.28	36.32
Cr2O3	0.10	0.12	0.00	0.14	0.12	0.05
FeO	0.09	0.35	0.05	0.06	0.10	0.09
MgO	1.71	0.50	0.63	0.84	0.90	0.97
MnO	0.07	0.00	0.00	0.00	0.08	0.03
CaO	0.02	0.14	0.00	0.03	0.02	0.31
BaO	0.73	0.46	0.63	0.60	0.31	0.34
CuO	0.01	0.00	0.00	0.07	0.06	0.00
Na2O	0.53	2.86	0.79	2.02	2.00	3.03
K20	9.86	5.87	9.60	7.62	7.92	6.11
Cl	0.00	0.01	0.02	0.01	0.00	0.00
Total	99.15	97.16	99.10	97.59	100.95	96.88
Mineral Formulas on Basis of 22 Oxygen						
V	0.13	0.04	0.07	0.05	0.04	0.04
Si	6.15	6.12	6.13	6.16	6.23	6.18
Ti	0.16	0.00	0.00	0.01	0.03	0.02
U	0.05	0.04	0.06	0.04	0.03	0.03
iv AL	1.85	1.88	1.87	1.84	1.77	1.82
vi AL	3.26	3.82	3.74	3.71	3.70	3.71
Cr	0.01	0.01	0.00	0.01	0.01	0.01
Fe	0.01	0.04	0.01	0.01	0.01	0.01
Mg	0.33	0.10	0.12	0.16	0.17	0.19
Mn	0.01	0.00	0.00	0.00	0.01	0.00
Ca	0.00	0.02	0.00	0.00	0.00	0.04
Ba	0.04	0.02	0.03	0.03	0.01	0.02
Cu	0.00	0.00	0.00	0.01	0.01	0.00
Na	0.13	0.71	0.20	0.51	0.48	0.76
K	1.63	0.96	1.58	1.26	1.26	1.01
Si + iv Al	8.00	8.00	8.00	8.00	8.00	8.00
Sum vi	3.77	3.96	3.87	3.88	3.92	3.93
Na+K+Ca+Ba	1.80	1.72	1.81	1.80	1.76	1.83
% Paragonite	0.07	0.41	0.11	0.28	0.27	0.42
% Muscovite	0.91	0.56	0.87	0.70	0.72	0.55
% Margerite	0.00	0.01	0.00	0.00	0.00	0.02
% Ba-Mica	0.02	0.01	0.02	0.02	0.01	0.01

*Locations of probe sites are in Appendix V

APPENDIX V

Photomicrographs of Grains Selected for Microprobe Analysis

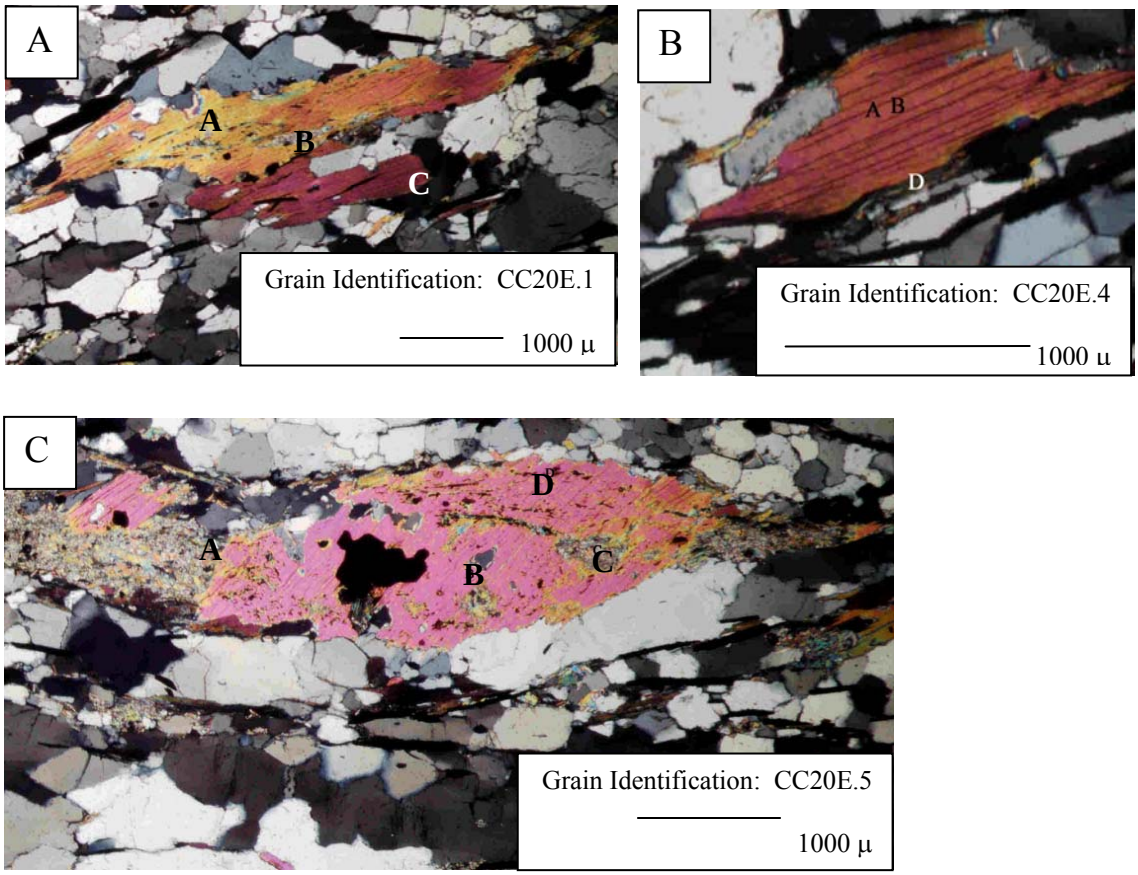

Fig. 49. Photomicrographs A, B and C are taken under crossed polarized light to show grains of muscovite within sample CC20E that were selected for microprobe analysis. Letters on the muscovite grains are used to label sites for analysis.

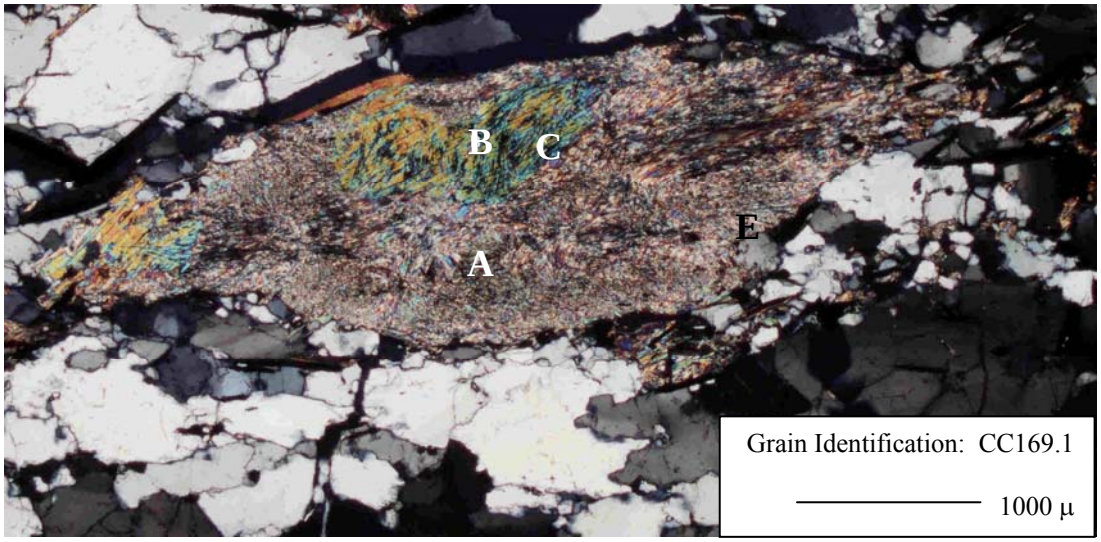

Fig. 50. Photomicrograph taken under crossed polarized light, showing the areas within sample CC169 that were selected for microprobe analysis. Letters on the grains are used to label analysis sites.

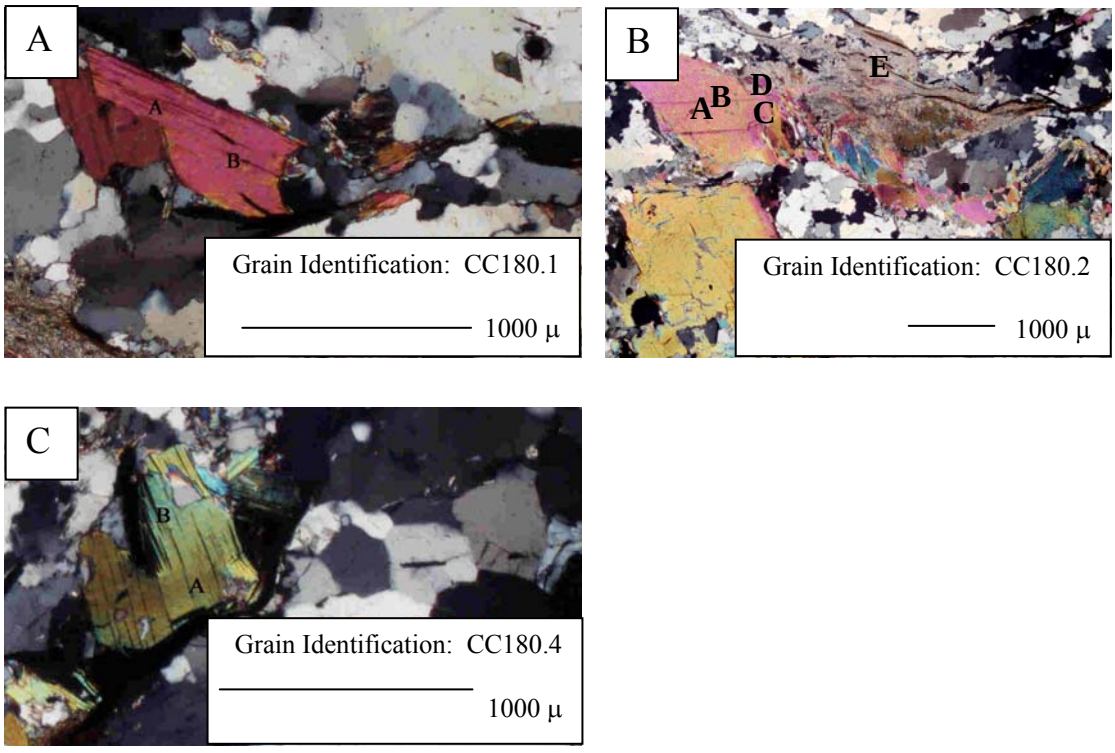

Fig. 51. Photomicrographs A, B and C are taken under crossed polarized light showing grains within sample CC180 that were selected for microprobe analysis. Letters on the muscovite and sericite grains are used to label sites for analysis.

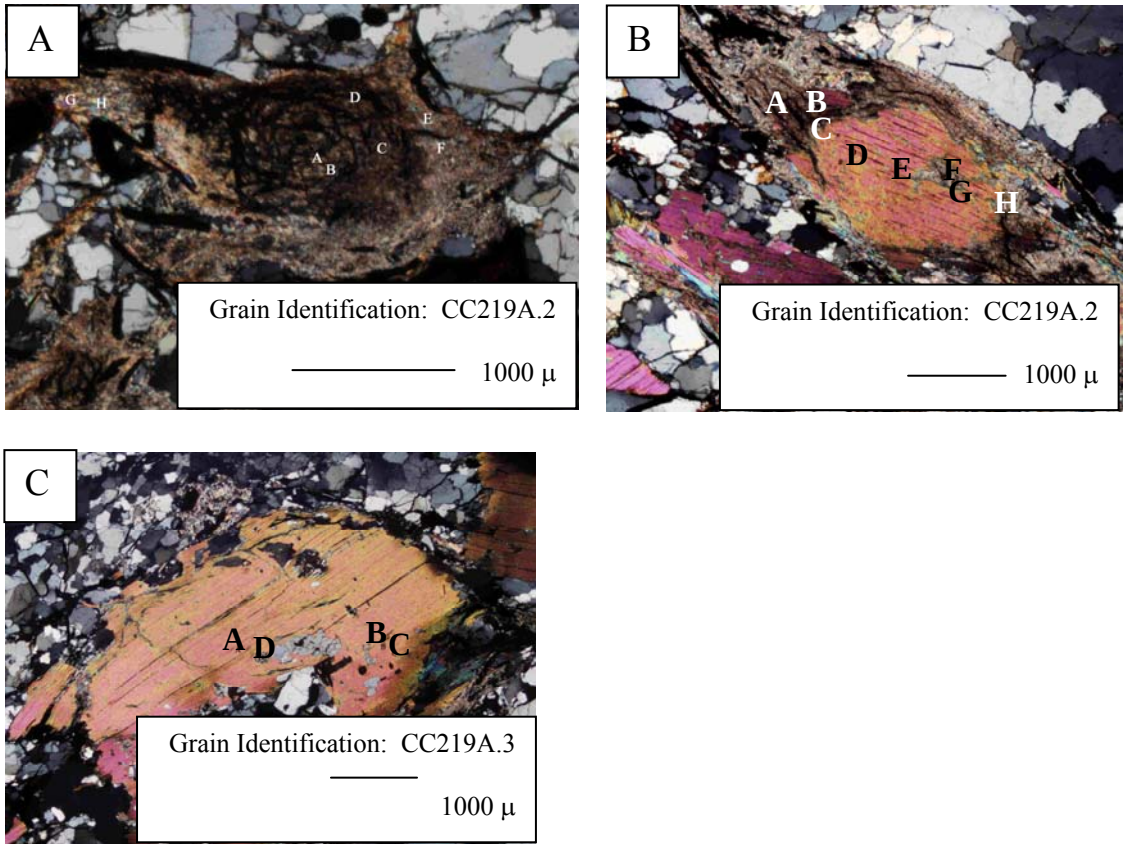

Fig. 52. Photomicrographs taken under crossed polarized light showing grains within sample CC219 that were selected for microprobe analysis. Letters on the muscovite and sericite grains denotes sites for analysis.

APPENDIX VI

Data CD

Table. 17 Rock Sample Pearson Correlation

	Ag	Ba	C	Ce	Co	Cr	Cs	Cu	Dy	Er	Eu	Ga	Gd	Hf	Ho	La	Lu	Mo	Nb	Nd	Ni	Pb	Pr	Rb	S	Sm	Sn	Sr	Ta	Tb	Th	Tl	Tm	U	V	W	Y	Yb	Zn
Ag	1.00																																						
Ba	-	1.00																																					
C	-	0.46	1.00																																				
Ce	-	0.07	-0.32	1.00																																			
Co	-	-0.23	-0.31	0.28	1.00																																		
Cr	-	-0.02	0.02	0.43	0.23	1.00																																	
Cs	-	0.37	0.14	0.42	0.17	0.27	1.00																																
Cu	-	0.18	0.13	0.02	0.00	-0.16	-0.04	1.00																															
Dy	-	-0.09	-0.19	0.63	0.58	0.43	0.36	0.06	1.00																														
Er	-	-0.06	-0.18	0.49	0.55	0.35	0.41	0.05	0.95	1.00																													
Eu	-	-0.07	-0.20	0.58	0.50	0.53	0.20	0.15	0.87	0.73	1.00																												
Ga	-	0.26	0.11	0.47	0.12	0.52	0.31	0.27	0.29	0.26	0.31	1.00																											
Gd	-	-0.11	-0.23	0.83	0.49	0.49	0.36	0.03	0.92	0.78	0.85	0.35	1.00																										
Hf	-	-0.17	-0.44	0.68	0.34	0.25	0.06	-0.23	0.39	0.30	0.31	0.22	0.51	1.00																									
Ho	-	-0.13	-0.24	0.53	0.42	0.44	0.23	0.00	0.85	0.85	0.72	0.29	0.76	0.37	1.00																									
La	-	0.06	-0.22	0.95	0.21	0.47	0.47	0.09	0.68	0.55	0.62	0.47	0.86	0.52	0.59	1.00																							
Lu	-	-0.02	-0.23	0.44	0.54	0.29	0.44	-0.01	0.86	0.97	0.63	0.24	0.67	0.31	0.78	0.48	1.00																						
Mo	-	0.67	0.73	-0.30	-0.28	-0.01	0.23	0.19	-0.26	-0.14	-0.30	0.35	-0.36	-0.41	-0.28	-0.23	-0.08	1.00																					
Nb	-	0.17	-0.14	0.66	0.18	0.32	0.34	-0.16	0.59	0.56	0.39	0.42	0.63	0.41	0.56	0.61	0.52	-0.05	1.00																				
Nd	-	-0.02	-0.22	0.92	0.34	0.48	0.41	0.02	0.79	0.65	0.71	0.43	0.95	0.54	0.68	0.96	0.55	-0.29	0.69	1.00																			
Ni	-	0.00	-0.13	0.10	0.43	-0.21	0.17	0.49	0.34	0.36	0.28	-0.10	0.25	-0.04	-0.05	0.11	0.36	-0.07	0.00	0.13	1.00																		
Pb	-	0.12	-0.18	0.40	-0.23	0.21	0.49	0.22	0.15	0.10	0.27	0.32	0.28	0.04	0.17	0.49	0.08	-0.16	0.01	0.36	0.01	1.00																	
Pr	-	0.01	-0.23	0.94	0.29	0.48	0.45	0.04	0.75	0.62	0.67	0.48	0.92	0.55	0.65	0.98	0.54	-0.27	0.68	0.99	0.11	0.43	1.00																
Rb	-	0.39	0.05	0.58	0.12	0.38	0.73	-0.07	0.39	0.42	0.17	0.35	0.44	0.25	0.36	0.59	0.43	0.14	0.63	0.56	0.05	0.32	0.59	1.00															
S	-	0.16	0.09	-0.03	0.32	-0.15	0.27	0.06	0.21	0.25	0.15	-0.10	0.11	-0.10	-0.27	-0.04	0.28	0.17	-0.05	0.00	0.78	-0.11	-0.02	0.01	1.00														
Sm	-	-0.05	-0.23	0.88	0.41	0.49	0.36	0.03	0.86	0.70	0.79	0.41	0.98	0.53	0.72	0.91	0.59	-0.33	0.69	0.98	0.18	0.31	0.96	0.51	0.05	1.00													
Sn	-	0.22	-0.12	0.56	0.12	0.53	0.47	0.12	0.52	0.52	0.51	0.65	0.53	0.17	0.60	0.65	0.52	0.12	0.37	0.60	-0.15	0.55	0.64	0.50	-0.16	0.56	1.00												
Sr	-	-0.10	-0.24	0.17	0.50	0.35	-0.06	-0.01	0.63	0.59	0.76	0.16	0.48	0.02	0.59	0.16	0.56	-0.20	0.26	0.27	0.13	-0.10	0.23	-0.09	0.08	0.39	0.34	1.00											
Ta	-	0.18	-0.05	0.50	0.04	0.20	0.27	-0.14	0.49	0.48	0.29	0.33	0.51	0.18	0.48	0.48	0.43	0.02	0.96	0.58	-0.02	-0.05	0.55	0.53	-0.06	0.58	0.30	0.26	1.00										
Tb	-	-0.12	-0.22	0.73	0.55	0.50	0.36	0.01	0.97	0.86	0.89	0.33	0.98	0.47	0.83	0.78	0.76	-0.33	0.60	0.88	0.25	0.23	0.85	0.40	0.14	0.94	0.54	0.59	0.49	1.00									
Th	-	0.12	-0.33	0.85	0.14	0.24	0.43	0.26	0.48	0.42	0.35	0.45	0.62	0.64	0.43	0.79	0.40	-0.20	0.65	0.74	0.22	0.43	0.77	0.65	-0.09	0.69	0.44	-0.08	0.50	0.53	1.00								
Tl	-	0.51	0.45	-0.15	-0.07	-0.01	0.70	-0.05	0.02	0.16	-0.13	0.00	-0.13	-0.24	-0.12	-0.10	0.25	0.57	0.05	-0.14	0.21	0.09	-0.12	0.49	0.38	-0.16	0.06	-0.15	0.06	-0.08	0.01	1.00							
Tm	-	-0.03	-0.20	0.45	0.55	0.32	0.46	0.00	0.89	0.99	0.66	0.25	0.71	0.28	0.81	0.50	0.99	-0.08	0.55	0.58	0.36	0.08	0.56	0.44	0.27	0.62	0.52	0.57	0.47	0.80	0.40	0.24	1.00						
U	-	0.32	0.17	-0.08	-0.06	-0.28	-0.05	0.27	-0.10	-0.18	-0.02	0.01	-0.08	-0.34	-0.37	-0.04	-0.23	0.25	-0.22	-0.06	0.36	0.02	-0.06	-0.24	0.52	-0.05	-0.14	-0.11	-0.15	-0.11	-0.21	-0.06	-0.21	1.00					
V	-	-0.17	0.28	-0.37	-0.26	0.22	-0.01	-0.19	-0.27	-0.16	-0.30	-0.03	-0.32	-0.43	-0.16	-0.24	-0.12	0.26	-0.15	-0.28	-0.24	-0.14	-0.27	-0.01	-0.14	-0.32	-0.17	-0.16	-0.05	-0.30	-0.35	0.20	-0.12	-0.12	1.00				
W	-	0.17	0.30	0.20	0.00	0.16	-0.07	0.14	0.26	0.21	0.20	0.24	0.26	0.07	0.25	0.18	0.12	0.12	0.33	0.25	-0.08	-0.15	0.23	0.21	-0.08	0.28	0.09	0.21	0.34	0.26	0.11	-0.13	0.14	0.06	-0.13	1.00			
Y	-	-0.04	-0.09	0.40	0.50	0.32	0.42	-0.03	0.89	0.97	0.64	0.18	0.70	0.21	0.75	0.46	0.96	-0.04	0.55	0.56	0.39	0.01	0.53	0.41	0.34	0.61	0.43	0.53	0.49	0.78	0.34	0.28	0.98	-0.17	-0.04	0.14	1.00		
Yb	-	-0.02	-0.21	0.47	0.55	0.31	0.45	0.00	0.89	0.98	0.64	0.26	0.71	0.31	0.80	0.51	0.99	-0.09	0.57	0.59	0.36	0.09	0.57	0.46	0.27	0.63	0.52	0.54	0.48	0.79	0.43	0.23	1.00	-0.21	-0.13	0.16	0.97	1.00	
Zn	-	-0.06	-0.22	0.02	0.19	-0.32	-0.04	0.77	0.13	0.14	0.16	-0.14	0.08	-0.13	-0.03	0.05	0.12	-0.18	-0.12	0.01	0.79	0.14	0.01	-0.07	0.30	0.05	-0.16	0.02	-0.11	0.06	0.29	0.00	0.12	0.19	-0.22	-0.13	0.12	0.12	1.00

Table 17. Green Mica Pearson Correlation

	Ag	Ba	Ce	Co	Cr	Cs	Cu	Dy	Er	Eu	Ga	Gd	Hf	Ho	La	Lu	Mo	Nb	Nd	Ni	Pb	Pr	Rb	Sm	Sn	Sr	Ta	Tb	Th	Tl	Tm	U	V	W	Y	Yb	Zn	Zr
Ag	1.00																																					
Ba	-0.09	1.00																																				
Ce	0.07	-0.05	1.00																																			
Co	-0.20	-0.28	0.84	1.00																																		
Cr	0.32	-0.38	-0.55	-0.63	1.00																																	
Cs	0.10	0.25	-0.62	-0.84	0.63	1.00																																
Cu	0.04	0.37	-0.34	-0.21	-0.32	-0.21	1.00																															
Dy	0.06	-0.61	0.44	0.67	-0.40	-0.65	-0.14	1.00																														
Er	0.07	-0.59	0.37	0.60	-0.39	-0.59	-0.13	0.99	1.00																													
Eu	0.14	-0.43	0.47	0.54	-0.49	-0.58	-0.06	0.90	0.90	1.00																												
Ga	0.28	-0.08	-0.34	-0.49	0.49	0.78	-0.42	-0.12	-0.08	-0.11	1.00																											
Gd	0.19	-0.60	0.58	0.65	-0.36	-0.56	-0.25	0.94	0.93	0.93	-0.02	1.00																										
Hf	-0.02	0.50	0.71	0.46	-0.48	-0.21	-0.19	-0.18	-0.24	-0.06	-0.19	-0.06	1.00																									
Ho	0.05	-0.61	0.40	0.65	-0.39	-0.63	-0.14	1.00	1.00	0.90	-0.11	0.94	-0.22	1.00																								
La	0.25	-0.56	0.70	0.63	-0.27	-0.49	-0.32	0.79	0.75	0.80	-0.02	0.94	0.08	0.77	1.00																							
Lu	0.27	-0.46	0.21	0.35	-0.29	-0.35	-0.12	0.89	0.93	0.89	0.16	0.86	-0.29	0.91	0.66	1.00																						
Mo	0.16	0.45	-0.45	-0.47	-0.23	0.10	0.87	-0.17	-0.12	0.04	-0.07	-0.20	-0.29	-0.15	-0.28	0.04	1.00																					
Nb	-0.19	0.71	-0.30	-0.40	-0.27	0.08	0.63	-0.52	-0.50	-0.22	-0.35	-0.55	0.14	-0.52	-0.58	-0.40	0.68	1.00																				
Nd	0.25	-0.55	0.70	0.64	-0.29	-0.50	-0.32	0.81	0.77	0.83	-0.01	0.95	0.09	0.79	1.00	0.69	-0.27	-0.56	1.00																			
Ni	-0.19	-0.26	0.52	0.45	-0.41	-0.18	-0.20	0.45	0.41	0.56	0.11	0.62	0.25	0.43	0.68	0.33	-0.12	-0.24	0.70	1.00																		
Pb	0.04	0.21	-0.25	-0.50	0.44	0.67	-0.46	-0.41	-0.35	-0.43	0.42	-0.34	-0.16	-0.39	-0.26	-0.18	-0.21	-0.12	-0.27	-0.31	1.00																	
Pr	0.26	-0.56	0.70	0.64	-0.28	-0.50	-0.32	0.80	0.77	0.82	-0.02	0.95	0.09	0.79	1.00	0.68	-0.27	-0.57	1.00	0.69	-0.28	1.00																
Rb	0.18	0.37	-0.33	-0.66	0.57	0.91	-0.38	-0.73	-0.70	-0.66	0.71	-0.60	0.15	-0.72	-0.45	-0.49	-0.13	0.03	-0.46	-0.22	0.67	-0.47	1.00															
Sm	0.24	-0.56	0.68	0.65	-0.33	-0.52	-0.31	0.86	0.83	0.88	-0.01	0.98	0.07	0.84	0.99	0.76	-0.25	-0.55	0.99	0.69	-0.30	0.99	-0.51	1.00														
Sn	-0.06	0.04	-0.39	-0.44	0.58	0.78	-0.37	-0.50	-0.49	-0.68	0.70	-0.47	-0.08	-0.49	-0.39	-0.42	-0.31	-0.36	-0.40	-0.14	0.53	-0.40	0.78	-0.44	1.00													
Sr	0.35	0.51	0.58	0.25	-0.17	-0.09	-0.21	-0.29	-0.33	-0.24	-0.12	-0.17	0.80	-0.31	0.01	-0.30	-0.27	0.01	0.00	-0.19	0.18	0.00	0.31	-0.04	0.02	1.00												
Ta	-0.15	0.67	-0.30	-0.42	-0.24	0.10	0.56	-0.48	-0.45	-0.15	-0.27	-0.49	0.12	-0.47	-0.51	-0.33	0.68	0.99	-0.50	-0.22	-0.10	-0.50	0.06	-0.48	-0.39	0.00	1.00											
Tb	0.11	-0.61	0.50	0.68	-0.39	-0.63	-0.18	0.99	0.98	0.91	-0.09	0.98	-0.13	0.99	0.85	0.89	-0.19	-0.55	0.87	0.52	-0.39	0.87	-0.69	0.91	-0.49	-0.24	-0.50	1.00										
Th	0.22	-0.37	0.79	0.68	-0.36	-0.54	-0.24	0.67	0.61	0.70	-0.09	0.83	0.25	0.65	0.95	0.50	-0.23	-0.48	0.94	0.64	-0.32	0.94	-0.42	0.91	-0.39	0.19	-0.42	0.74	1.00									
Tl	0.02	0.44	-0.47	-0.76	0.26	0.81	-0.03	-0.50	-0.45	-0.25	0.66	-0.38	-0.11	-0.49	-0.32	-0.18	0.39	0.38	-0.32	0.03	0.47	-0.33	0.71	-0.33	0.39	-0.11	0.46	-0.47	-0.30	1.00								
Tm	0.13	-0.56	0.32	0.54	-0.36	-0.54	-0.12	0.98	0.99	0.91	-0.01	0.92	-0.26	0.99	0.73	0.96	-0.08	-0.48	0.75	0.39	-0.32	0.75	-0.66	0.82	-0.47	-0.33	-0.43	0.97	0.59	-0.39	1.00							
U	0.69	0.02	-0.13	-0.43	0.25	0.47	-0.16	0.10	0.16	0.29	0.71	0.25	-0.16	0.11	0.24	0.48	0.26	-0.10	0.26	0.07	0.31	0.25	0.41	0.27	0.09	0.05	0.01	0.15	0.16	0.59	0.24	1.00						
V	0.40	-0.11	-0.40	-0.67	0.64	0.79	-0.45	-0.19	-0.12	-0.09	0.81	-0.06	-0.36	-0.17	-0.02	0.17	-0.03	-0.19	-0.02	-0.07	0.70	-0.03	0.69	-0.03	0.46	-0.13	-0.10	-0.15	-0.17	0.69	-0.05	0.79	1.00					
W	-0.06	0.12	-0.50	-0.56	0.23	0.69	-0.16	-0.10	-0.02	-0.11	0.62	-0.11	-0.48	-0.07	-0.19	0.21	0.18	-0.08	-0.19	-0.05	0.75	-0.20	0.45	-0.17	0.46	-0.32	-0.05	-0.12	-0.33	0.62	0.04	0.49	0.72	1.00				
Y	0.09	-0.58	0.35	0.57	-0.37	-0.55	-0.15	0.99	1.00	0.90	-0.03	0.92	-0.25	0.99	0.74	0.95	-0.12	-0.50	0.76	0.40	-0.31	0.76	-0.67	0.82	-0.47	-0.33	-0.45	0.97	0.60	-0.41	1.00	0.20	-0.07	0.03	1.00			
Yb	0.18	-0.51	0.26	0.44	-0.33	-0.44	-0.14	0.94	0.97	0.90	0.07	0.89	-0.29	0.95	0.69	0.99	-0.03	-0.43	0.72	0.36	-0.23	0.71	-0.57	0.78	-0.45	-0.33	-0.37	0.93	0.53	-0.28	0.99	0.36	0.07	0.14	0.98	1.00		
Zn	0.66	0.15	0.42	0.14	-0.12	0.00	-0.24	0.25	0.27	0.26	0.24	0.36	0.23	0.25	0.41	0.44	-0.07	-0.34	0.41	-0.03	0.37	0.40	0.14	0.40	-0.04	0.59	-0.31	0.30	0.41	0.00	0.32	0.61	0.33	0.25	0.30	0.37	1.00	
Zr	-0.01	0.49	0.69	0.43	-0.44	-0.17	-0.21	-0.22	-0.28	-0.10	-0.15	-0.08	1.00	-0.25	0.06	-0.32	-0.30	0.14	0.07	0.25	-0.14	0.07	0.19	0.04	-0.04	0.80	0.12	-0.17	0.24	-0.07	-0.30	-0.14	-0.33	-0.47	-0.29	-0.32	0.22	1.00

Table 18. Microprobe Pearson Correlation

	Si	Ti	Al	Mg	Fe	Ca	Mn	K	Na	Cl	F	Cr	Ba	Cu	U	V	O
Si	1.00																
Ti	0.48	1.00															
Al	0.46	0.40	1.00														
Mg	0.33	0.74	0.59	1.00													
Fe	-0.11	-0.20	0.16	0.08	1.00												
Ca	-0.23	-0.52	-0.21	-0.20	-0.15	1.00											
Mn	-0.01	-0.03	0.20	-0.10	-0.15	0.17	1.00										
K	-0.21	0.24	0.63	0.31	0.15	-0.24	0.19	1.00									
Na	-0.43	-0.43	0.27	0.06	0.24	0.41	0.18	0.30	1.00								
Cl	-0.07	0.21	0.17	0.24	-0.29	0.00	0.20	0.28	0.05	1.00							
Fe	-	-	-	-	-	-	-	-	-	-	1.00						
Cr	0.14	-0.17	0.04	0.04	0.45	0.09	0.13	-0.30	0.24	-0.24	-	1.00					
Ba	0.16	0.50	0.59	0.69	0.17	-0.15	-0.15	0.43	0.30	0.01	-	-0.08	1.00				
Cu	0.14	-0.25	0.19	-0.23	0.07	0.01	-0.10	0.13	0.11	-0.11	-	0.00	-0.23	1.00			
U	0.34	0.61	0.80	0.77	0.13	-0.23	0.18	0.53	0.12	0.13	-	-0.12	0.62	-0.15	1.00		
V	0.42	-0.06	0.36	0.13	0.01	0.18	0.19	-0.19	0.23	-0.06	-	0.38	-0.09	0.43	0.16	1.00	
O	0.55	0.50	0.99	0.64	0.13	-0.26	0.18	0.60	0.17	0.17	-	0.03	0.60	0.17	0.81	0.35	1.00

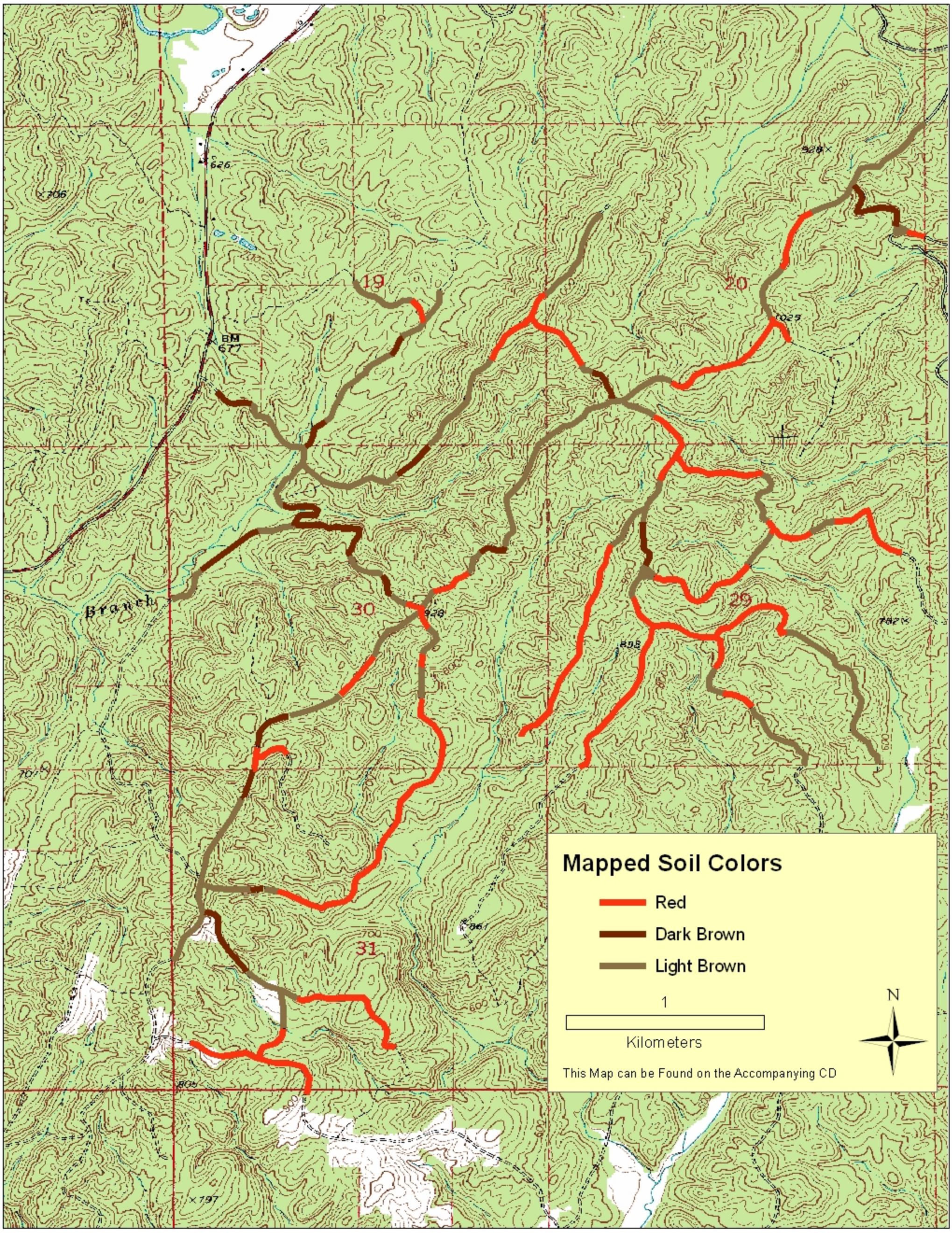
19
20
30
29
31
626
BM
677
928
858
861
1025
Branch
Mapped Soil Colors
Red
Dark Brown
Light Brown
1
Kilometers
N
This Map can be Found on the Accompanying CD

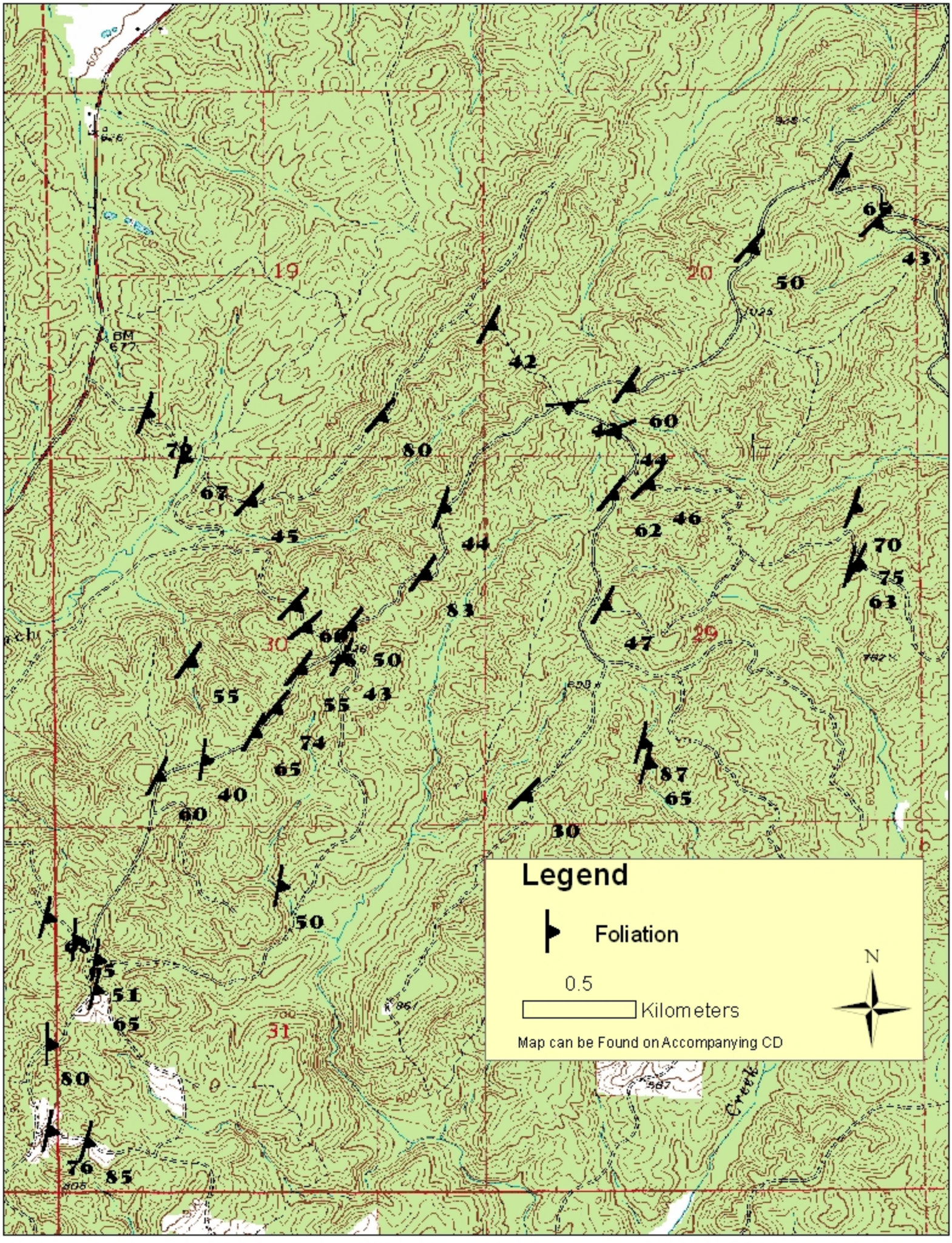
19
20
30
29
31
42
60
80
67
45
44
83
50
55
43
74
65
40
60
50
51
65
80
76
85
70
75
63
47
87
65
62
46
Legend
Foliation
0.5
Kilometers
Map can be Found on Accompanying CD
N

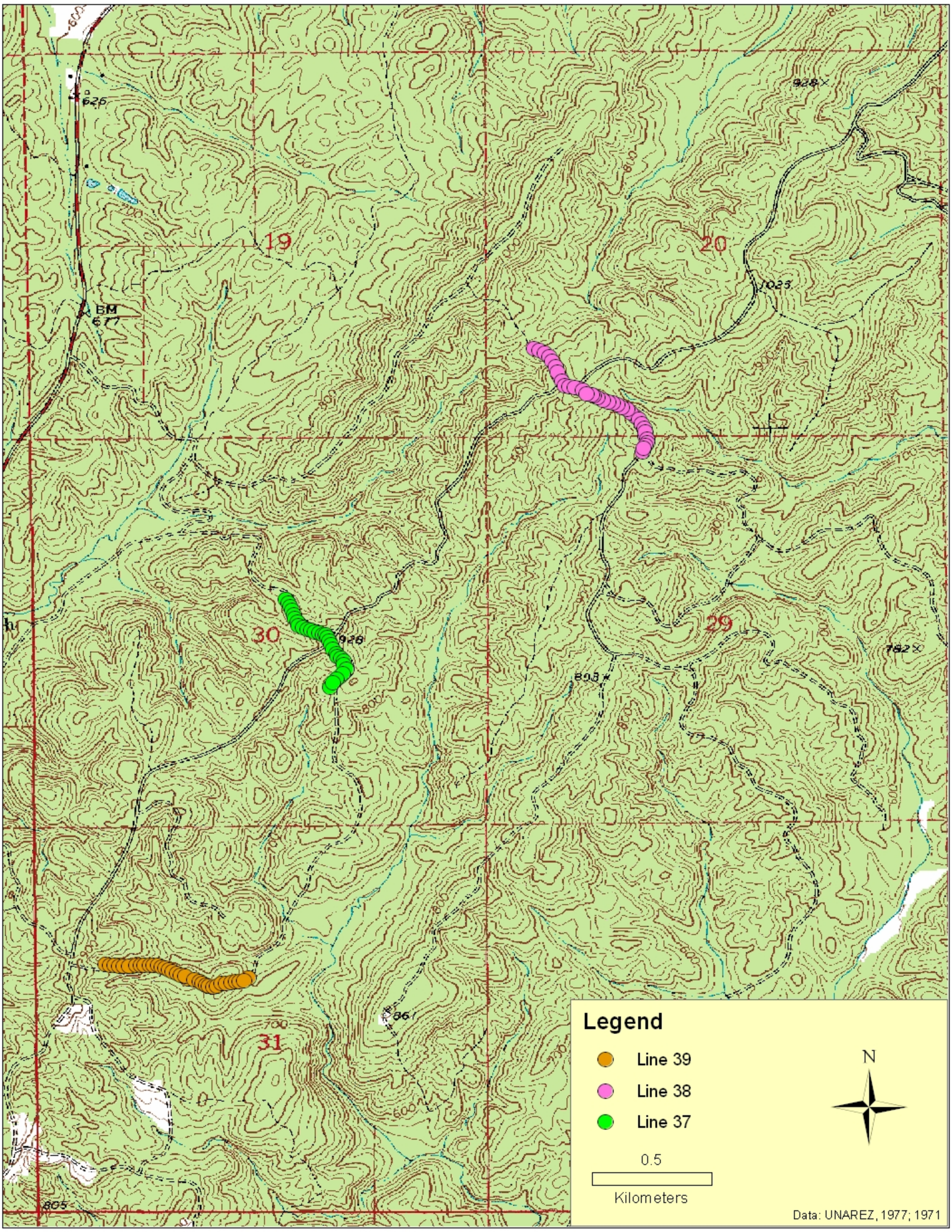
19
20
30
29
31
626
677
928
1023
928
803
782
886
805
Legend
Line 39
Line 38
Line 37
0.5
Kilometers
N
Data: UNAREZ, 1977; 1971

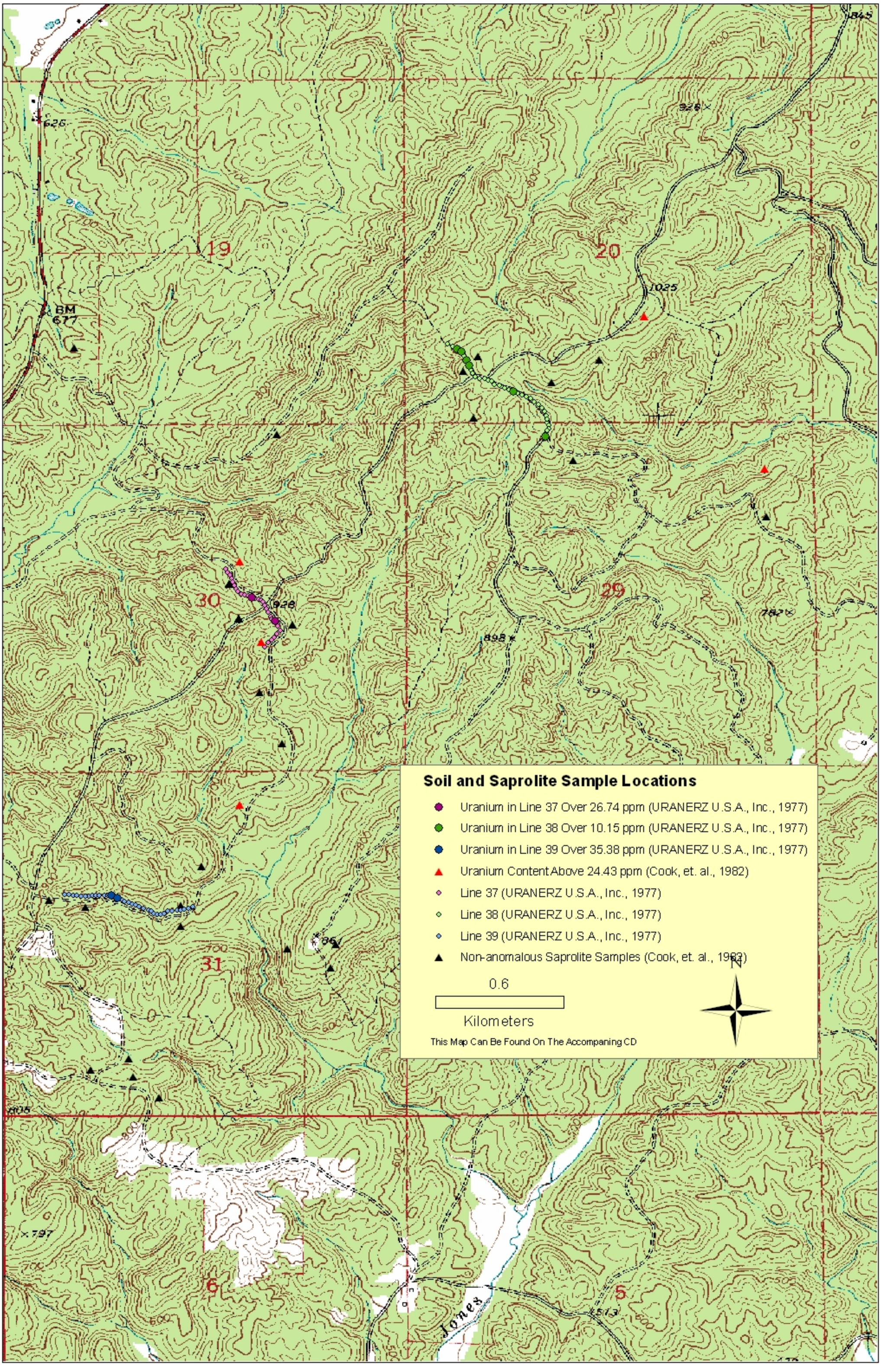
19
20
30
29
31
6
5
BM
677
1025
928
898
Jones
Soil and Saprolite Sample Locations
Uranium in Line 37 Over 26.74 ppm (URANERZ U.S.A., Inc., 1977)
Uranium in Line 38 Over 10.15 ppm (URANERZ U.S.A., Inc., 1977)
Uranium in Line 39 Over 35.38 ppm (URANERZ U.S.A., Inc., 1977)
Uranium Content Above 24.43 ppm (Cook, et. al., 1982)
Line 37 (URANERZ U.S.A., Inc., 1977)
Line 38 (URANERZ U.S.A., Inc., 1977)
Line 39 (URANERZ U.S.A., Inc., 1977)
Non-anomalous Saprolite Samples (Cook, et. al., 1982)
0.6
Kilometers
N
This Map Can Be Found On The Accompaning CD

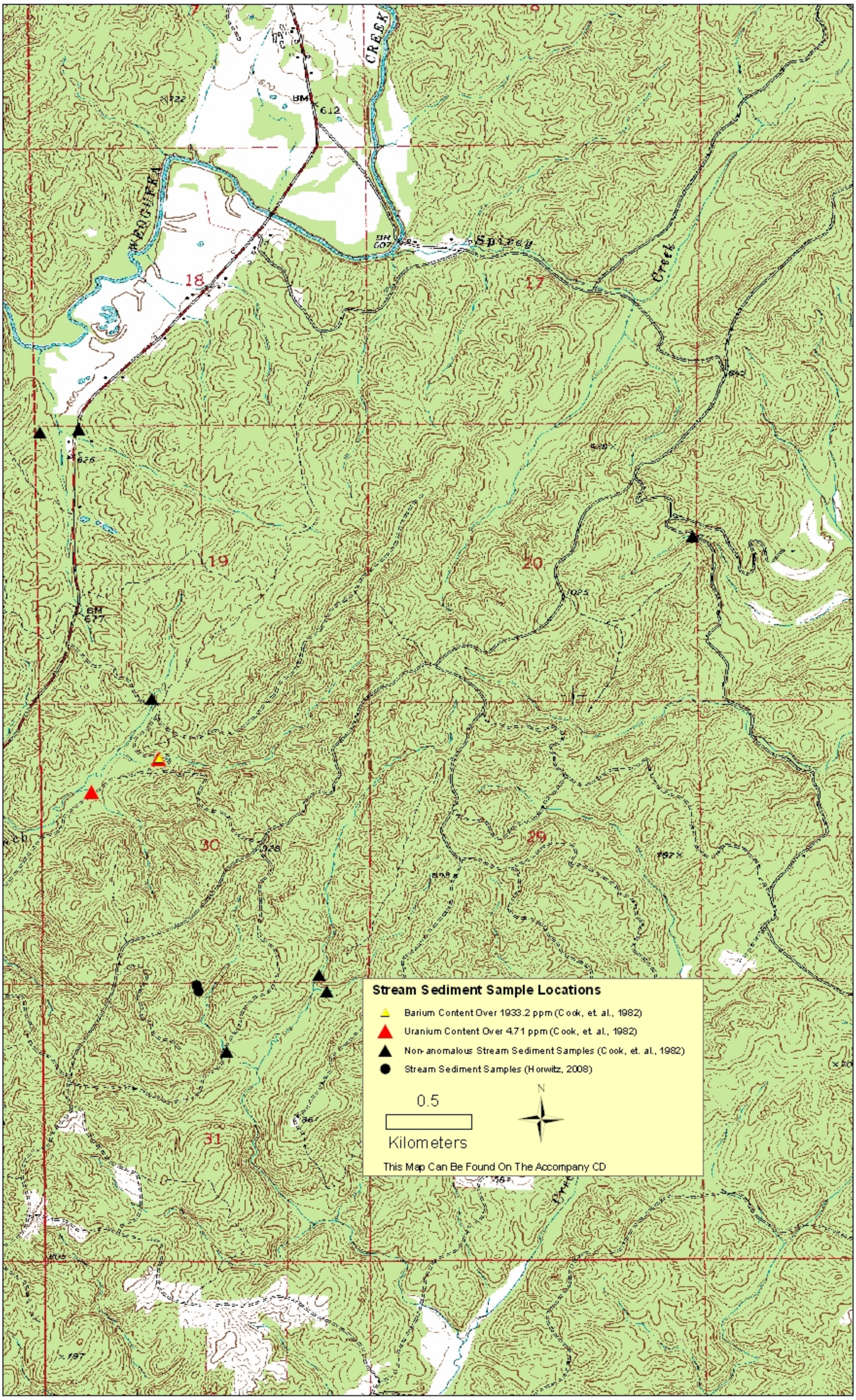
CREEK
Spivey
Creek
BM
612
18
17
19
20
30
29
31
BM
677
626
1025
642
Stream Sediment Sample Locations
Barium Content Over 1933.2 ppm (Cook, et. al., 1982)
Uranium Content Over 4.71 ppm (Cook, et. al., 1982)
Non-anomalous Stream Sediment Samples (Cook, et. al., 1982)
Stream Sediment Samples (Horwitz, 2008)
0.5
Kilometers
N
This Map Can Be Found On The Accompany CD

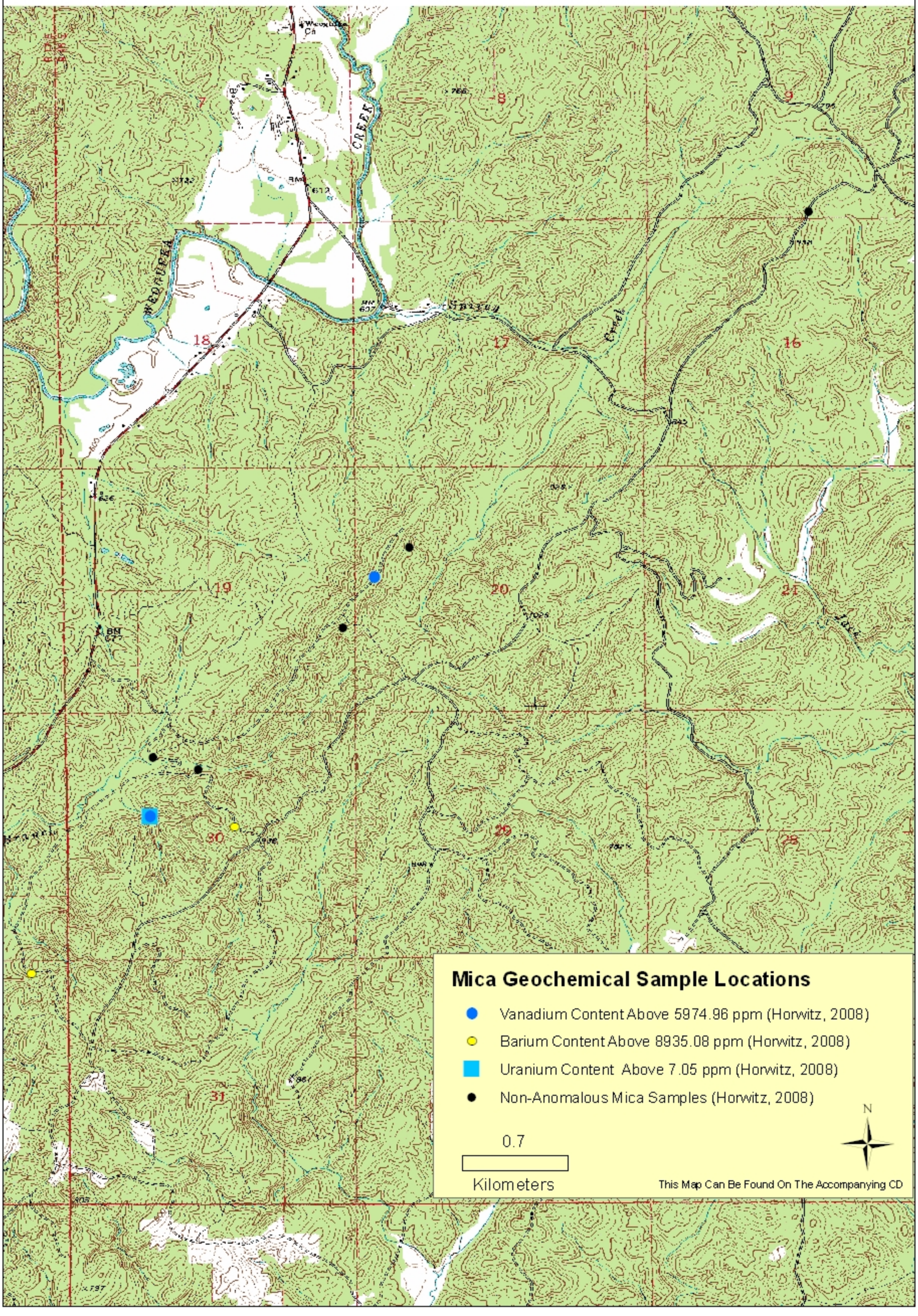
Mica Geochemical Sample Locations
Vanadium Content Above 5974.96 ppm (Horwitz, 2008)
Barium Content Above 8935.08 ppm (Horwitz, 2008)
Uranium Content Above 7.05 ppm (Horwitz, 2008)
Non-Anomalous Mica Samples (Horwitz, 2008)
0.7
Kilometers
N
This Map Can Be Found On The Accompanying CD

WEOGUFKA STATE FOREST
Water Tank
Flagg Mountain
Weoguefka Creek
Spivey Creek
Mill Branch
Moriah
Mt Moriah Ch
Cem
Flint Hill Ch
Tyler Ford
Jones Creek
HATCHET CREEK
Beaver Creek
BM 617
BM 692
BM 528
BM 555
BR 384
14
13
18
17
16
23
24
19
20
21
26
25
30
29
28
35
36
31
32
33
2
1
6
5
4
12
7
8
9
11
3
18
17
16

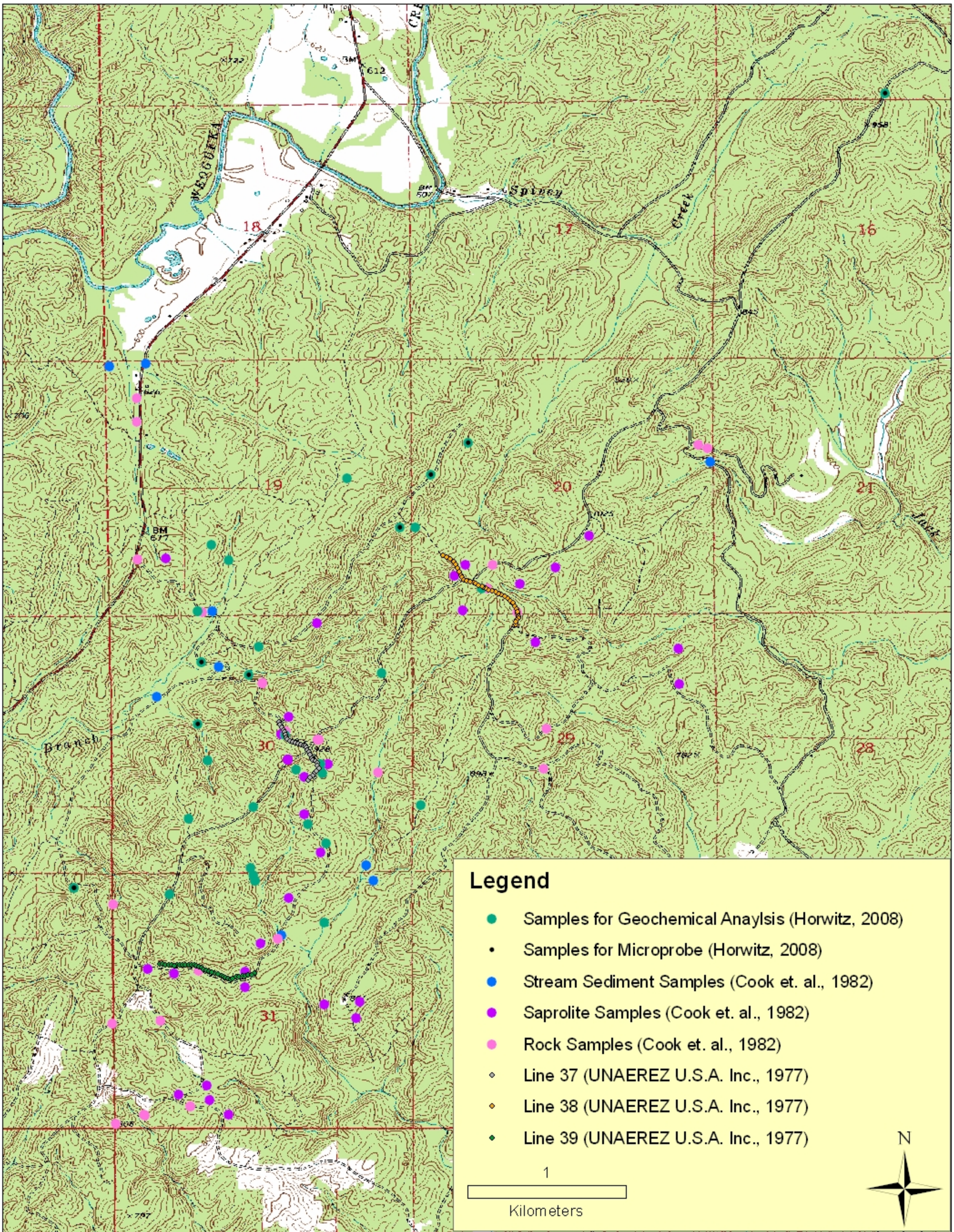
Legend
Samples for Geochemical Anaylsis (Horwitz, 2008)
Samples for Microprobe (Horwitz, 2008)
Stream Sediment Samples (Cook et. al., 1982)
Saprolite Samples (Cook et. al., 1982)
Rock Samples (Cook et. al., 1982)
Line 37 (UNAEREZ U.S.A. Inc., 1977)
Line 38 (UNAEREZ U.S.A. Inc., 1977)
Line 39 (UNAEREZ U.S.A. Inc., 1977)
1
Kilometers
N
Spivey
Creek
Branch
WEOGUFKA
BM 612
BM 677
18
17
16
19
20
21
30
29
28
31
958

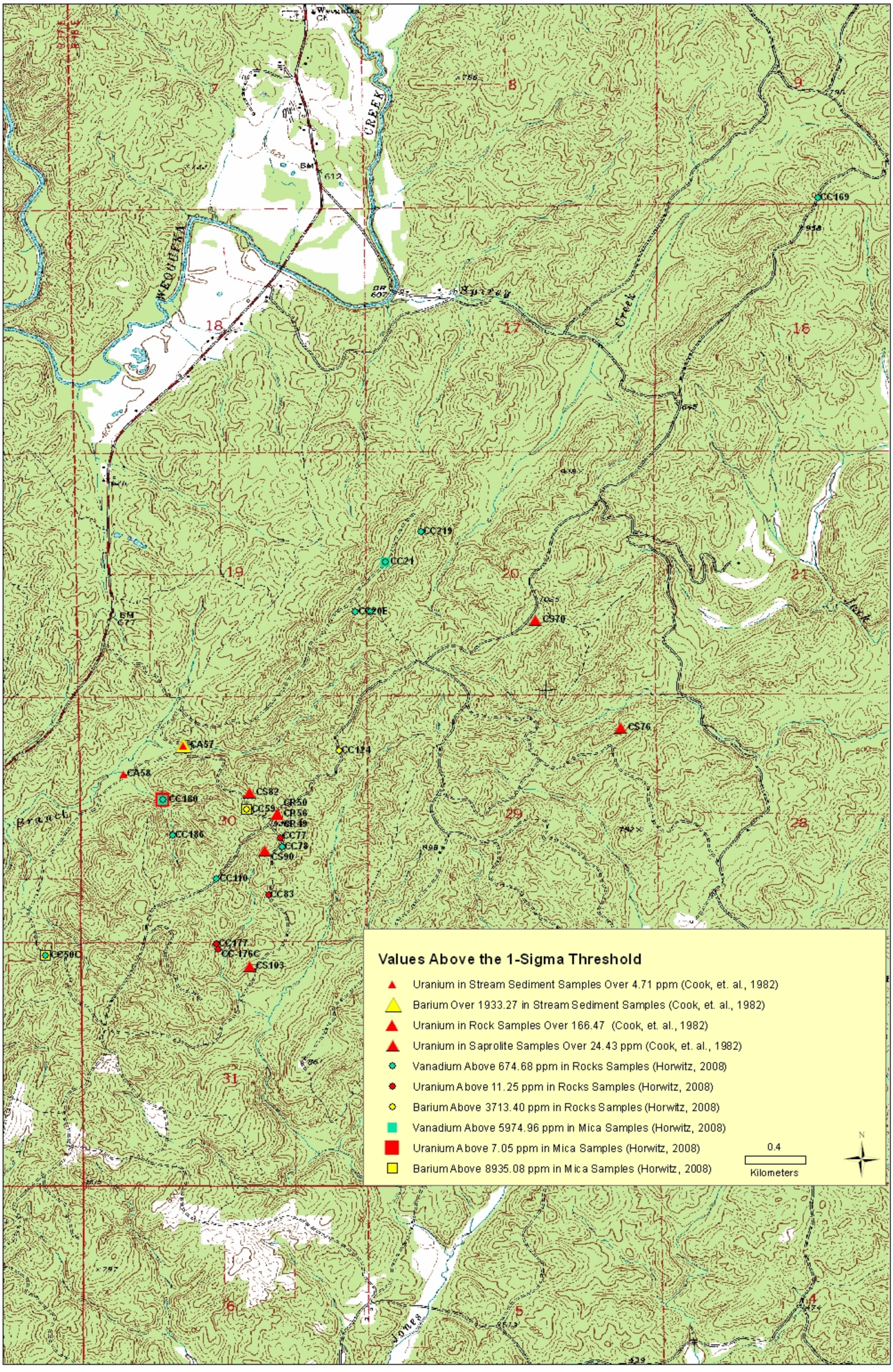
CREEK
WEQUEAK
Spivey
Creek
Branch
Jones
7
8
9
17
16
18
19
20
21
29
28
30
31
6
5
4
CC169
CC219
CC21
CC20E
CC124
CC180
CC186
CC77
CC78
CC110
CC83
CC177
CC176C
CC50C
CA57
CA58
CS82
CS90
CS103
CS70
CS76
CR50
CR56
CR49
BM
612
DR
607
Values Above the 1-Sigma Threshold
Uranium in Stream Sediment Samples Over 4.71 ppm (Cook, et. al., 1982)
Barium Over 1933.27 in Stream Sediment Samples (Cook, et. al., 1982)
Uranium in Rock Samples Over 166.47 (Cook, et. al., 1982)
Uranium in Saprolite Samples Over 24.43 ppm (Cook, et. al., 1982)
Vanadium Above 674.68 ppm in Rocks Samples (Horwitz, 2008)
Uranium Above 11.25 ppm in Rocks Samples (Horwitz, 2008)
Barium Above 3713.40 ppm in Rocks Samples (Horwitz, 2008)
Vanadium Above 5974.96 ppm in Mica Samples (Horwitz, 2008)
Uranium Above 7.05 ppm in Mica Samples (Horwitz, 2008)
Barium Above 8935.08 ppm in Mica Samples (Horwitz, 2008)
0.4
Kilometers
N